Summer 2021

The Impact of Nanopulse Treatment on the Tumor Microenvironment in Breast Cancer: Overturning the Treg Immunosuppressive Dominance

Anthony Nanajian
Old Dominion University, anthony8n@gmail.com

THE IMPACT OF NANOPULSE TREATMENT ON THE TUMOR MICROENVIRONMENT IN BREAST CANCER: OVERTURNING THE TREG IMMUNOSUPPRESSIVE DOMINANCE

by

Anthony Nanajian
B.S. August 2010, Old Dominion University
M.S. December 2013, Old Dominion University
M.D. May 2019, St. George's University, Grenada

A Dissertation Submitted to the Faculty of
Old Dominion University in Partial Fulfillment of the
Requirements for the Degree of

DOCTOR OF PHILOSOPHY

BIOMEDICAL SCIENCES

OLD DOMINION UNIVERSITY
August 2021

Approved by:

Stephen J. Beebe (Co-Director)

Siqi Guo (Co-Director)

Christopher Osgood (Member)

Woong-Ki Kim (Member)

ABSTRACT

THE IMPACT OF NANOPULSE TREATMENT ON THE TUMOR MICROENVIRONMENT IN BREAST CANCER: OVERTURNING THE TREG IMMUNOSUPPRESSIVE DOMINANCE

Anthony Nanajian
Old Dominion University, 2021
Co-Directors: Dr. Stephen J. Beebe, Dr. Siqi Guo

Nanopulse treatment (NPT) is a high-power electric engineering modality that has been shown to be an effective local tumor treatment approach in multiple cancer models. Our previous studies on the orthotopic 4T1-luc breast cancer model demonstrated that NPT ablated local tumors. The treatment consequently conferred protection against a second live tumor challenge and minimized spontaneous metastasis. This study aims to understand how NPT mounts a potent immune response in a predominantly immunosuppressive tumor.

NPT changed the local and systemic dynamics of immunosuppressive cells by significantly reducing the numbers of regulatory T cells (Tregs), myeloid-derived suppressor cells (MDSCs), and tumor-associated macrophages (TAMs) that contribute to the dominant immunosuppressive environment in the 4T1-luc mouse breast cancer model. The Treg suppression capacity and activation markers, including 4-1BB and TGFβ, were diminished post-treatment, and the Treg activation profile shifted from a predominantly activated ($CD44^{+}CD62L^{-}$) to a naïve ($CD44^{-}CD62L^{+}$) profile. Furthermore, we observed an increase in apoptosis among Tregs and TAMs followed by a concomitant M1-macrophage polarization of the surviving TAMs. Meanwhile, a continuing rise in the effector T cell (Teff) / Treg ratio and among resident memory CD8 T cells hinted at the

expansion of antitumor specific cytotoxic T cells. Overall, these findings suggest that NPT is a potent tumor microenvironment (TME) modifier that can effectively reverse the tumor's immunosuppressive barrier by decreasing MDSCs, TAMs and functionally suppressive Tregs. Thus, the TME modification by NPT confers cytotoxic T cell function and immune memory formation contributing to the tumor challenge rejection and reduction in metastasis risk.

Future studies will investigate the underlying mechanisms of NPT-induced T cell immunity by determining the changes it creates among Treg and Teff T cell receptor (TCR) clonality in both mice and humans. Control studies on human blood indicated that peripheral Tregs are predominantly polyclonal in nature among healthy donors. Overall, these findings on NPT-induced immunity can help develop novel immunotherapeutic approaches to effectively treat poorly immunogenic cancers, such as breast and pancreatic cancers, that are largely resistant to current systemic immunotherapies.

This work is dedicated to my family Catharina Gräbe, Dr. Joanna Kogan, Joanna Nanajian, Dr. Haroutioun Nanajian and Eva Nanajian who supported me through the day-to-day challenges and without whom I could not have completed this degree. Thank you to the Gräbe family, Lee Kulas and my friends who stood by me throughout this journey.

ACKNOWLEDGEMENTS

I am very grateful to Dr. Stephen J. Beebe and Dr. Siqi Guo for providing me with the mentorship and support I needed to complete the PhD degree. It was an absolute privilege to have them as my advisors. I am especially grateful for the sense of independence and ownership of the project that I got to experience under their guidance. I would like to thank Dr. Christopher Osgood and Dr. Woong-Ki Kim on my committee for their support over the years and for making my completion of this degree possible. I am very grateful to Dr. Robert Wojtowicz for his tireless dedication to student advocacy and for getting me through the most challenging hurdles while completing the program. Thank you to Dr. Lesley Greene and Dr. Wayne Hynes for their support and guidance over the years. Thank you to Dr. Piotr Kraj for his expertise on Tregs and his much-needed help during the COVID-19 shutdown period. I am grateful to my current lab colleagues Megan Scott, Brittney Ruedlinger, Lucas Potter, Tatiana Zvonareva, Edwin Oshin for the daily teamwork and moral support, as well as to my former lab colleagues Raquel Judy, Joanna Kyriakidis and Lisa Merritt. I acknowledge my former advisors Dr. Emilia Oleszak and Dr. Chris Platsoucas. Thank you to Dr. Maisoun Bani Hani, Dr. Yu Jing and Dr. Lauren Browning for their guidance through some of the more complex lab techniques. Thank you to Dr. Nikolaos Zacharakis who is an expert in his field and taught me many of the lab techniques that I know today. Special thank you to Dr. Wassim Obeid and Dr. Anthony Asmar for their readily available advice (in science and beyond), and for being great friends over the years. Thank you to Dr. Ralph W. Stevens III and Dr. Lytton John Musselman who stood by my side ever since I first joined ODU. Thank you to everyone who helped at ODU Bioelectrics, EVMS flow facility, SoBran, Department of Biology, ODU Graduate school and at the College of Sciences.

NOMENCLATURE

APC	Antigen-presenting cells
CD	Cluster of differentiation
cDNA	Complimentary DNA
CDR3	Complementarity-determining region 3
CFSE	Carboxyfluorescein succinimidyl ester
dLN	Tumor-draining lymph node
FACS	Fluorescence-activated cell sorting
FOXP3	Forkhead box P3
irAE	Immune-related adverse event
IRE	Irreversible electroporation
MHC	Major histocompatibility complex
MDSC	Myeloid-derived suppressor cell
ND	Normal donor
NPT	Nanopulse treatment
nsEP	Nanosecond electric pulse
PCR	Polymerase chain reaction

RFA	Radio frequency ablation
TAA	Tumor-associated antigen
TAM	Tumor-associated macrophage
TCR	T cell receptor
Tconv, Teff	Conventional (or effector) $CD4^+$ T cell
TIL	Tumor infiltrating lymphocytes
TME	Tumor microenvironment
Treg	Regulatory T cell
Trm	Resident memory T-cells
TSA	Tumor specific antigen

TABLE OF CONTENTS

LIST OF TABLES

LIST OF FIGURES

CHAPTER 1

INTRODUCTION

1.1 Background on the tumor microenvironment and Tregs

The tumor microenvironment (TME) is a complex network of tumor cells, T cells, B cells, myeloid-derived suppressor cells (MDSCs), tumor-associated macrophages (TAMs), tumor-associated neutrophils, natural killer (NK) cells, dendritic cells (DCs), cancer-associated fibroblasts (CAFs), vascular endothelial cells, adipocytes, pericytes, as well as extracellular matrix (ie. collagen, fibronectin, hyaluronan, laminin) and signaling components (ie. cytokines, chemokines, exosomes). Among the cellular components, immunosuppressive cells, such as regulatory T cells (Tregs), MDSCs and TAMs play a critical role in suppressing antitumor immunity and promoting tumor growth (1,2).

1.1.1 Tregs

Tregs represent a small subset (5-10%) of the total circulating $CD4^+$ T cell population (3) and have an essential role in maintaining immune homeostasis and preventing autoimmunity (4). Their expression of CD4 and CD25 cell surface antigens and the Foxp3 transcription factor distinguishes them from the effector (or conventional) $CD4^+$ T cells (Teff) (5). Immune dysregulation polyendocrinopathy, enteropathy, X-linked (IPEX) is an uncontrolled systemic autoimmune condition that occurs in the absence of Tregs or when the Foxp3 locus is disrupted. This condition is lethal to patients and requires a bone marrow transplant (6). A ‘scurfy mutation’ in mice is the absence of Foxp3 expression through genetic deletion, which similarly manifests in autoimmune complications (6).

While Tregs represent around 10% of the total $CD4^+$ T cell population in healthy peripheral organs, their proportions are increased in the TME where they can constitute 30-50% of the total $CD4^+$ population (7,8). These TME Tregs are found to be functionally immunosuppressive via *in vitro* suppression assays, which are the 'gold standard' for confirming *bona fide* functional Tregs in tumors by measuring how intensely their presence suppresses effector T cell proliferation (9).

Treg presence in the TME diminishes antitumor immunity, and their immunosuppressive function is a dominant mechanism in the tumor cell evasion of immune responses (6,7). $CD4^+CD25^+$ Tregs in the tumor infiltrating lymphocytes (TIL) population isolated from cancer patients suppress autologous effector T cells in a cell-contact manner (PD-1, CTLA-4, 4-1BB) and by producing immunosuppressive cytokines TGFβ and IL-10 (4-6). These intratumoral Tregs mediate stronger suppression in comparison to Tregs isolated from peripheral blood mononuclear cells (PBMCs) (10,11). High frequencies of Tregs in the TME, affected lymph nodes and/or in the peripheral blood have been reported in a variety of human cancers (12,13), including lung cancer (14), liver cancer (15), head and neck cancer (16), lymphoma (17), breast cancer (18-20), ovarian cancer (21,22) and melanoma (5,6,23).

In multiple tumor types, including breast cancer, Treg presence in the TME worsens the prognosis and reduces patient survival (20,21,23,24), and a high intratumoral $CD8^+$ effector T cell to Treg ratio is associated with a favorable prognosis and better survival (8,13,23-26). Tregs' ability to suppress not only spontaneous T cell response, but also to hamper immunotherapeutic interventions aimed at inducing antitumor responses, makes them an attractive target for improving clinical outcomes in cancer patients (23).

1.1.2 MDSCs

MDSCs are a heterogeneous population of myeloid cells that can be identified by their expression of the Gr-1 and CD11b cell surface markers (27,28). MDSCs promote tumor progression via several mechanisms including immune suppression (29), particularly of T cells. MDSC immunosuppressive mechanisms include (27): a) ARG1-dependent depletion of L-arginine (30) and L-cysteine sequestration (31). This mechanism depletes CD3ζ chain (of the TCR complex, see **Fig. 1**) amino acids required for antigen-mediated T cell activation and proliferation (27). b) Disruption of T cell viability and trafficking via Galectin 9 and ADAM17 molecules expressed on MDSCs (32,33). Galectin 9 binds to TIM3 on lymphocytes to induce T cell apoptosis (33), while ADAM17 decreases the lymphocyte-expressed L-selectin and disrupts T cell recruitment in LNs (27,32,33). c) Treg activation and expansion with concomitant Tconv suppression (34), a process associated with the CD40-CD40L interaction, whereby CD40L is T cell-expressed and CD40 is MDSC-expressed. MDSC IL-10 and TGFβ cytokine secretion and PD-L1 expression further contribute to the above process (27,35,36). d) Generation of oxidative stress, which nitrates TCRs and limits their response to the MHC-antigen complex (27,37,38).

1.1.3 TAMs

TAMs can be classified as cytotoxic antitumor M1 macrophages ($CD206^-$ with high MHC-II expression) and immunosuppressive tumor-promoting M2 macrophages ($CD206^+$ with low MHC-II expression) (36,39,40). TAMs in breast cancer have been demonstrated to have an M2 phenotype in gene expression studies. (36,41-43). TAM polarization towards an M2 phenotype, via secreted molecules, has been observed in in basal-like

breast cancer (44) and in brain metastasis in breast cancer (36,45). TAMs in the 4T1 murine mammary cancer models and the MDA-MB-231 human breast cancer model demonstrate MHC-II downregulation (36,46). The presence of M1 TAMs in breast cancer, on the other hand, is associated with decreased cancer invasion and metastasis, and increased cancer cell apoptosis (36,47,48).

1.2 T cell antigen-specificity in cancer and its significance in current therapies

1.2.1 Tumor-infiltrating lymphocytes

The host immune system generally recognizes tumor cells as non-self and may initiate a cellular (**Fig. 1**) and/or humoral immune response to eliminate them (49). Human and animal tumors are infiltrated by lymphocytes known as tumor-infiltrating lymphocytes (TILs), primarily composed of $CD4^+$ and $CD8^+$ T cells, that may represent the host immune response to the tumor (49-51). TILs represent the immune response of the host to the tumor, and their presence in certain tumors has been associated with improved prognosis and higher survival (9,49-53). These TILs recognize autologous tumor cells in an antigen-specific manner (49).

1.2.2 Tumor vaccines and adoptive cell therapy

Tumor vaccine strategies initially relied on targeting tumor associated antigens (TAAs), such as HER2, MART-1, MUC1, and NY-ESO-1, which are self-antigens common to both the tumor and normal cells (54). Vaccines generated to the above TAAs conferred some degree of response, however, side effects were common (54). Current approaches are more focused on targeting neoantigens, a subset of tumor-specific antigens (TSAs) (54,55). Neoantigens are highly individual-specific, arise by somatic

mutations and, compared to TAAs, are more immunogenic as they are not expressed on normal tissue cells (55). Successful designs and applications of neoantigen vaccines in breast cancer and other cancers have been expanding rapidly (54,56). A current clinical trial (NCT03412877) at the National Cancer Institute actively recruits patients with incurable or metastatic cancers, including breast cancer, with the objective of treating them with neoantigen-reactive TCRs transduced into autologous peripheral lymphocytes (54,57).

Adoptive cell transfer of antigen-specific T cells is another method of "harnessing the immune system to combat cancer (58)". In adoptive cell transfer, antigen-specific T cells are isolated from cancer patients, expanded *ex vivo* then re-admitted to the patient in activated form to target and eliminate tumor cells (58). A clinical trial (NCT03970382) proposed by PACT Pharma Inc. utilizes autologous T cells engineered to express autologous TCRs reactive to unique patient-specific neoantigens (54).

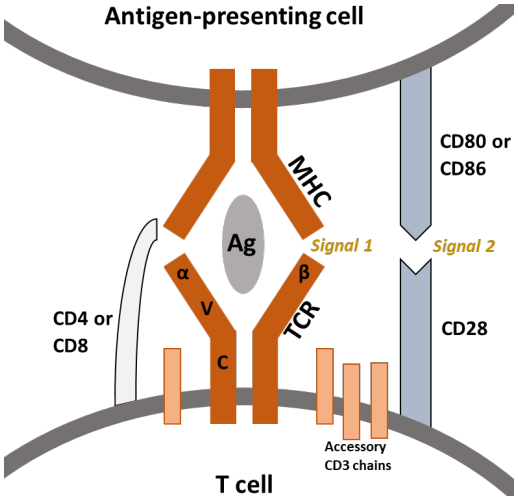

Figure 1.

Antigen-mediated T cell stimulation. The α and β chains of the TCR recognize the MHC-bound antigen on an APC, and the CD4 (or CD8) co-receptor molecule interacts with the MHC. These events (1st signal) stimulate the T cell through the accessory CD3 chains (γ, ε, δ, ζ).

Figure 1. *(Continued.)* Co-stimulation (2nd signal) is then delivered via the CD28-CD80/86 interaction. TCR α and β chains each have a constant (C) and variable (V) region. This figure was designed using Microsoft Word Office 365.

1.3 Targeting Tregs in cancer

In tumor immunity, Tregs become activated in tumor tissues and tumor-draining lymph nodes (dLN) by antigen recognition (59). These Tregs exhibit significant proliferative potential *in vivo* (9,59), and suppress effector T cell proliferation and cytokine secretion (59). In mouse studies, antigen-specific Tregs exhibit superior suppressive capacities when compared to non-antigen-specific Tregs (60). In order to understand how Tregs accumulate in tumors, a recent study demonstrated that the intratumoral Tregs and Tconv had distinct TCR repertoires (61).

Their findings suggested that circulating Tregs selectively migrate into the tumor where they are activated and undergo clonal expansion in an antigen-specific manner rather than in a non-specific polyclonal manner (61). The most dominant TCRs from these intratumoral Tregs had tumor- and neoantigen-specific reactivity (61).

Strategies aimed at evoking antitumor immunity may focus on better controlling the Treg-Tconv balance by tipping it away from the immunosuppressive Treg activity and towards an antitumor effector T cell response (59).

1.3.1 Immune checkpoint inhibitors

In addition to the TCR-antigen/MHC interaction (**Fig. 1**), antigen-mediated T cell activation and expansion require co-stimulatory cell surface signaling (62). This signaling process involves an interaction between co-stimulatory molecules, such as CD28, present on T cells with the CD80/CD86 molecules on APCs (**Fig. 1**) (35). Alternatively, T

cells can express cell surface co-inhibitory receptors, such as cytotoxic T-lymphocyte-associated antigen-4 (CTLA-4), which compete against CD28 and attenuate the T cell response (35).

Such immune checkpoints are required to prevent T cell autoreactivity and maintain immune homeostasis under physiological conditions (62). Tumor cells themselves may express inhibitory signaling molecules, such as CTLA-4, and influence the immune checkpoint pathway to obstruct the antitumor T cell response (35,62). The inhibitory interaction of the programmed cell death-1 (PD-1) receptor on T cells with the programmed cell death ligand 1/2 (PD-L1, PD-L2) expressed on tumor cells is another example of checkpoint pathway manipulation by the tumor (35,62). Tregs that are abundant in the TME also express immune checkpoint molecules, including PD-1, CTLA-4, that contribute to the contact-mediated immunosuppression.

Immune checkpoint inhibitors were developed to target these tumor-hijacked pathways with the hope of restoring normal T cell immunosurveillance and tumor clearance (6,35). Such immunotherapeutic approaches gained growing interest in 2010 when Ipilimumab, now an FDA-approved antibody targeting CTLA-4, demonstrated a 20% improvement in the overall survival of patients with metastatic melanoma (6,63,64). Nivolumab, an antibody targeting PD-1, was approved in 2014 after showing a 40% objective response rate in melanoma patients (6,65). And in 2018, the Nobel Prize in Medicine was awarded for the checkpoint inhibitor immunotherapy (35,66). Unfortunately, the presence of suppressor cells such as Tregs, MDSCs and TAMs, coupled with few pre-existing TILs, in low immunogenic tumors prevents widespread applicability of checkpoint inhibitors and leaves many patients unresponsive to the treatments (9,35).

Ipilimumab and tremelimumab, both anti-CTLA therapies, were tested in breast cancer with limited efficacy (62,67,68). Triple Negative Breast Cancer (TNBC) is an example of a genetically unstable malignancy that demonstrates a limited response to checkpoint inhibitor immunotherapy (35,69,70). Significant variations in patient treatment responses are even seen within the same cancer type, such as in advanced ER^+ breast cancer (35,71,72). Furthermore, these systemic therapies carry the risk of toxic and severe adverse effects, including severe immune-related adverse events (irAEs) (73,74).

1.3.2 Manipulating Treg chemokine-mediated recruitment to the tumor

Chemokine ligands (CCL, CXCL) secreted by the TME promote the recruitment of chemokine receptor-expressing (CCR, CXCR) Tregs in various tumor types (75,76). CCL22 is reported to attract $CCR4^+$ Tregs to the TME in breast cancer (75,76). Other chemokines and their corresponding receptor in various types of tumors include CCR8 (77) and CCR5-CCL5 in pancreatic cancer (75,78) , and CCR4-CCL22, CCR10-CCL28, and CXCR4-CXCL12 in ovarian cancer (75,79).

Chemotaxis-blocking antibodies or small molecules have been used to reduce Treg accumulation in tumors (75), which in turn, increases antitumor immunity (80). CCR4 is a key marker used in the specific depletion of Tregs. The use of anti-CCR4 therapy has been shown to simultaneously deplete Tregs and increase $CD4^+$ and $CD8^+$ T cells (and their activation (79,81). Activated human Tregs have a high CCR4 expression, unlike naïve Tregs or most effector T cells (80,82). Mogamulizumab, an anti-CCR4 mAb has been implemented in clinical trials to evoke antitumor immunity by selectively depleting activated Tregs (80,83). The drug was shown to significantly reduce activated Treg cells in the peripheral blood patients with advanced or recurrent solid tumors (80,83).

1.3.3 Treg reprogramming

While some studies show the pro-tumorigenic effects of Th17 cells, recent advances in immunotherapy have demonstrated strong antitumor effects and clinical benefits in tipping the Treg/Th17 axis towards a Th17 profile (84). Though the Th17 antitumor mechanism is not yet clear, studies suggest Th17 cells may exert their mechanism through direct tumor lysis or CD8 cell synergism (84). Furthermore, Th17 cells have demonstrated apoptosis and activation-induced cell death (AICD) resistance and a strong ability to retain antitumor efficacy when compared to Th1 cells (84).

1.3.4 Manipulating antigen-specific Tregs in cancer

Analyzing the *in vivo* Treg TCR distribution is critical to determine Treg antigen-specificity in cancer (and autoimmune disease) patients given Tregs' ability to obstruct not only spontaneous immunity, but also immunotherapeutic interventions. Many tumor antigen-based vaccines intended to bolster antigen-specific immunity have been demonstrated to counterproductively elicit Treg immunosuppressive response (85). In a study on mice, an immunization course lead to *in vivo* expansion of Tregs that were demonstrated to efficiently suppress the expansion and function of activated T cells (85). In another study, antigen-specific Tregs were shown to be induced after vaccinating melanoma patients with cancer-testis antigen NY-ESO-1 (86). Following patient vaccination, tumor digests analyzed by flow cytometry –prior to culture– revealed Tregs constituted 41% of the total $CD4^+$ population in the tumor site, a value 10-fold greater than Treg representation in blood (86). TILs were then cultured in IL-2 and stimulated with antigenic peptides NY-ESO-$1_{85\text{-}102}$ and NY-ESO-$1_{115\text{-}132}$ (86). No significant response was reported for NY-ESO-$1_{85\text{-}102}$. Whereas with NY-ESO-$1_{115\text{-}132}$, both effector T cells and

Tregs, within the expanded TIL population, exhibited antigen-specific response determined by CD3 downregulation (86). The Treg response to this peptide was ~4-fold greater than that of effector T cells, with more than 40% of Tregs exhibiting CD3 downregulation (86).

Determining the tumor antigen recognition patterns of Tregs (60,87) will therefore permit new considerations to be taken into account when selecting for the optimal tumor antigen for vaccine development (49). It will be critical to select for tumor antigen peptides that stimulate an exclusively effector T cell, without inadvertently inducing a concomitant Treg response (85). More recently, the Treg and Tconv TCR repertoires have been found to be distinct with minimal overlap (61), and tumor vaccine strategies now favor targeting neoantigens over TAAs (54). These recent findings and advances have positive implications for improving the efficacy of tumor vaccine designs.

1.4 Nanopulse treatment and other local cancer therapies

Targeting intratumoral Tregs locally, whether by downregulating activated Tregs or inducing Treg cell death, may help reverse the imbalance between immunosuppression and immunostimulation, and avoid toxic systemic effects (88). However, this idea has not been studied as extensively as systemic approaches.

1.4.1 Local tumor ablation therapies

Local tumor ablation therapies have the potential to treat tumors with fewer severe side effects. Irreversible electroporation (IRE), electrochemotherapy, cryoablation, laser ablation, radio frequency ablation (RFA), and radiotherapy (RT) are some examples of such ablation therapies (89,90). Unfortunately, these therapies either cannot generate an

effective antitumor immunity, or they require additional treatment with immune-modulators such as the addition of immune checkpoint inhibitors (PD-1 inhibition) or antitumor cytokines (IL-15) (89). Radiotherapy combination treatments show promising antitumor response (90). However, radiotherapy alone has been shown to increase Tregs in the TME, and it requires the combined use of immunomodulators and other systemic therapies in order to reduce Treg number and effectively treat tumors (90).

1.4.2 Nanopulse treatment of tumors

Nanopulse Treatment (NPT), also known as Nanopulse Stimulation (NPS) or nanosecond electric pulses/pulsed electric fields (nsEPs/nsPEFs), is a high-power electric engineering technology that generates an ultra-short (pulse durations 1 to 999 nanosecond) and high intensity (electric fields 5 to 68 kV/cm) electrical pulses to ablate tumors in multiple animal models, including mouse melanoma, breast cancer, pancreatic cancer, lung squamous cell carcinoma, rat hepatocellular carcinoma, xenograft pancreatic cancer, etc. (89,91,92). Unlike many systemic immunotherapies and chemotherapy, which are often long-term treatments associated with many serious side effects, NPT is minimally invasive and only requires short (5-7 minute) intervals when the tumor is covered within the electrode array (91).

1.4.3 Investigating the impact of NPT on Tregs and other immunosuppressive cells in breast cancer

In our previous study, NPT ablated primary breast tumors in a poorly immunogenic breast cancer model (orthotopic mouse 4T1-luc). The treatment resulted in a strong vaccine effect that rejected 100% (11/11) of live secondary tumor challenges and significantly reduced spontaneous metastasis by 83% (from 82% to 14%) (92). The 4T1

tumor model is a very aggressive and spontaneously metastatic malignancy with abundant immune suppressive cells, including Tregs, TAMs and MDSCs in the TME (93,94). Successful treatments of the above model and the Pan02 pancreatic cancer model also showed a reduction in intratumoral and blood Tregs several days after NPT (89).

However, we still do not know the underlying mechanism of the NPT impact on Tregs and other immunosuppressive cells. Investigating the NPT-associated changes in Treg, MDSC and TAM dynamics may further clarify the treatment's antitumor effect. Elucidating the mechanisms impacted by NPT may help develop novel immunotherapeutic approaches to effectively treat poorly immunogenic cancers like breast cancer.

Tumors contain Treg infiltrates that have accumulated and become activated to create a barrier to the tumor-eliminating immune response. I hypothesize that NPT of mouse breast cancer induces Treg cell death and reduces their functional capacity to diminish the immunosuppressive barriers. To test my hypothesis, I characterized NPT-induced local and systemic changes in immune profiles, particularly among Tregs.

In this study, I showed that NPT altered Treg phenotypic dynamics and reduced their suppressive capacity by diminishing activated Tregs and inducing Treg cell death, thus releasing a major immunosuppressive brake. MDSCs and TAMs were also dramatically reduced in the TME but exhibited distinct dynamics and cell death changes following NPT. Conventional CD4 T cells (Tconv) were more resilient to NPT-induced apoptosis compared to Treg, CD8 T cells were preserved, and CD8 resident memory

cells (Trm) significantly increased over time post-NPT**.** An investigation of the Treg signaling and functional changes post-treatment demonstrated that NPT is quite adept at bringing down the immunosuppressive barrier.

CHAPTER 2

METHODS

2.1 Mouse Nanopulse treatment studies

2.1.1 Mice

Female Balb/c mice (8–10 weeks of age) were purchased from Jackson Laboratory. The mice were housed and maintained at the ODU AAALAC approved animal facility. All animal procedures in this study were approved by the IACUC (protocol 18-008) at Old Dominion University.

2.1.2 *In vivo* Nanopulse treatment

Tumors were initiated by subcutaneously injecting female Balb/c mice with $1x10^6$ 4T1-luc cells in 50 µL DPBS (Life Technologies) in the left posterior mammary fat pad. NPT was performed on Day 11 following tumor inoculation when average tumor sizes were 6-8 mm or 60-100 mm^3. Prior to treatment, hair was thoroughly removed. The tumor mass and electrodes were covered with ultrasound gel to maintain uninterrupted tumor-electrode contact and prevent air accumulation that creates electrical breakdowns. I delivered the high-voltage pulses (**Fig. 2**) making sure only the tumor mass receives treatment. Nanosecond electric pulses were delivered to the tumor tissue using a two-plate pinch electrode with an 8 mm diameter. The NPT parameters were: pulse duration 100 ns with fast rise-fall times, pulse frequency 3 Hz, applied electric field 50 kV/cm and a pulse number of 1000 pulses. Depending on the experimental design, mice were euthanized 4 hours (4hr), 8 hours (8hr), Day 1, Day 3, and Day 7 post-treatment (**Fig. 3**).

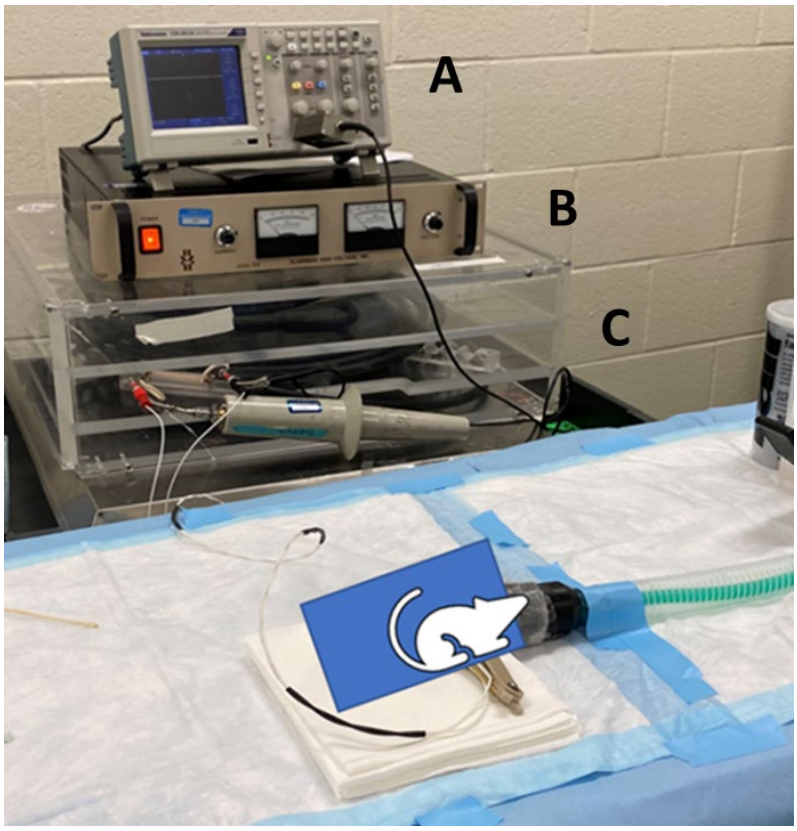

Figure 2.

Nanopulse treatment pulser setup. **A-C,** Components of the NPT pulser include the oscilloscope **(A)**, power supplier **(B)** and fixed 100 ns Nanopulser **(C)**. High-power ultra-short pulses are delivered to the mouse breast tumor via a pinch electrode covering the entire tumor mass.

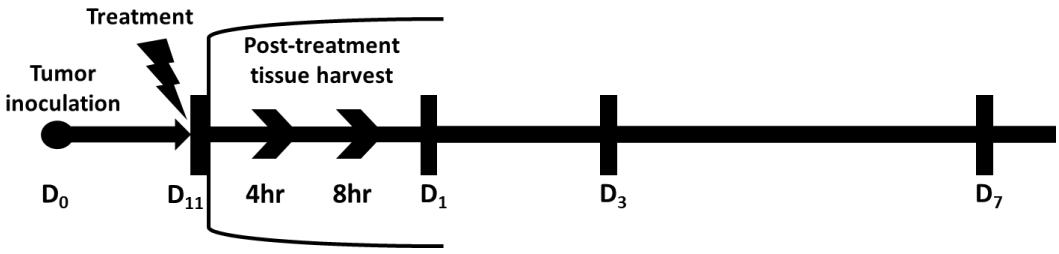

Figure 3.

In vivo NPT experimental design. $1x10^6$ 4T1-luc cells were injected subcutaneously into the posterior part of the mammary fat pad. The control group (n=4) received the tumor inoculation only.

Figure 3. *(Continued.)* The remaining mice underwent NPT (100 ns pulses, 50 kV/cm, 1-3 Hz, 1000 pulses) on Day 11 following tumor inoculation. The treated mice were euthanized 4 hours, 8 hours (for local tissues only), and on Day 1, Day 3, and Day 7 post-NPT. Their tumor tissues, tumor-draining lymph nodes (dLN), blood and spleens were harvested. Control tissues were obtained from mice with untreated tumors. Single cell suspensions from each tissue were prepared.

2.1.3 Preparation for single cell suspensions

The primary solid tumor (**Fig. 4**), dLN, blood and spleen were collected and prepared into single cell suspensions for downstream analysis. Spleen and dLN were gently mashed through a 70 μm cell strainer into a conical tube. The dissociated spleen and the blood underwent RBC lysis to make cell suspensions for further analysis. For solid tumor processing, fat and other surrounding tissues were removed and the tumor samples were washed with RPMI 1640 (Life Technologies) and cut into 1-5 mm^3 pieces. The cut pieces were then dissociated with the Miltenyi Biotec tumor dissociation kit and the Gentlemacs Octo-dissociator (with heater) using the tough tumor dissociation protocol. The digest was then passed through a 70 μm cell strainer to remove clumps. Tumor single cell suspensions then underwent magnetic bead based CD45 TIL isolation (Miltenyi Biotec) to obtain $CD45^+$ cells for downstream flow cytometric analysis.

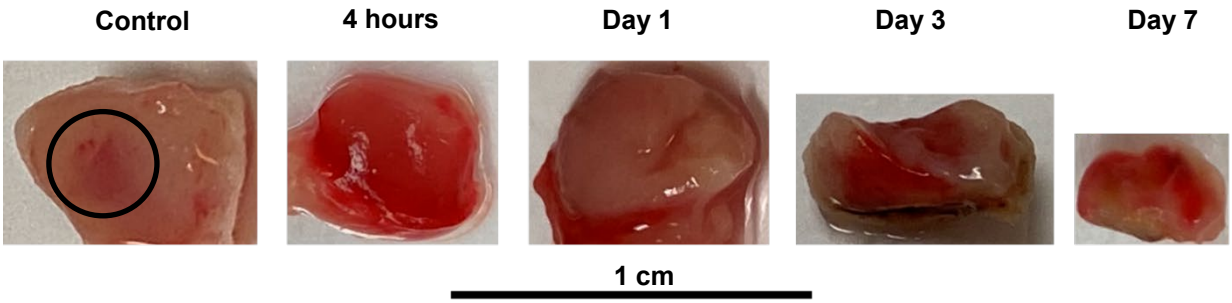

Figure 4.

Changes in 4T1-luc solid tumor morphology following NPT. Breast cancer tumors were surgically resected on post-inoculation Day 11 from tumor-bearing mice (control) and from NPT-mice at 4 hours, Day 1, Day 3, Day 7 post-treatment timepoints.

2.1.4 Flow Cytometry

To perform cell surface staining, cells were washed with FACS buffer then incubated with anti-FcR (TruStain FcX™ PLUS, Biolegend) for 10 min on ice to block unspecific binding of antibodies. The following fluorochrome-labeled antibodies were used for Treg, MDSC and TAM labelling: CD4 FITC, CD8 APC/Cy7, CD3 BV510, CD25 APC, CTLA-4 PerCP/Cy5.5, PD-1 PE/Cy7, CCR4 BV421, 4-1BB APC, TGFβ BV421, CD45 Pacific Blue, CD11b PE, Gr-1 PE/Cy7, F4/80 FITC, and CD86 APC/Cy7. All cell surface antibodies were purchased from Biolegend.

For intracellular and intranuclear staining, single cell suspensions were first labelled with cell surface antibodies, followed by fixation and permeabilization using the Foxp3 transcription factor buffer set (Thermofisher Scientific). Permeabilized cells were then labelled with Foxp3 PE, Helios PerCP/Cy5.5, IL-17 PE/Cy7, RORγt PerCP-Cy5.5 and/or IFN-γ PerCP-Cy5.5 primary antibodies (Thermofisher Scientific). Cytokine staining using the above buffer and cytokine antibodies from Thermofisher Scientific was verified

with the company's in-house data as well as our own experimental data. This technique allowed us to co-stain for Foxp3, RORγt, IL-17 and IFN-γ in the same panel to investigate for reprogramming.

For cell apoptosis studies, cells were labelled with Zombie NIR and Annexin V (Biolegend). Due to the sensitivity of the phosphatidylserine bond (for Annexin V binding) to the fixation/permeabilization process (for Foxp3 analysis), I did not incorporate Annexin V and Foxp3 co-staining in the same panel. To perform the cell apoptosis studies, freshly obtained single cell suspensions were first labelled with Zombie NIR using a serum-free PBS buffer. Cells were then washed with FACS buffer to perform cell surface staining. The labelled cells were then washed and resuspended in Annexin V binding buffer, stained with Annexin V, and immediately acquired by flow cytometry.

Stained cells were analyzed on a MACSQuant 10 Analyzer, BD FACS Calibur and BD FACS Canto II at Old Dominion University and Eastern Virginia Medical School. The acquired data was analyzed using FlowJo software (**Fig. 5** and **6**).

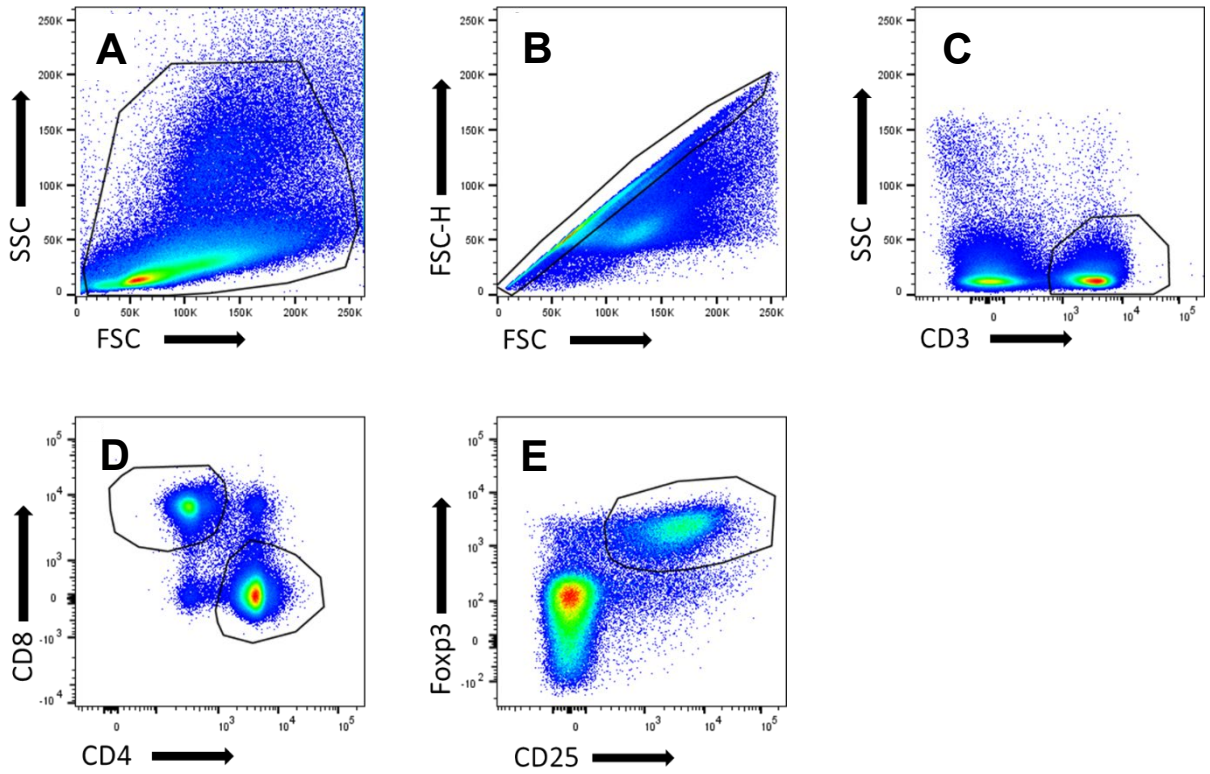

Figure 5.

CD25⁺Foxp3⁺ Treg gating strategy. **A-E,** Summary flow plots representing the Treg gating strategy. **A,** Single cell suspensions from the dLN of 4t1-luc tumor-bearing mice were gated on the forward scatter (FSC) vs side scatter (SSC) dot plot to select lymphocytes. **B,** Lymphocytes were then gated on the FSC-Height vs FSC axis to eliminate doublets. **C** and **D,** CD3 cells were selected **(C)** and gated on the CD4 vs CD8 axis to separate CD4-single positive and CD8-single positive T cells **(D)**. **E,** CD4-single positive T cells were then gated on the CD25 vs Foxp3 axis to select CD25⁺Foxp3⁺ Tregs.

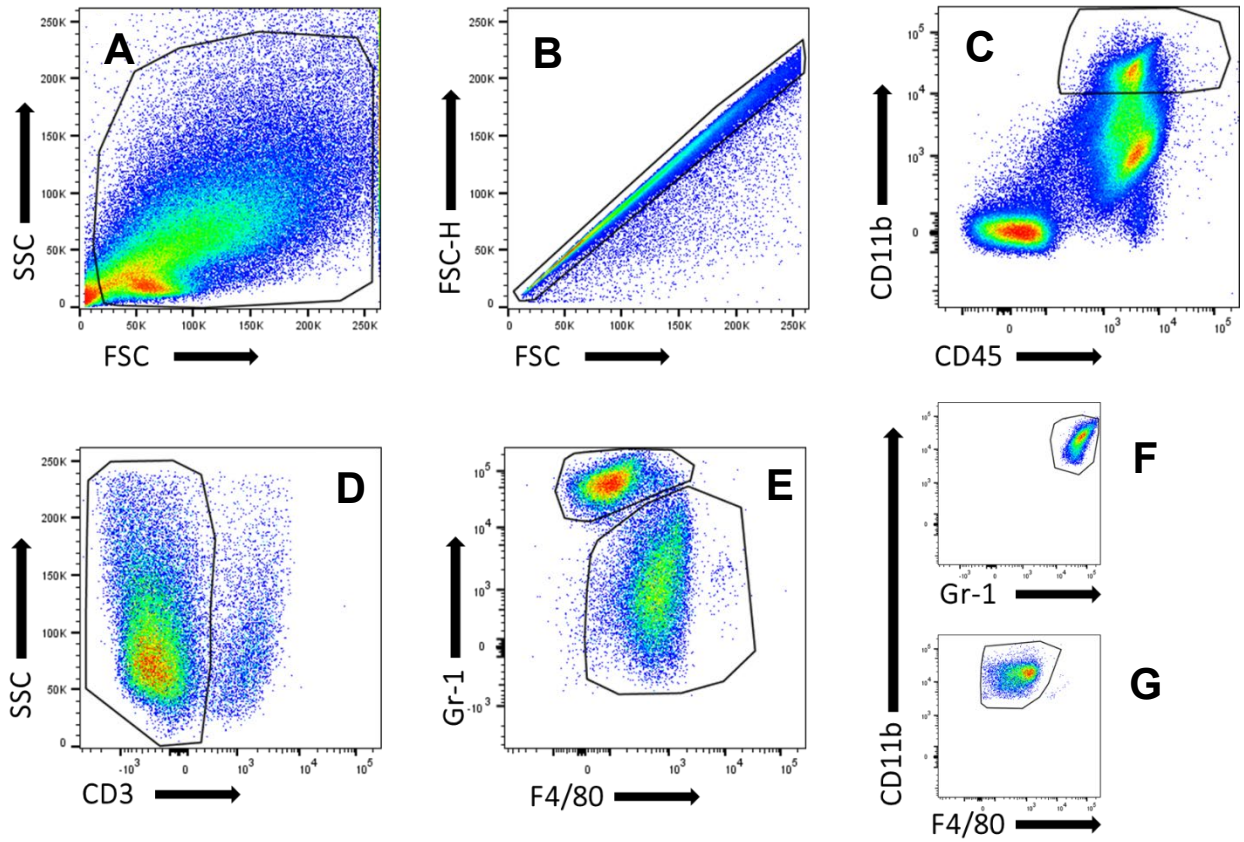

Figure 6.

MDSC and TAM gating strategy. **A-G,** Summary flow plots representing the MDSC gating strategy. **A,** Single cell suspensions from surgically resected tumors of 4t1-luc tumor-bearing mice were gated on the forward scatter (FSC) vs side scatter (SSC) dot plot to select lymphocytes. **B,** Lymphocytes were then gated on the FSC-Height vs FSC axis to eliminate doublets. **C,** $CD45^+$ $CD11b^+$ leukocytes were selected. **D,** $CD3^+$ cells were excluded (negative selected). **E,** The remaining $CD3^-$ T cells were then gated on the Gr-1 vs F4/80 axis to separate MDSCs and TAMs. **F,** $Gr\text{-}1^+F4/80^-$ cells were subgated on the Gr-1 vs CD11b axis to identify $Gr\text{-}1^+CD11b^+$ MDSCs. **G,** $F4/80^+Gr\text{-}1^-$ cells were subgated on the Gr-1 vs CD11b axis to identify $F4/80^+CD11b^+$ TAMs.

2.1.5 *In vitro* Treg suppression assay

$CD4^+CD25^+$ Tregs were isolated from dLN of tumor-bearing mice and NPT-treated mice on post-treatment Day 2. To obtain a sufficient number of Tregs, dLN from 2-3 mice were pooled together for each group. Spleen-derived CD8 responder (Tresp) cells were isolated from naïve mice by negative selection using magnetic beads (Stemcell Technologies). Purified responder cells were labelled with 5 μM CFSE (ThermoFisher Scientific) and plated in a 96-well round-bottom plate at a density of 4×10^4 responder cells per well. $CD4^+CD25^+$ Tregs were co-incubated with CFSE-labelled responder cells at the Treg:Tresp ratios 1:1, 1:2 and 1:4. The plates were incubated at 37°C with 5% CO_2 for 60 hours in the presence of CD3/CD28 activation beads (ThermoFisher Scientific). Responder cell proliferation was quantified by flow cytometry based on the dilution of the CFSE dye. Treg suppression was calculated in the following manner: %Suppression = [1-(%proliferating Tresp at Treg:Tresp ratio / %proliferating Tresp-only cells)] x100.

2.1.6 Statistical Analysis

P-values were generated using one-way ANOVA with a minimum of n=3. P-values <0.05 were considered to be statistically significant.

2.2 Human TCR studies

2.2.1 Isolation of mononuclear cells from human peripheral blood using density gradient centrifugation

100 mL of freshly drawn blood was shipped on ice overnight and sample processing was initiated immediately upon arrival. 50 mL of blood was diluted 2x by adding 100 mL of Calcium-free, Magnesium-free PBS buffer (Miltenyi Biotec). The total

150 mL blood-buffer solution was divided equally among five conical tubes for density gradient centrifugation:

15 mL of Ficoll-Paque (GE Healthcare) was added to each (of five) 50 mL conical tubes. 30 mL (from a total of 150 mL) of diluted blood-buffer suspension was carefully layered, drop-by-drop, over the Ficoll layer, making sure not to disrupt the Ficoll cushion in the process.

The conical tubes were centrifuged at 400xg for 35 minutes at 18°C in a swinging bucket rotor. Brakes were disabled; acceleration set to low. The plasma layer was aspirated leaving the mononuclear cell Buffy coat (lymphocytes, monocytes, thrombocytes) undisturbed at the interphase. The buffy coat layers were then extracted and combined in a new 50 mL conical tube. Up to 5 mL of the buffy coat content was placed in the new tube (to allow for 10X dilution with PBS buffer).

Each conical tube was then topped with fresh PBS buffer (for a total of 50 mL; 10x dilution) and centrifuged at 300xg for 10 minutes at 18°C. Brakes were enabled; normal acceleration. The cell pellet was then washed twice with PBS at 200xg for 10 minutes to thoroughly remove platelets that can interfere with the purification process. After the final wash, the cell pellet was resuspended in 15 mL Microbead buffer (Calcium-free, Magnesium-free PBS supplemented with 0.5% FBS and 2 mM EDTA) to prepare for the $CD4^+$ cell microbead enrichment step.

2.2.2 $CD4^+$ T cell microbead-based enrichment

To perform $CD4^+$ T cell enrichment, microbead-bound antibodies (Miltenyi Biotec) against CD8, CD14, CD15, CD16, CD19, CD36, CD56, CD123, TCRγ/δ and CD235a

were used to label non-$CD4^+$ peripheral blood cells. These antibody-labelled non-CD4 peripheral blood cells were then run through the microbead column, causing them to bind, while the unlabeled $CD4^+$ cell-enriched effluent was collected and prepared for automated cell sorting. The non-$CD4^+$ cells bound to the column were discarded.

2.2.3 Fluorescence-antibody tagging of enriched $CD4^+$ T cells

A cell count was performed, and the enriched $CD4^+$ cells were washed twice with ice cold PBS at 300xg for 7 minutes at 4°C. After the final wash, the pellet was vortexed and resuspended in the ~50 µL leftover buffer. For FACS sorting, the cells were labelled using the following dyes: eBioscience CD4 eFluor 450, CD25 APC and CD127 PE. 35 µL of each dye was added to the cells. The tube was incubated for 30 minutes on ice, in the dark.

Five tubes were prepared for sorting: Tube 1 contained the enriched $CD4^+$ cells that were labeled with all three dyes. To setup dye controls, three separate single stain PBMC controls were prepared: Tube 2 CD4 eFluor 450, Tube 3 CD4 APC, Tube 4 CD4 PE. An unstained PBMC control (Tube 5) was also prepared. Following incubation, cells were washed twice in PBS, filtered, and placed in a 15 mL FBS pre-coated polypropylene tube to prepare for cell sorting.

2.2.4 Regulatory T cell isolation using multicolor FACS sorting

The following gating strategy was setup to isolate $CD4^+CD25^+$CD127lo Tregs:

1) FSC-A vs SSC-A gate to identify live lymphocytes
2) FSC-A vs FSC-Peak gating to exclude doublets
3) Singlets were gated for $CD4^+$ T cells

4) The $CD4^+$ T cell subset was then gated for $CD25^+$ and CD127lo Tregs

Cell sorting was performed to obtain the $CD4^+CD25^+$CD127lo pure Treg population (positive faction). A post-sort FACS purity analysis was then performed on a fraction (>20,000 cells) of the obtained Tregs. A negative fraction containing non-Treg $CD4^+$ T cells was also obtained and analyzed post sorting.

2.2.5 RNA Isolation

Both, the purified Treg population and the non-Treg $CD4^+$ T cells, were immediately resuspended in Trizol solution (Life Technologies) and placed in -80°C for RNA precipitation.

2.2.6 cDNA synthesis

RNA was extracted and purified using the PureLink Mini Kit (Life technologies). RNA was then reverse transcribed using the Superscript III RT kit (Life Technologies). The reverse transcribed cDNA product was divided into three batches for the following downstream applications. Batch 1: analysis of Treg FOXP3 expression. Batch 2: amplification of alpha-chain Treg TCR. Batch 3: amplification of beta-chain Treg TCR.

2.2.7 PCR amplifications

2.2.7.1 Semi-quantitative PCR analysis of FOXP3 expression among the purified Treg population

To assess FOXP3 expression in the purified $CD4^+CD25^+$CD127lo cells, cDNA (from Batch 1) was used to set up a PCR reaction and assess the expression of actin (housekeeping gene), CD4 and FOXP3. A similar PCR reaction was setup using the non-Treg $CD4^+$ T cells (negative fraction).

2.2.7.2 Amplification of Treg TCR transcripts using two rounds of nested family-specific PCRs

The remaining reverse transcribed Treg cDNA products were used for two rounds of TCR chain PCR amplifications.

2.2.7.2a First PCR reaction

To amplify each of the 32 α-chain (Batch 2 cDNA) TCR transcript families, 32 PCR reactions were prepared, each containing the hCα3 primer (5`CTGGATTTAGGTCTCTCAGCTGGTAC3`) as the 3` Constant (C) region primer, and one of the thirty-two 5` Variable (V) region α-chain family primers (detailed in Xu et al. 2003) (95).

A similar process was employed to amplify each of the 24 β-chain (Batch 3 cDNA) TCR transcript families using the hCβ3 (5`CAGGCAGTATCTGGAGTCATTGA3`) as the 3` primer C-region primer and each of twenty-four 5` V-region β-chain family primers (detailed in Sakkas et al. 2002) (96).

2.2.7.2b Second PCR reaction

The amplified products from the first PCR reaction were used to perform a second nested PCR reaction using the hCα1 (GTTGCTCCAGGCCACAGCACTG) primer to amplify the 3` C region and each of the family specific α-chain primers to amplify the 5` V region. For the beta-chain, the hCβ1 (CAGGCAGTATCTGGAGTCATTG) primer was used for the 3` C region, along with each of the 24 β-chain family primers to amplify the 5` V region.

2.2.8 Cloning and sequencing

Amplified samples were then separated by base pair size using agarose gel electrophoresis. The gel bands were visualized using ethidium bromide under UV light, followed by excision of the bands containing the desired amplified DNA sequences. Next the Purelink Quick Gel Extraction Kit (Invitrogen) was used to purify and recover DNA fragments from the agarose gel bands. The purified PCR product was then ligated into the pCR 2.1-TOPO vector (Invitrogen TOPO TA Cloning kit). Ligated plasmid vector containing our desired PCR insert was then transformed into One Shot chemically competent E. coli cells (Invitrogen) via heat-shock, followed by a 1 hour incubation of the transformed cells in SOC medium on a shaker at 37°C.

E. coli doubling time is 20 minutes under ideal conditions (97); however, the heat shock stress should prevent E. coli from duplicating during this 1 hour incubation period. Though unlikely, duplication may occur before plating, resulting in two E. coli cell colonies carrying the same insert. The result would be 2 identical CDR3 sequences that have originated from premature bacterial doubling rather than from *in vivo* T cell clonal expansion.

After the 1 hour incubation period, the E. coli bacteria were spread on agar plates containing X-Gal and ampicillin, then incubated at 37°C overnight. The TOPO vector containing an ampicillin resistance gene confers ampicillin antibiotic resistance upon, and allows growth of, successfully transformed E. coli cells. The TOPO vector also contains the *lacZa* gene at the insertion site for the PCR products. The *lacZa* gene encodes β-galactosidase enzyme, which breaks down X-Gal in the culture plate to create blue colonies. Successful insertion of PCR product into the vector, on the other hand, would

disrupt the *lacZa* gene, thus creating white colonies. Following overnight incubation at 37°C, blue/white screening was performed to identify and pick successfully transformed white E. coli colonies containing the PCR product.

Picked colonies were cultured in separate Falcon tubes containing Luria-Bertani broth suplemented with ampicillin. The tubes were incubated overnight at 37°C to allow for bacterial multiplication and cloning of the inserted PCR product. Next, the plasmid was prepared using the Promega Wizard Plus Minipreps DNA Purification System. E. coli cells were lysed, and the plasmids were isolated, purified and stored in nuclease-free water.

The isolated plasmids containing the amplified TCR transcripts were then prepared for sequencing. Dideoxy chain termination sequencing PCR using BigDye Terminator v3.1 Cycle Sequencing kit was carried out. The sequencing PCR products were purified using microspin columns followed by vacuum drying and resuspension in Hi-Di formamide. The resuspended products were loaded onto a 96-well plate and TCR transcripts were read by an automated sequence analyzer. The manufacturer's software provided raw nucleotide sequence data, which were analyzed using the IMGT online software (imgt.org).

V(D)J regions were analyzed to determine the presence of CDR3 nucleotide sequences for each of the α- and β- chain TCR transcripts expressed on the Tregs. The corresponding amino acid sequences for each TCR transcript were derived through the ExPASy proteomics website (expasy.org). Treg TCR transcript sequences were analyzed for clonal expansion.

CHAPTER 3

RESULTS

3.1 Overturning the immunosuppressor cell dominance in the TME following NPT

3.1.1 NPT-induced shift from a Treg- to a Tconv-dominant environment

I evaluated Treg prevalence among CD4 T cells in systemic and local tissues (**Fig. 7**), including the blood (**Fig. 7A** and **B**), spleen (**Fig. 7C**), dLN (**Fig. 7D** and **E**), and tumor (**Fig. 7F** and **G**) tissues. In untreated mice, I found the Treg percentage among CD4 T cells was 18.6% in blood (**Fig. 7B**), 23.8% in spleen (**Fig. 7C**), 20.6% in dLN (**Fig. 7D**), and 49.5% in tumor tissues (**Fig. 7F**). After 4T1-luc tumor-bearing mice were treated with 100 ns NPT, I observed a significant and sustained drop in this Treg prevalence. Tregs were noted to decrease post-treatment by 52.1% in the tumor (4 hour) (**Fig. 7F**), 42.2% in the dLN (Day 3) (**Fig. 7D**), 52.3% in the blood (Day 3) (**Fig. 7B**) and 19.7% in the spleen (Day 7) (**Fig. 7C**).

Total TIL numbers were found to decrease rapidly following treatment (**Fig. 8A**). Following NPT, the Treg cell count underwent a 4.4-fold reduction by 4 hours and an 8.1-fold reduction by Day 3 from its untreated intratumoral baseline (**Fig. 7G**). Tconv, in contrast, only experienced a 1.4-fold reduction by 4 hours and a 2.3-fold reduction from baseline by Day 3 post-treatment. This occurrence shifted the ratio of intratumoral Treg vs Tconv from 1:1 in untreated tumors, to 1:3 by 4 hours, and 2:7 by Day 3 post-treatment (**Fig. 7G**).

While the observed intratumoral Treg reduction is favorable for cancer treatment outcomes, the resulting low post-treatment Treg count (**Fig. 8B**) makes it challenging to

study the treatment impact on their phenotypic dynamics. To address this challenge, I used dLN, spleen, and blood tissues to better explore these dynamics. I found that the percentage of Tregs among CD4 cells significantly decreased (**Fig. 7B** and **D**) and the CD4 Tconv:Treg ratio increased in the dLN (**Fig. 7E**) following NPT. These changes were seen rapidly (by 4 hours) in the local tumor and dLN (**Fig. 7D** and **F**) and in the blood (by Day 1) (**Fig. 7B**). On the other hand, the spleen, which is used to assess long-term changes in immunity, demonstrated a significant reduction in Tregs by Day 3 post-treatment and maintained its status at Day 7 post-treatment (**Fig. 7C**).

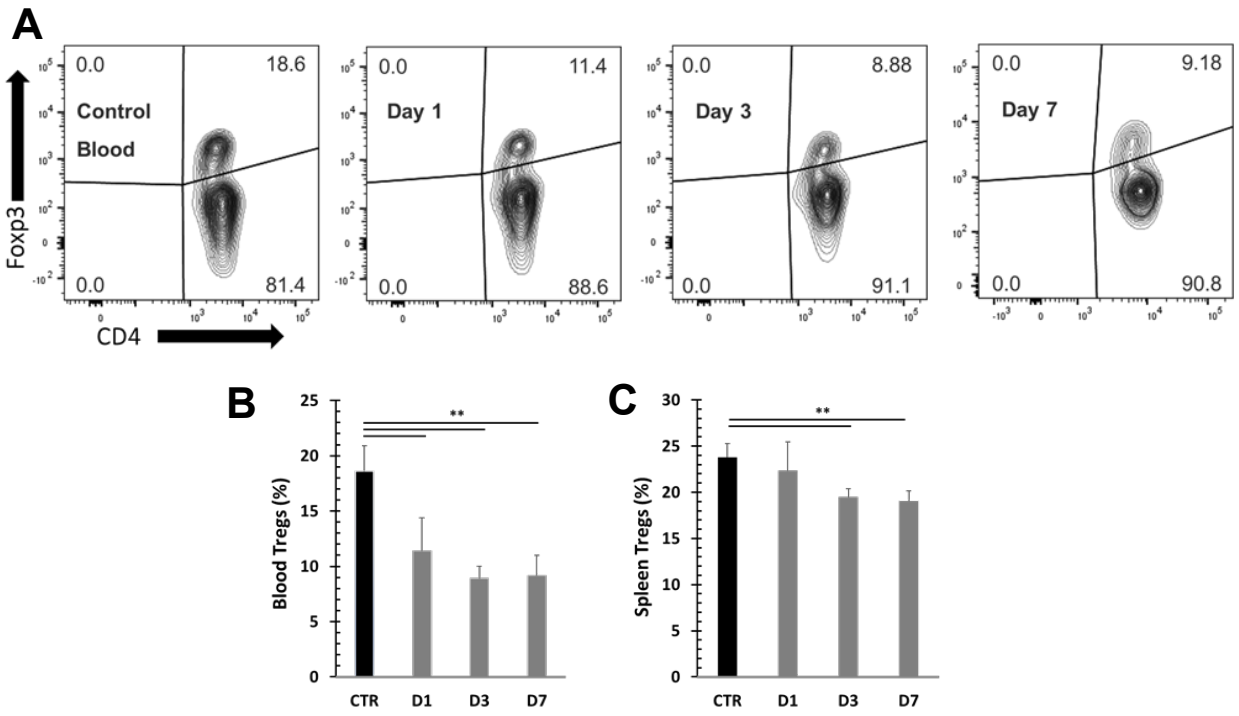

Figure 7.

Treg frequency is reduced in local and systemic tissues following NPT. **A,** Summary flow plots represent Foxp3^{+} Tregs and Foxp3^{-} Tconv among the total CD4^{+} T cell population in the blood. The control group received the tumor inoculation only.

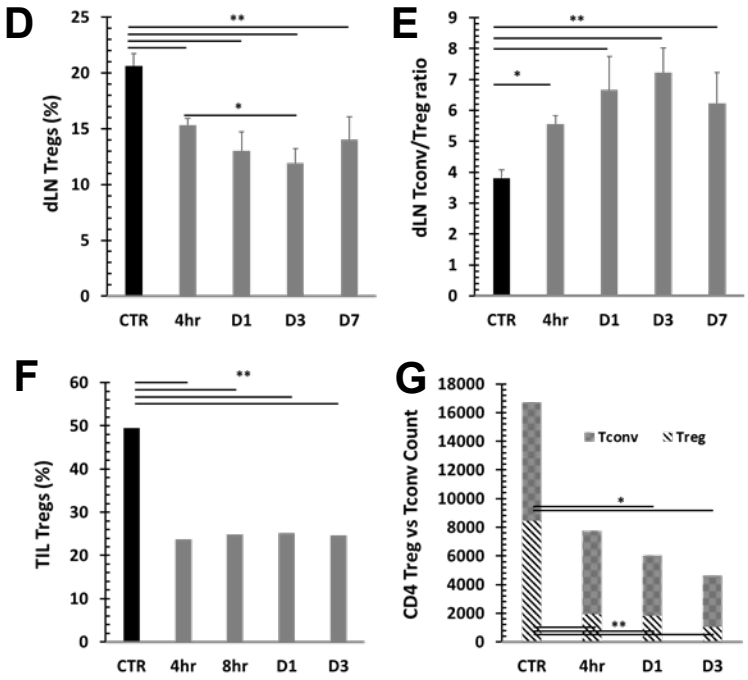

Figure 7. *(Continued.)* **A,** The treated mice were euthanized at 4 hours, 8 hours (for local tissues only), and on Day 1, Day 3, and Day 7 post-NPT. Their tumor tissues, tumor-draining lymph nodes (dLN), blood and spleens were harvested. Control tissues were obtained from mice with untreated tumors. **B-F,** Quantitative bar graphs depict the percentage of Tregs among the $CD4^+$ T cell population (**B-D**) and the Tconv/Treg ratios (**E**) in the blood (**B**), spleen (**C**) and dLN (**D** and **E**). TIL Tregs are represented in quantitative bar graphs as the percentage of Tregs among $CD4^+$ TILs (**F**) and as a standardized CD4 Treg vs CD4 Tconv cell count (**G**). N=4 per group. Error bars, SD. ** $p < 0.01$ and * $p < 0.05$ determined by one-way ANOVA.

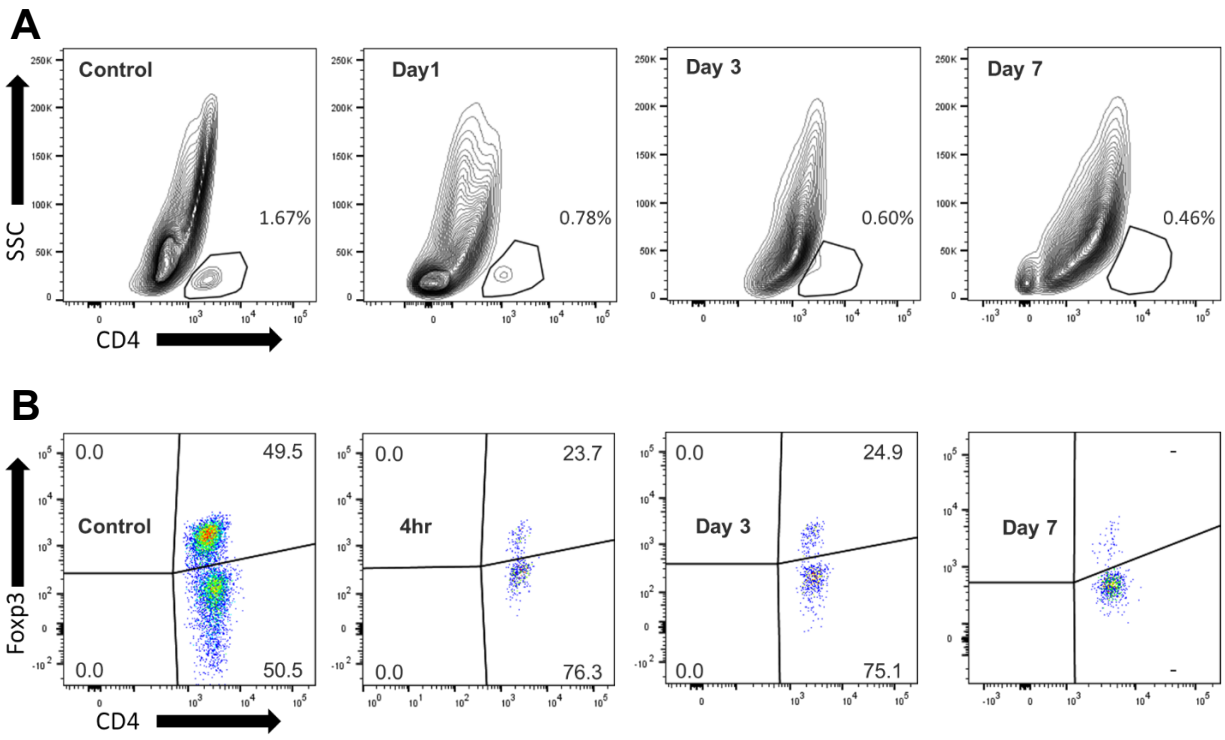

Figure 8.

NPT reduces intratumoral T cells. **A** and **B,** Summary flow plots demonstrate the impact of NPT on the total $CD4^+$ TIL population (**A**) and on Tregs vs Tconv (**B**) in untreated mice and at 4 hours (shown only in **B**), Day 1 (shown only in **A**), Day 3 and Day 7 post-NPT.

3.1.2 Decline in Treg activation after NPT

When evaluating for changes in the activated ($CD44^+CD62L^-$) vs naïve ($CD44^-CD62L^+$) Treg distribution (**Fig. 9A**), I found that activated Tregs were the initially dominant Treg population -in the dLN of tumor-bearing mice- and outnumbered naïve Tregs at a 2:1 ratio. Following NPT, this activated:naïve Treg ratio shifted to 1:1 by Day 1, and naïve Tregs became the dominant Treg population by post-treatment Day 3, at an activated:naïve Treg ratio 1:2 (**Fig. 9A** and **B**).

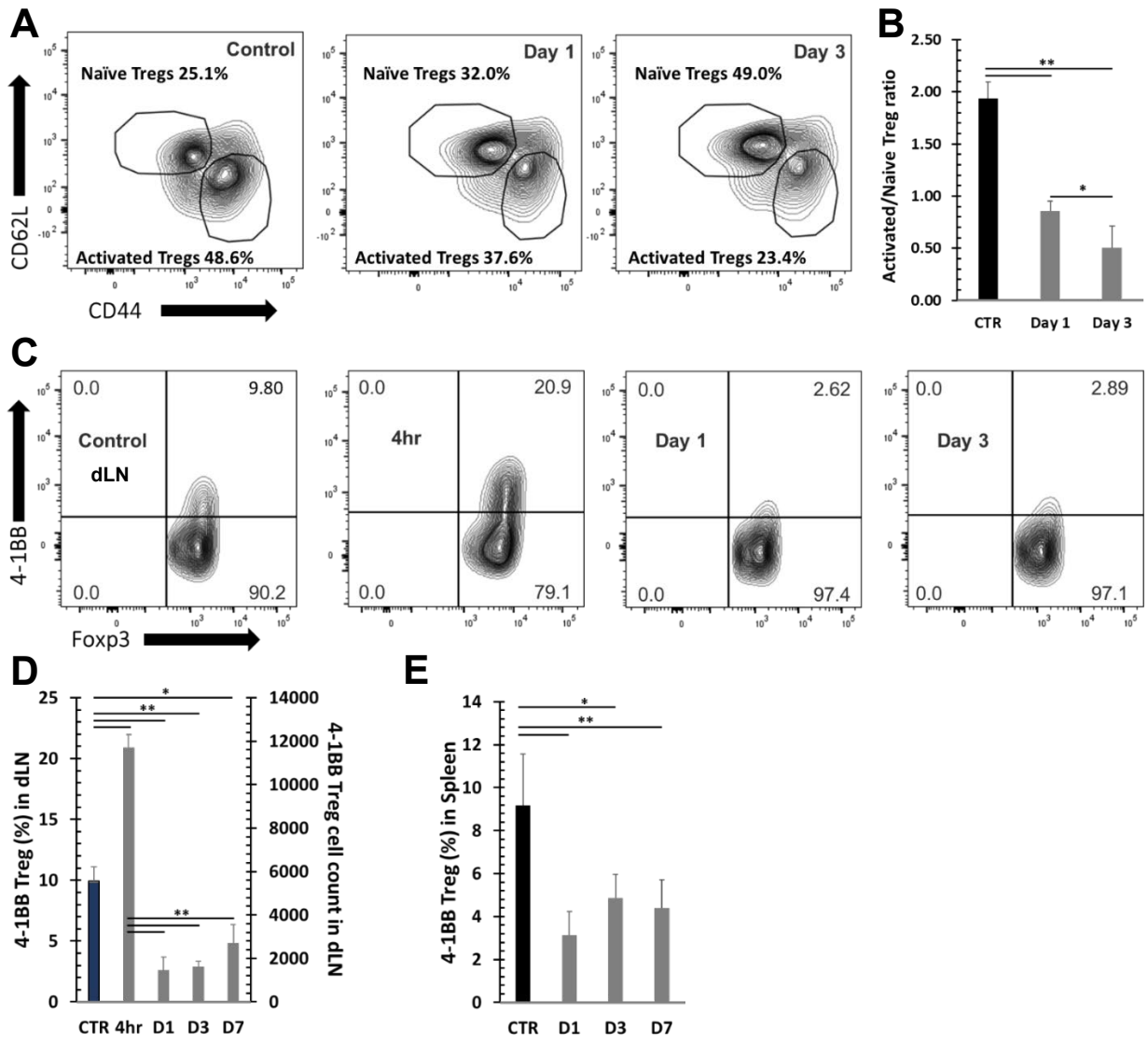

Figure 9.

Treg activation is reduced following NPT. **A** and **B,** Changes in activated and naïve Treg distribution in the dLN are represented in the summary flow plots (**A**) and quantitative bar graphs (**B**). **C-E,** Phenotypic changes in the 4-1BB activation marker expression among Foxp3^{+} Tregs are represented in the summary flow plots (**C**) and quantitative bar graphs (**D** and **E**) in the dLN (**C** and **D**) and spleen (**E**). N=4 per group. Error bars, SD. ** $p < 0.01$ and * $p < 0.05$ determined by one-way ANOVA.

I examined different Treg phenotypic markers, including CTLA-4, PD-1, CD39, Helios, 4-1BB, and TGFβ among $CD4^+$ T cells in the dLN of tumor-bearing mice (**Fig. 10** and **11**). CTLA-4, PD-1 and CD39 (not shown) were expressed in both Tconv and Tregs (**Fig. 10**) and did not demonstrate significant and consistent changes post-NPT. 4-1BB, Helios and TGFβ, on the other hand, were exclusively seen among the Treg population (**Fig. 11**) and were used to further determine how NPT affects Treg dynamics.

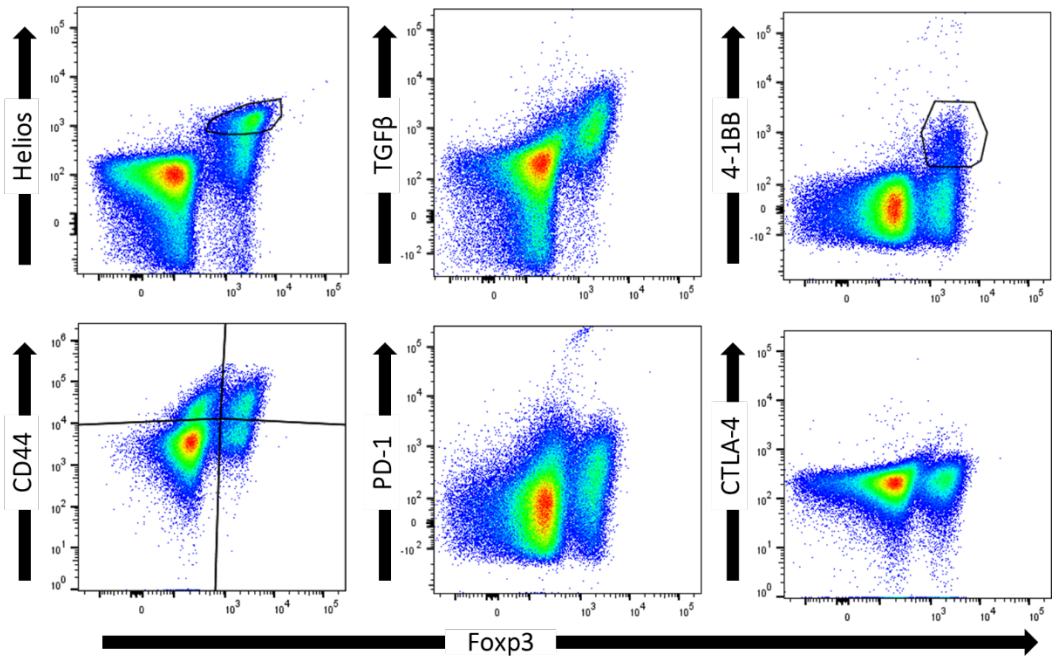

Figure 10.

Treg activation marker expression among total $CD4^+$ T cells in the dLN of untreated mice. Flow plot summaries of Foxp3 co-expression with Treg phenotypic markers including Helios, TGFβ, 4-1BB (upper panel) and CD44, PD-1, CTLA-4 (lower panel).

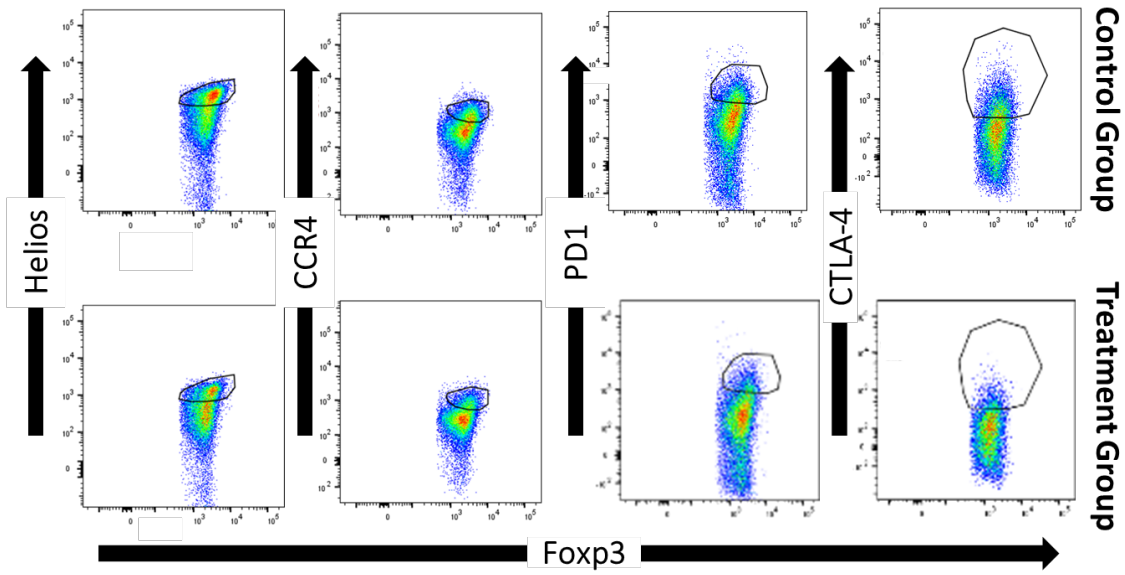

Figure 11.

Changes in dLN Treg activation marker expression following NPT. dLN were analyzed from mice with untreated control tumors and post-NPT treatment Day 2. Flow plots represent the expression of Helios, CCR4, PD-1 and CTLA-4 markers among Foxp3$^+$ Tregs.

4-1BB, a T cell activation marker with significant immunotherapeutic potential, was found to be expressed among Tregs in the dLN, tumors and spleens of tumor-bearing mice. 4-1BB expression was not found among a) Tregs in the blood, b) Tregs in any healthy (naïve) mouse tissues, or c) conventional CD4 or CD8 T cells of healthy or tumor-bearing mice (**Fig. 12**). A significant reduction in the total number of 4-1BB$^+$ Tregs in the dLN and spleen was observed in days 1-7 following NPT (**Fig. 9C** and **E**). Interestingly, there was an early transient peak among 4-1BB$^+$ Tregs, around 2-fold increase from baseline, by 4 hours post-NPT in the dLN followed by a 7-fold drop by 24 hours post-treatment (**Fig. 9C** and **D**).

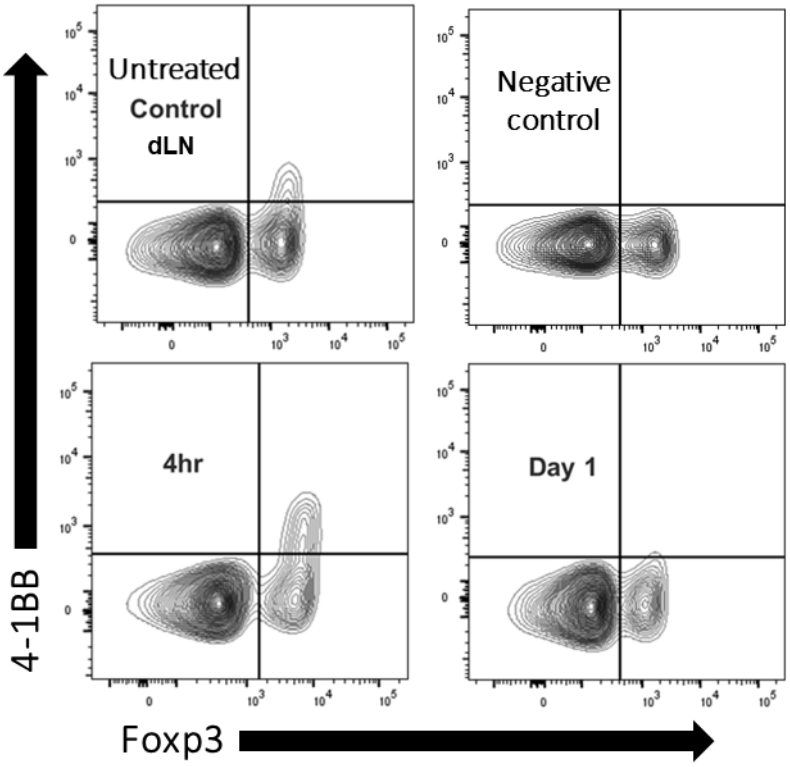

Figure 12.

NPT-induced changes in 4-1BB and Foxp3 co-expression among $CD4^+$ T cells in the dLN. Flow plots represent 4-1BB and Foxp3 analysis in $CD4^+$ T cells in the dLN of untreated tumor-bearing mice (untreated control), tumor-naïve mice (negative control) and treated mice from the post-NPT 4 hours and Day 1 timepoints.

$4\text{-}1BB^+$ Tregs were further found to be exclusively expressed among activated Tregs and mostly absent among naïve Tregs in dLN of tumor-bearing mice (**Fig. 13A**). A higher TGFβ expression was also found among $4\text{-}1BB^+$ and activated Tregs (**Fig. 13B**) when compared to their $4\text{-}1BB^-$ and naïve Treg counterparts. Similar to the changes in Treg $4\text{-}1BB^+$ expression, this elevated TGFβ expression among dLN Tregs had a transient increase from 33.2% among untreated mice to 39.2% at 4 hours post-NPT, followed by a reduction in expression in the days following treatment, lowest at 23.8% on

Day 3 post-NPT (**Fig. 14A** and **B**). High-level TGFβ expression among activated Tregs also dropped post-treatment (**Fig. 14C**). While we could clearly observe the above phenotypic changes among dLN Tregs, the few remaining intratumoral Tregs post-NPT made it challenging to properly describe such phenotypic changes among TILs (**Fig. 15**).

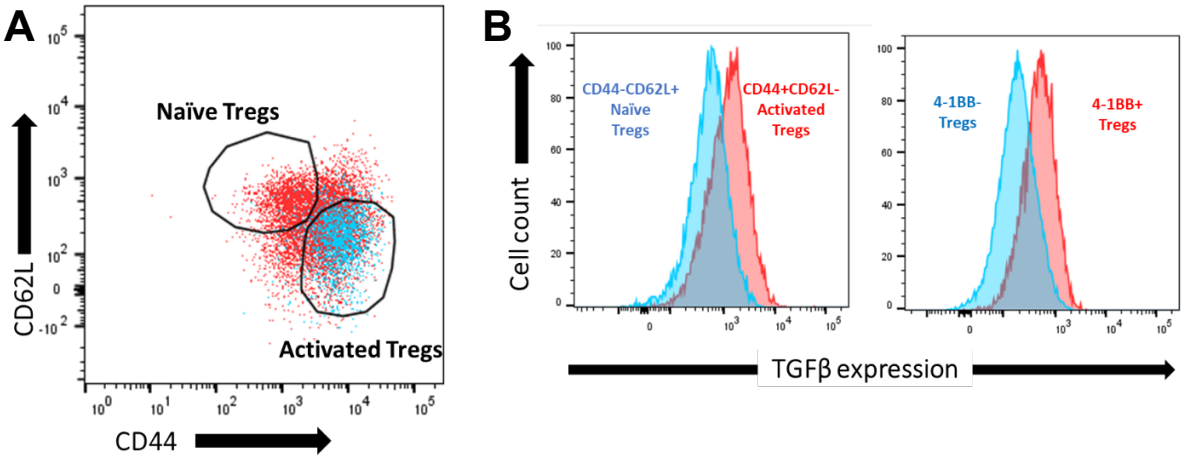

Figure 13.

Comparing phenotypic characteristics among different Treg subsets in the untreated tumor dLN. **A,** Flow plots represent CD44/CD62L expression among the total Treg population (red) and 4-1BB^{+} subgate (blue). **B,** TGFβ expression among naïve vs activated Tregs (left) and 4-1BB^{+} vs 4-1BB^{-} Tregs (right).

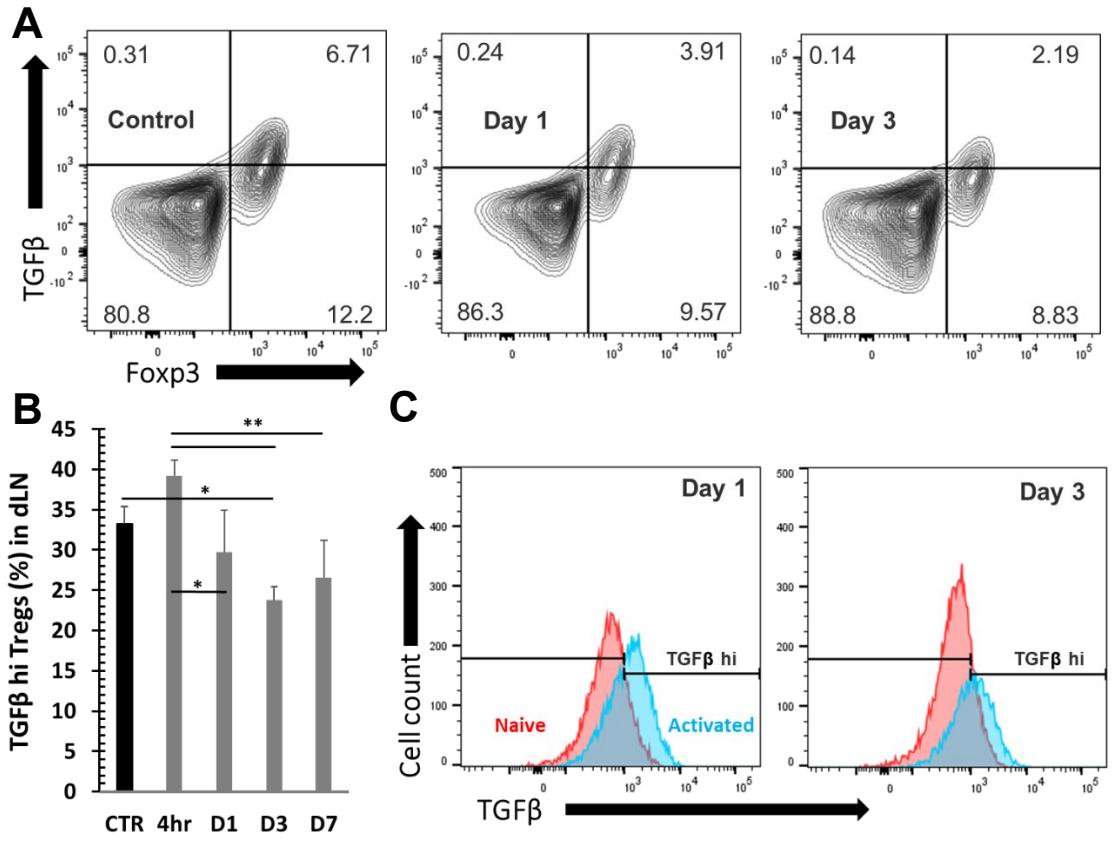

Figure 14.

NPT reduces TGFβ expression among Tregs in the dLN. **A,** Flow plots represent changes in TGFβ and Foxp3 expression among $CD4^+$ T cells. **B,** Quantitative graph of changes in TGFβ-hi expression among Tregs. **C,** Flow plots of TGFβ expression among activated vs naïve Tregs on Day 1 and Day 2 post-NPT. N=4 per group. Error bars, SD. ** $p < 0.01$ and * $p < 0.05$ determined by one-way ANOVA.

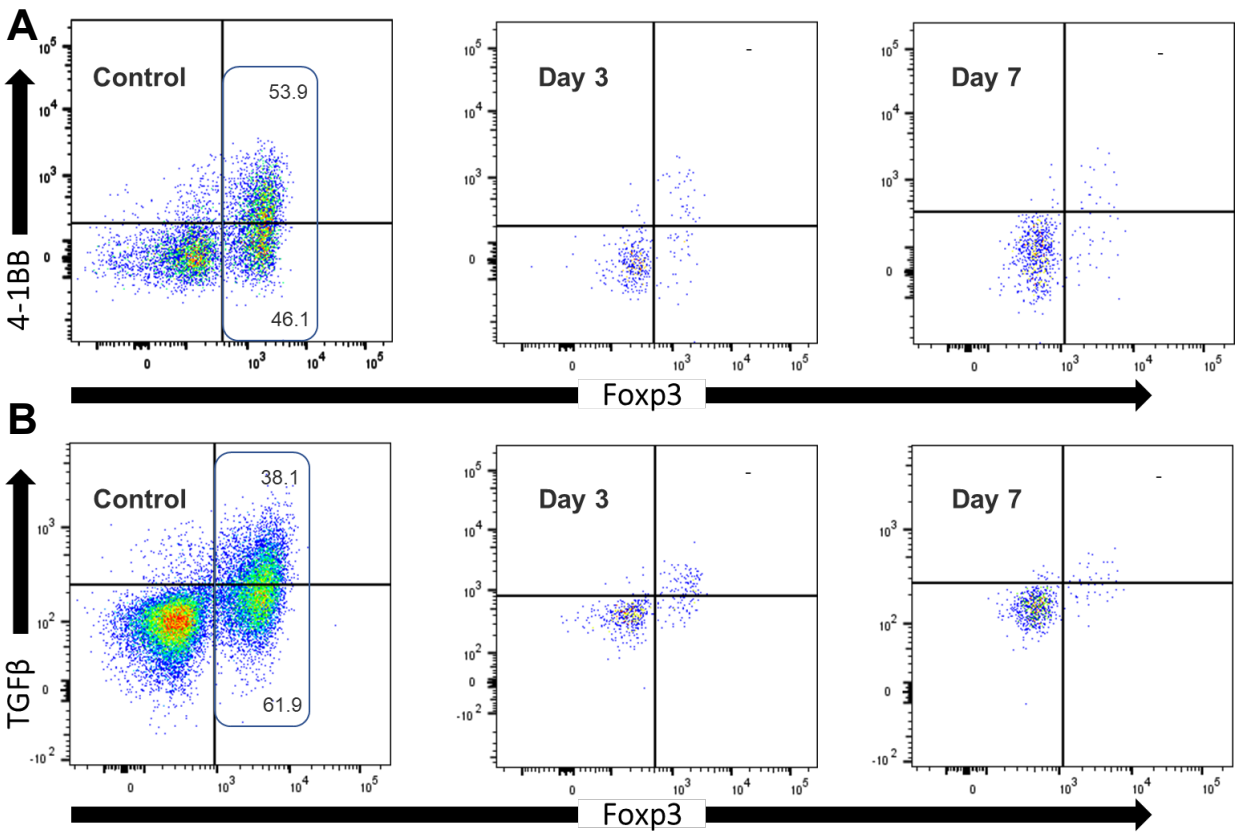

Figure 15.

NPT severely reduces intratumoral Tregs making their activation marker expression unquantifiable post-treatment. **A** and **B**, Flow plots representing Foxp3 co-expression with 4-1BB (**A**) and TGFβ (**B**) among $CD4^+$ TILS in untreated tumors and on Day 3 and Day 7 post-NPT.

3.1.3 Selective eradication of Tregs by NPT with a conservation of CD8 and CD4 Tconv

To understand why NPT resulted in a remarkable decrease in Tregs but less so among Tconv (**Fig. 7G**), I next determined whether cell death occurred differentially in various subsets of T cells (**Fig. 16**). As we can see from Figure 16A-C, Tregs, including both activated ($CD44^+CD62L^-$) and naïve ($CD44^-CD62L^+$) Treg subsets, were the only T

cell populations to exhibit statistically significant increases in apoptotic changes. Activated Tregs exhibited the highest level of apoptosis, seen at 4 hours post-treatment (**Fig. 16B** and **D**). Importantly, CD4 Tconv and CD8 T cells showed little or no change in apoptosis following NPT.

Noticeably, all T cell groups, except for the naïve Treg subset, exhibited various levels of apoptotic death in the control mice (**Fig. 16C**). Therefore, I also evaluated the percent change among the T cell subsets from their baseline apoptotic status to post-NPT apoptosis at 4 hours post-treatment (change in T cell subset apoptosis = % apoptosis at 4 hour post-treatment / % apoptosis in untreated control sample). Tregs exhibited the highest change in apoptosis at 4 hours post-NPT. Activated Tregs, in particular, demonstrated a 53.7% increase in apoptosis (**Fig. 16D**), whereas CD8 T cells showed no change and CD4 Tconv had a small but insignificant increase in apoptotic death.

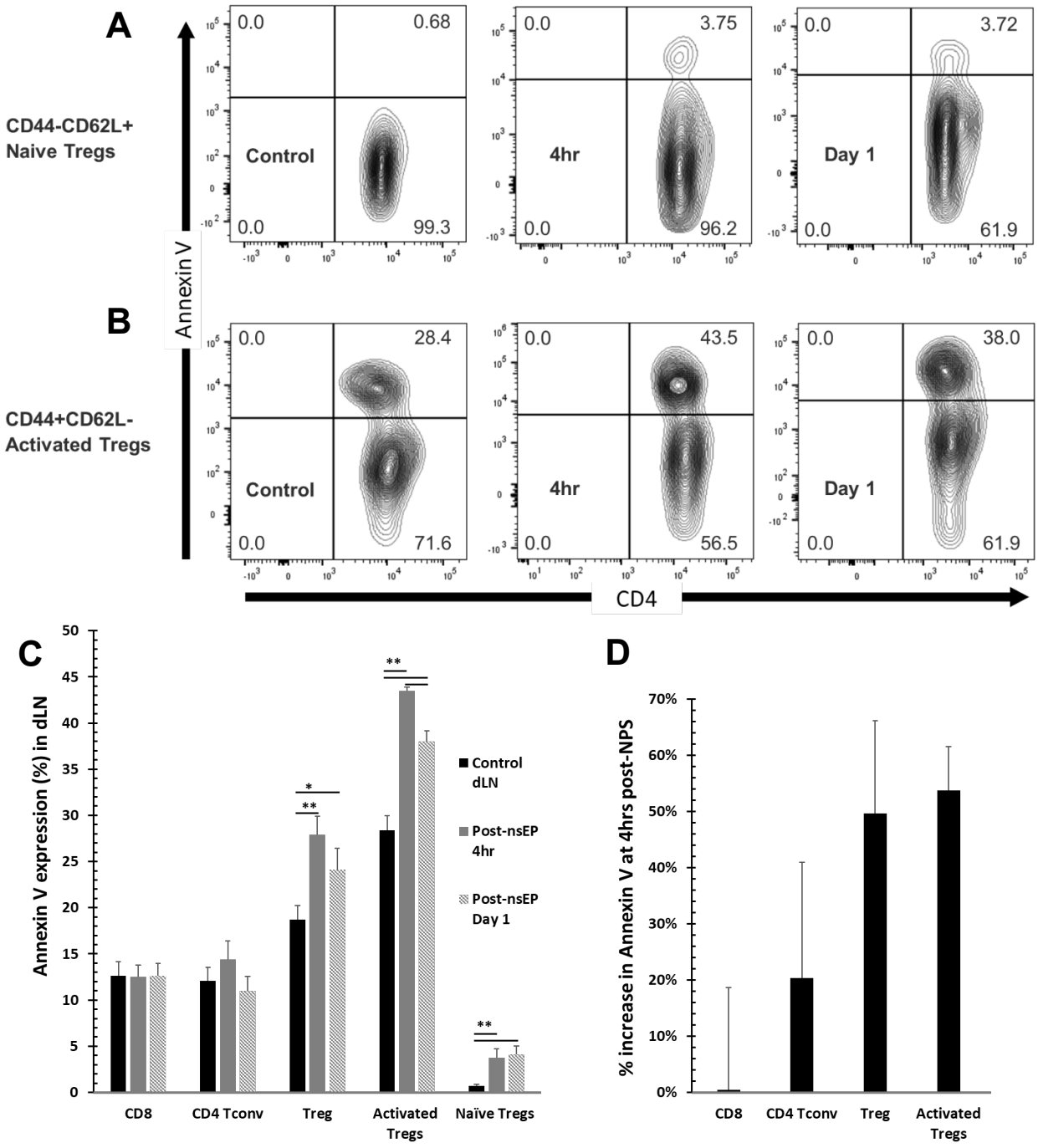

Figure 16.

Changes in apoptosis among T cells subsets following NPT. **A** and **B,** Summary flow plots represent Annexin V expression among activated and naïve Treg subsets in the dLN at 4 hours and Day 1 post-NPT. **C,** Quantitative graph shows Annexin V expression among CD8, CD4 Tconv, CD4 total Treg, activated Treg and naïve Treg subsets in the dLN at 4 hours and Day 1 post-NPT.

Figure 16. *(Continued.)* **D,** Quantitative graph shows the percent increase in Annexin V expression from the untreated Control to Day 1 post-treatment among T cell subsets. N=4 per group. Error bars, SD. ** $p < 0.01$ and * $p < 0.05$ determined by one-way ANOVA.

To gain a better understanding of how NPT impacts tumor cells and their subsequent interaction with T cells, I pulsed cultured 4T1-luc tumor cells *in vitro* then co-cultured them with healthy dLN lymphocytes. I found that healthy Tregs underwent apoptosis within 24 hours when co-cultured with NPT-treated tumor cells (**Fig. 17A**). On the other hand, healthy lymphocytes cultured with unpulsed (control) tumor cells were still alive in the co-culture after 48-72 hours, suggesting that Tregs heavily rely on healthy tumor presence for their survival (**Fig. 17A**). Tregs demonstrated increased apoptosis marker upregulation when compared to their CD8 and CD4 Tconv counterparts (**Fig. 17C**).

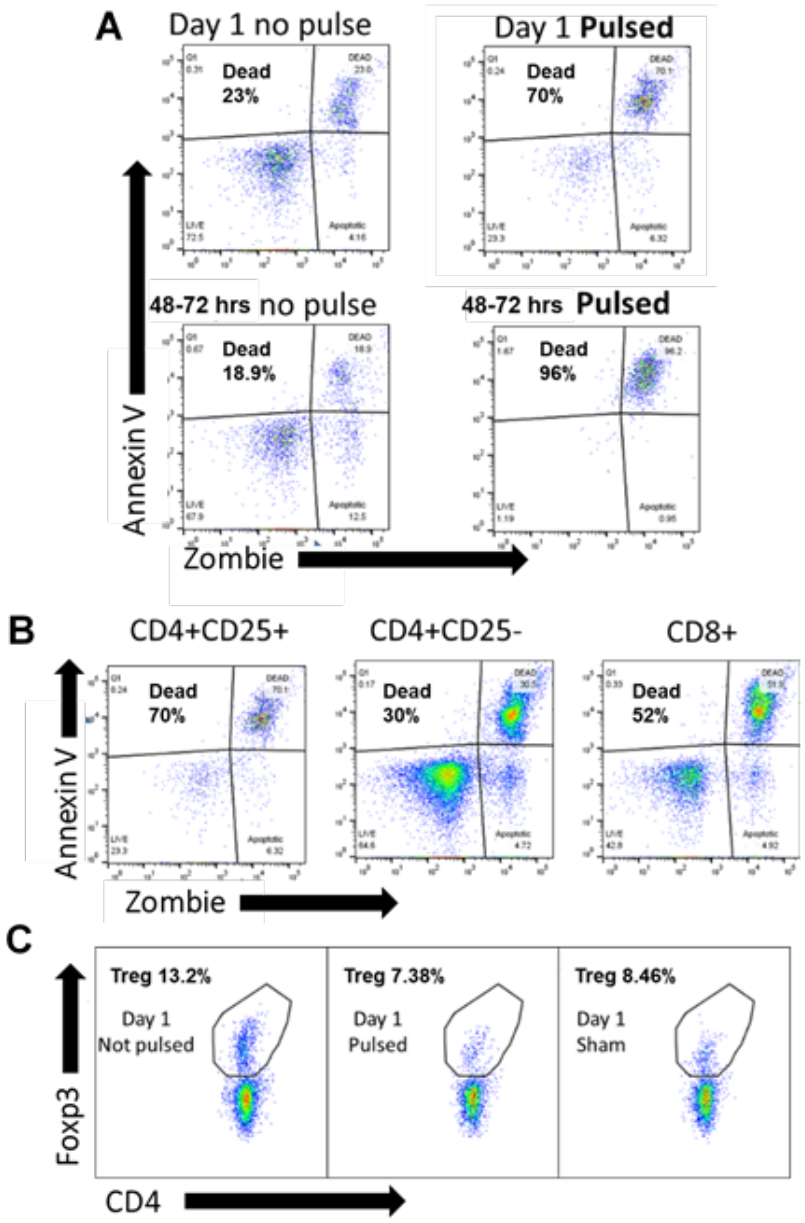

Figure 17.

T cells co-cultured with NPT-treated 4T1-luc cells demonstrate an increased expression in apoptosis markers. **A,** Changes in Treg apoptosis markers after 1 day and 48-72 hours in a culture with NPT-treated 4T1-luc cells. **B,** Expression of apoptosis markers among different T cell subsets (Treg and CD4/CD8 Tconv) after 1 day in a culture with NPT-treated 4T1-luc cells. **C,** Changes in Treg percentage among $CD4^+$ T cells after 1 day in a culture with NPT-treated 4T1-luc cells. Sham experiment represents T cells cultured in complete medium in the absence of tumor cells.

3.1.4 NPT is unlikely to influence Treg reprogramming

I investigated for NPT-induced Treg reprogramming to a Th17 (IL-17, RORγt expression) or Th1 (IFNγ expression) profile but were unable to find any significant changes. No FOXP3-RORγt co-expression was found in untreated or days 1, 3, 7 post-treatment groups in local or systemic organs.

3.1.5 No conclusive findings on the NPT impact on chemotaxis

Our studies on the NPT-associated changes among Treg vs Tconv CCR4 expression are currently inconclusive and require further *in vitro* investigations using transwell assays.

3.1.6 Differential changes in MDSCs and TAMs following NPT

In addition to Tregs, there are other immunosuppressive cells influencing the TME, including MDSCs and TAMs. TAMs (**Fig. 18A** and **B**) along with the systemic (**Fig. 18C** and **D**) and local (**Fig. 18E** and **F**) MDSC populations were significantly reduced following NPT. While investigating the intratumoral immune cell changes, I performed backgating to study the distribution of intratumoral TAMs, MDSCs and CD3 lymphocytes on the forward and side scatter plot and found that NPT affected these cell populations differently (**Fig. 19A-D**). TAMs showed a rapid decrease in cell count (by 4 hours post-treatment) (**Fig. 19A** and **B**), associated with a significant increase in apoptosis (**Fig. 19D** and **E**) and remained below control levels on days 1 and 3 post treatment (**Fig. 19B**). In contrast, MDSCs remained at control levels 1 day after treatment, but decreased by Day 3 (**Fig. 19A** and **B**). While CD3 TILs had a similar decrease in cell count 4 hours after treatment (**Fig. 19A** and **B**), they exhibited no significant change in apoptosis in the tumor. By 4 hours post-treatment, TIL apoptosis was detected in the dLN (**Fig. 17C**) but not in the

tumor. By Day 3, as MDSCs regressed, there was a significant increase in antitumor CD86^{+} M1 TAMs (**Fig. 19C**).

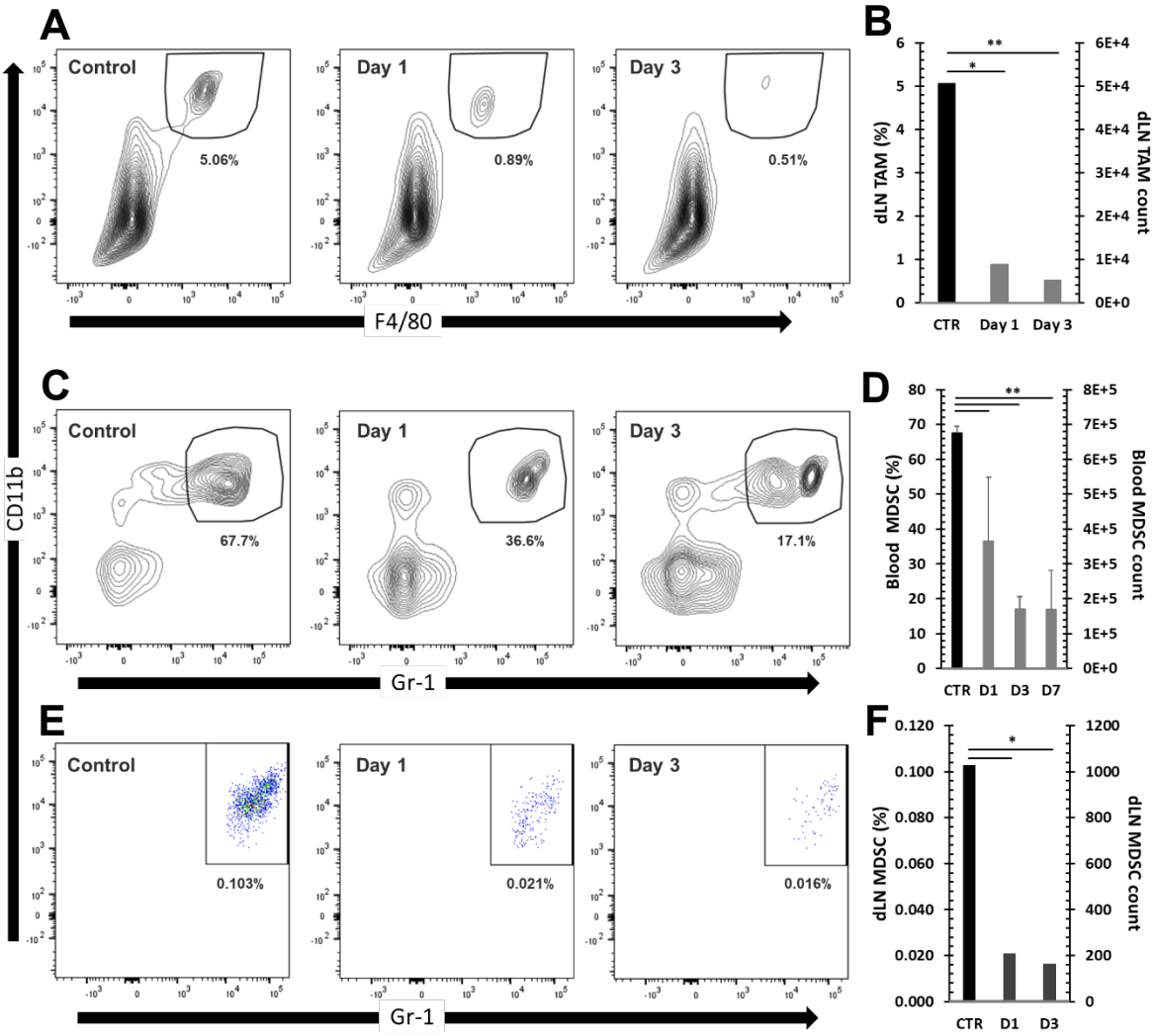

Figure 18.

MDSCs and TAMs are decreased following NPT. F4/80^{+}CD11b^{+} TAMs in the dLN (**A** and **B**) and Gr-1^{+} CD11b^{+} MDSCs in the blood (**C** and **D**) and dLN (**E** and **F**) are represented as a percentage among total single events in the summary flow plots (**A, C** and **E**) and quantitative bar graphs (**B, D** and **F**). A standardized cell count is represented for TAMs in the dLN (**B**) and MDSCs in the blood (**D**) and dLN (**F**). N=4 per group. Error bars, SD. ** $p < 0.01$ and * $p < 0.05$ determined by one-way ANOVA.

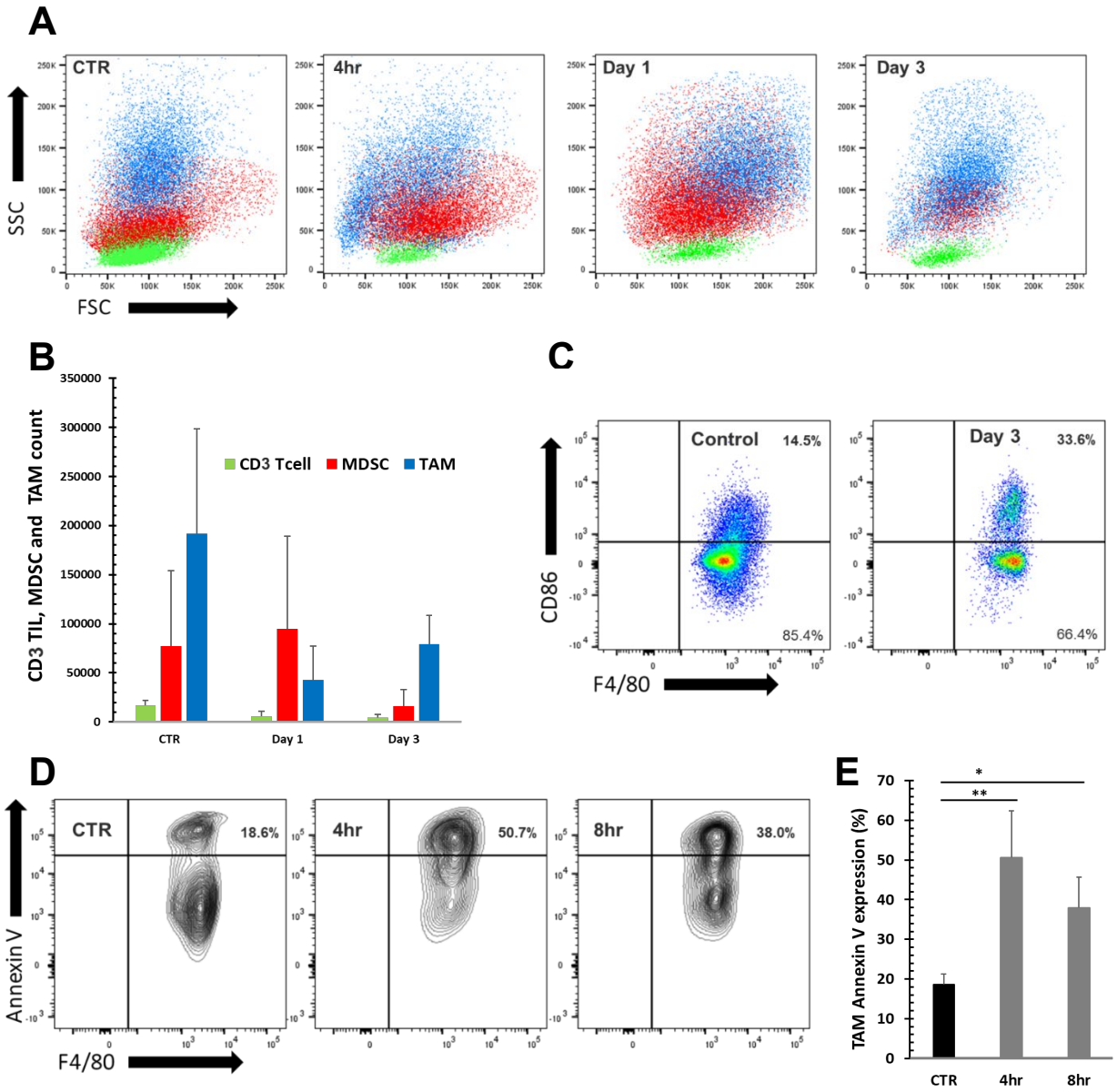

Figure 19.

The impact of NPT on intratumoral TAM and MDSC characteristics. **A** and **B,** Changes in intratumoral TAMs, MDSCs and CD3 lymphocytes distribution at 4 hours, Day 1 and Day 3 post-treatment shown in a summary flow plot (**A**) and quantitative graph (**B**). **C,** Changes in the CD86 activation marker expression among TAMs is investigated on the third day post-treatment, represented in a summary flow plot. **D** and **E,** Intratumoral TAM apoptosis summary flow plot (**D**) and quantitative graph (**E**) are shown at 4 hours and 8 hours post-NPT. N=4 per group. Error bars, SD. ** $p < 0.01$ and * $p < 0.05$ determined by one-way ANOVA.

3.1.7 CD8 resident memory cells increase following NPT

To further evaluate the antitumor immune response, I investigated for the presence of resident memory T cells (Trm) following NPT. I found an increase in the expression of the CD103 Trm marker among CD8 T cells in the dLN (**Fig. 20A-C**). The frequency of Trms among the $CD8^+$ T cell population (**Fig. 20A** and **B**) and the total number of CD8 Trms (**Fig. 20C**) significantly increased to 2.5-fold in the dLN following NPT. To assess whether this shift held potential clinical relevance, I evaluated the CD8 Trm / CD4 Treg ratio and found a significant 2-3-fold increase in the ratio by days 3 and 7 post-treatment (**Fig. 20D**).

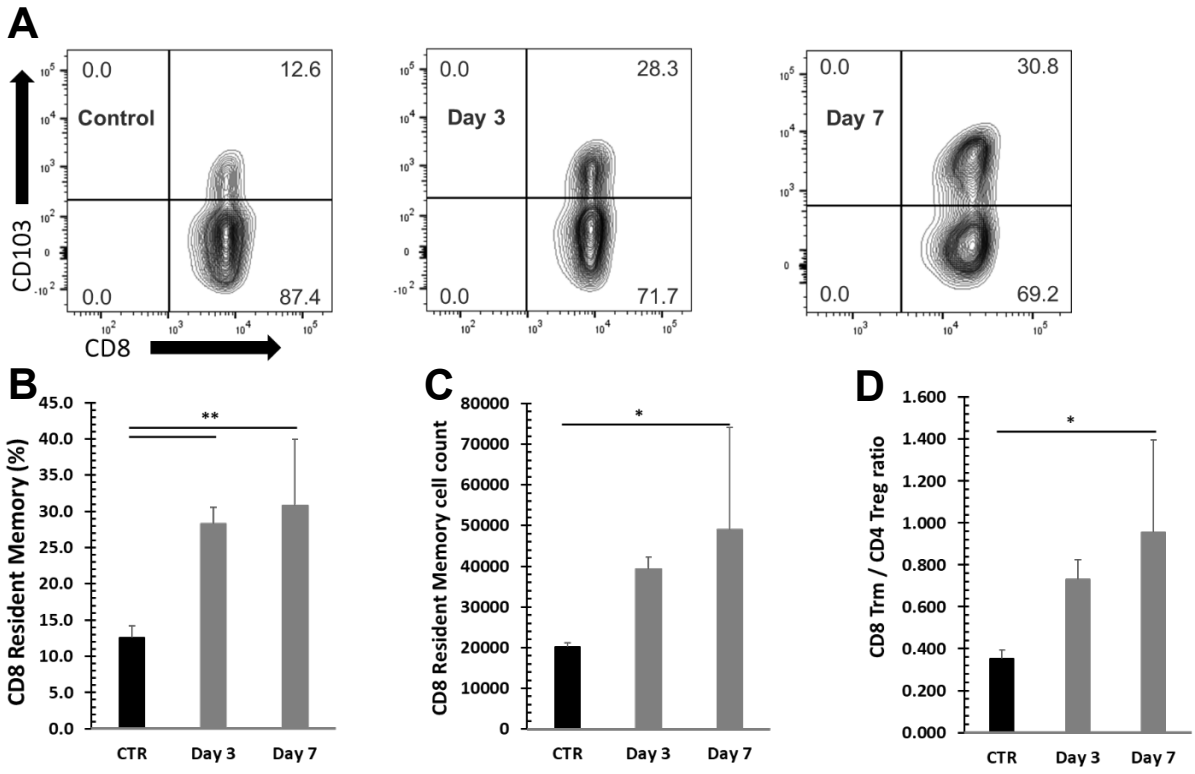

Figure 20.

CD8 Trm increase in the dLN following NPT.

Figure 20. *(Continued.)* **A** and **B,** Summary flow plot (**A**) and quantitative bar graph (**B**) represent CD103 expression among the total CD8 T cell population in the dLN on days 3 and 7 following NPT. **C** and **D,** The Trm standardized cell count (**C**) and CD8 Trm / CD4 Treg ratio (**D**) are represented in quantitative graphs. N=4 per group. Error bars, SD. ** $p < 0.01$ and * $p < 0.05$ determined by one-way ANOVA.

3.2 Reduction in Treg suppression capacity following treatment

To show the effect of NPT on the Treg suppression capacity, I isolated dLN $CD4^+CD25^+$ Tregs using magnetic beads and incubated them with CFSE-labelled CD8 cells at different Treg:CD8 ratios in the presence of activation beads. Tregs isolated from dLNs of NPT-treated mice exhibited a reduced suppression capacity compared to those from untreated tumors, particularly at the Treg:CD8 1:1 and 1:2 ratios (**Fig. 21**). Tregs from both control and treatment groups were stained with Foxp3 following bead-based isolation, and the post-isolation purity was analyzed (**Fig. 22**).

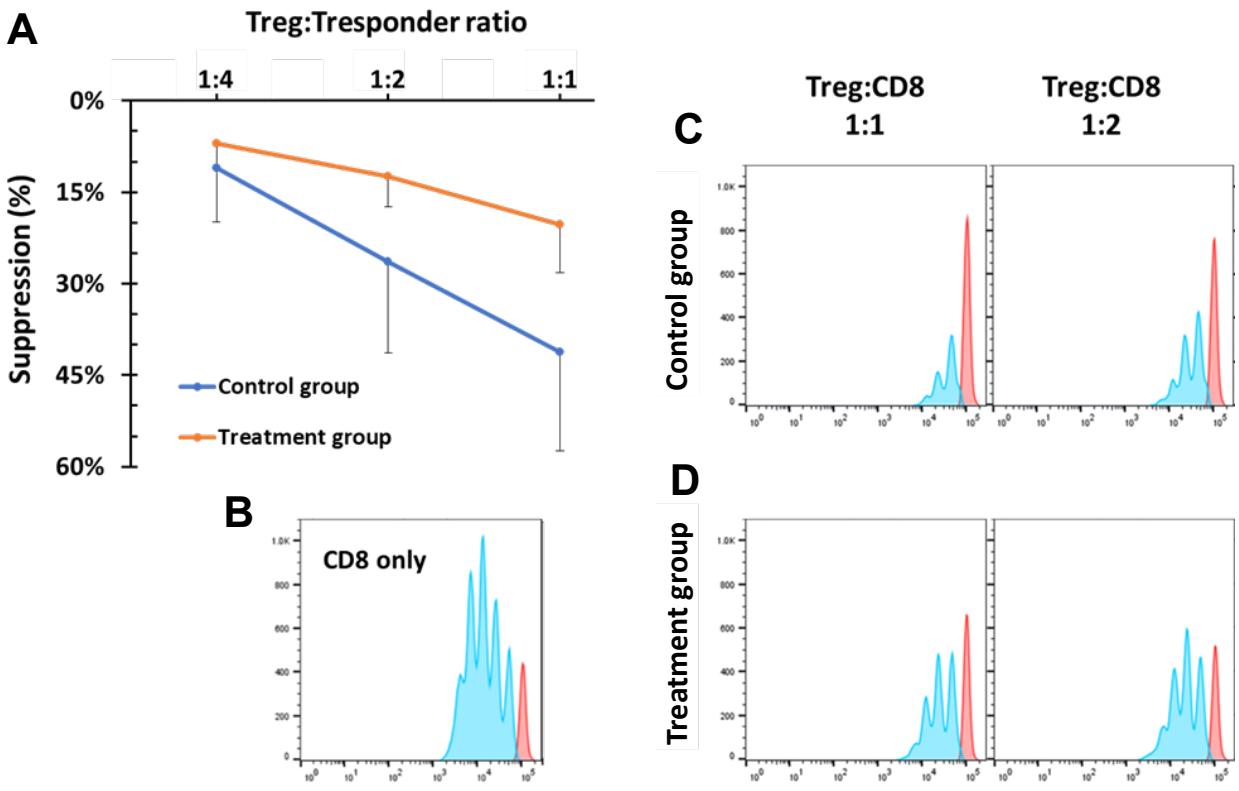

Figure 21.

Treg suppressive function is reduced following NPT. **A,** Tregs from dLN of NPT-treated mice have a reduced functional suppression capacity as shown in the *in vitro* suppression assay quantitative plot. dLN Tregs were incubated with CFSE-labelled CD8 responder cells at the Treg:Tresponder ratios 1:1, 1:2 and 1:4 for 60 hours in the presence of CD3/CD28 activation beads. %Suppression = [1-(%proliferating Tresp at Treg:Tresp ratio / %proliferating Tresp-only cells)] x100. **B,** Representative histogram plots of responder cell proliferation alone (proliferating cells shown in the blue histogram; non-proliferating cells shown in the red histogram). **C** and **D,** Representative histogram plots of responder cell proliferation in the presence of Tregs from untreated tumor-bearing mice (control group) (**C**) or Tregs from NPT-treated mice (treatment group) (**D**) at different Treg:Tresponder ratios. N=3 per group.

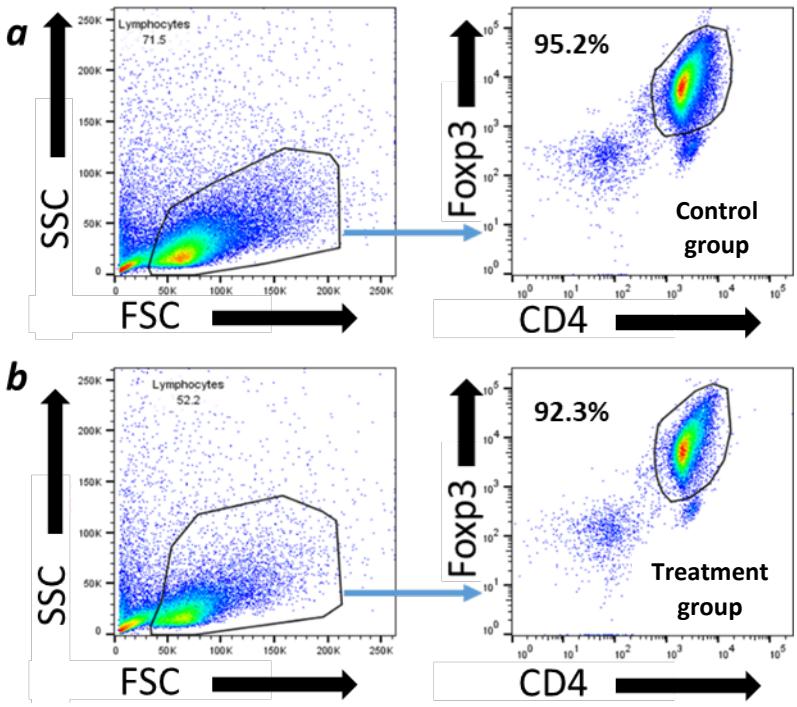

Figure 22.

Purity analysis of Tregs isolated from dLNs. **A** and **B,** Summary flow plots demonstrate Foxp3 expression among $CD4^+CD25^+$ T cells isolated from untreated tumor-bearing mice (control group) (**A**) or NPT-treated mice (treatment group) (**B**). The percentage of $CD4^+Foxp3^+$ Tregs is represented among the total isolated $CD4^+CD25^+$ cell population.

3.3 Treg TCR studies, human

Since functionally superior Tregs were downregulated, and activated Tregs underwent apoptosis following NPT, I hypothesize that the above NPT-impacted population consisted of clonally expanded antigen-specific Tregs. The increased vulnerability of activated Tregs to apoptosis in comparison to Tconv and naïve Tregs is discussed further in Section 4.2. The future goal of this project is to determine whether NPT downregulates activated Tregs in humans to subsequently lead to a vaccine-like

immunity, similar to the way it does in mice. To initiate such studies on human tissue, I first investigated the Treg TCR clonality in normal donor blood samples.

3.3.1 Pure Tregs were isolated through automated cell sorting

To investigate the Treg TCR clonality among healthy donors, 7 blood samples from 7 different donors were obtained from BioChemed Services. Donors were from both sexes; all were non-smokers and reported to be healthy. PBMCs were isolated from freshly drawn blood, and $CD4^+$ cells were enriched using microbeads. The cells were then labeled with fluorochrome-conjugated antibodies and automated cell sorting was performed using the gating strategy discussed in Section 2.2.4 for the isolation of human peripheral blood $CD4^+CD25^+CD127$lo Tregs (**Fig. 23**).

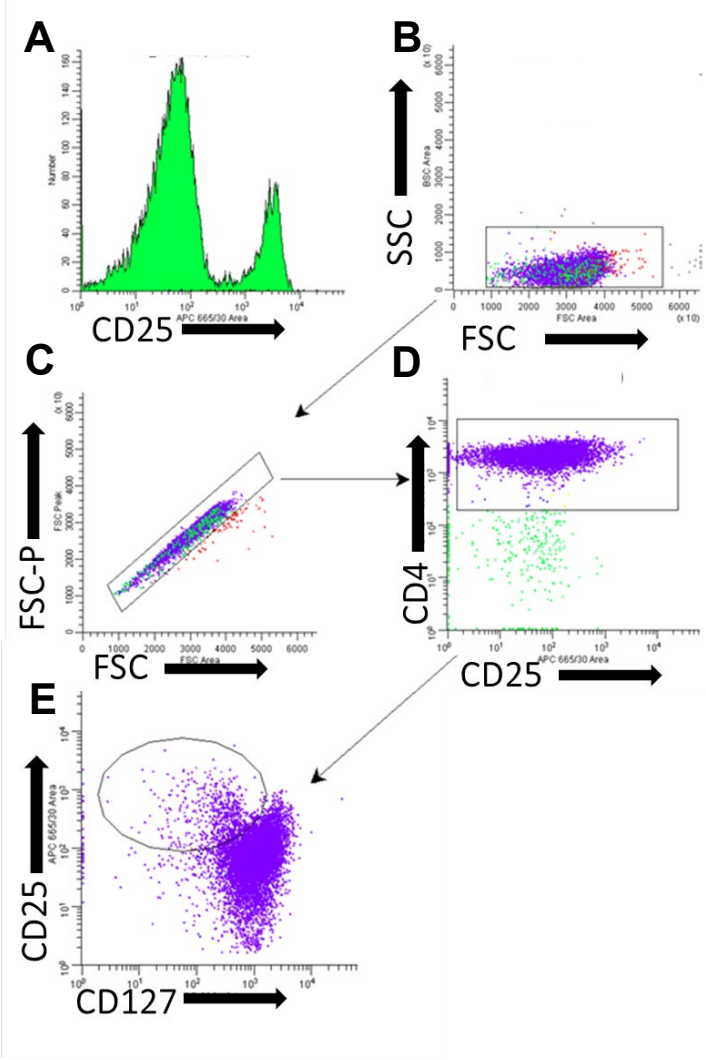

Figure 23.

Gating strategy for isolation of human CD4⁺CD25⁺CD127lo Tregs from enriched peripheral blood CD4⁺ T cells using automated cell sorting. **A,** Microbead-enriched CD4⁺ T cells from the peripheral blood of normal donor were initially assessed for their CD25⁺ expression, represented on a histogram. **B,** The forward scatter (FSC) vs side scatter (SSC) flow plot was used to select lymphocytes. **C** and **D,** Lymphocytes were then gated on the FSC-A vs FSC-P axis to eliminate doublets (**C**) and CD4⁺ singlets were selected (**D**). **E,** CD4⁺ T cells then gated on the CD25 vs CD127 axis to select for CD4⁺CD25⁺CD127lo Tregs.

The percentage of Tregs among the CD4 population was analyzed prior to sorting. Among the 7 normal donor blood samples, Tregs represented 7.06% of the CD4 cell population. The range was 4.37 - 9.10% (Table 1).

Following cell sorting, the isolated pure Treg population and the non-Treg $CD4^+$ cells were analyzed. The post-sort (**Fig. 24**) $CD4^+CD25^+CD127lo$ Treg purity ranged from 87 - 95%. The average Treg purity was 91.45%, calculated from 6 recorded samples (Table 1).

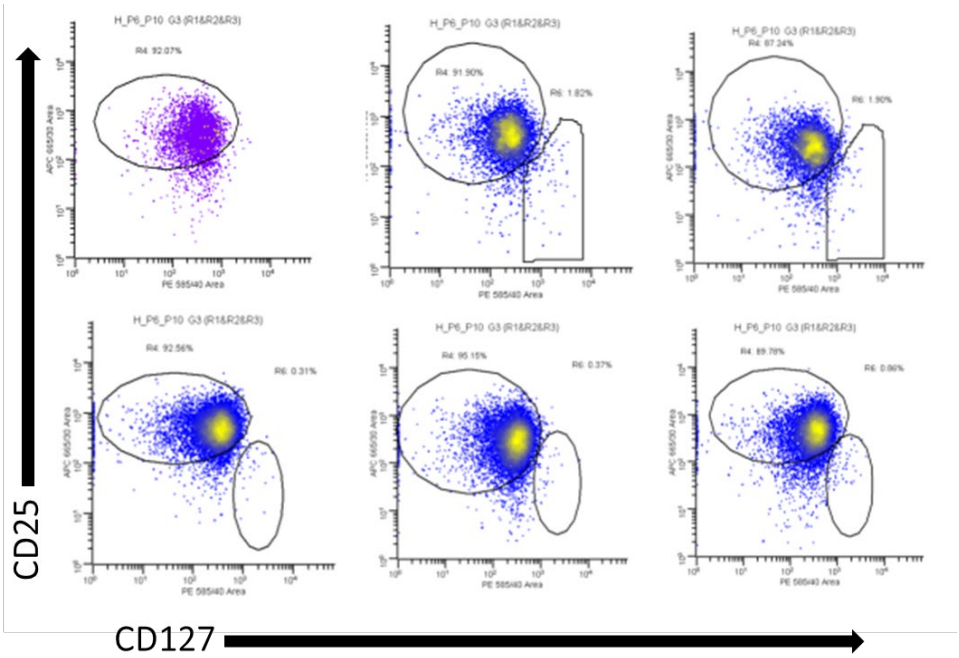

Figure 24.

Post-sort analysis of isolated human peripheral blood Tregs. Flow plots represent $CD4^+CD25^+CD127lo$ Tregs isolated from the peripheral blood of different healthy donors using automated cell sorting.

Table 1. Percentage of pre- and post-sort Tregs among the total $CD4^+$ T cell population in healthy donor blood.

	Tregs	
Normal Donor	**Pre-sort**	**Post-sort**
1st	4.37	N/A
2nd	8.04	92.07
3rd	9.10	91.90
4th	6.67	87.24
5th	7.80	92.56
6th	6.19	95.15
7th	7.23	89.78
Range	**4.37 - 9.10**	**87 - 95**
Mean	**7.06**	**91.45**

The percentage of $CD4^+CD25^+CD127lo$ Tregs among $CD4^+$ T cells from the peripheral blood of different healthy donors was recorded before (n=7) and after (n=6) automated cell sorting. The mean and range were calculated.

3.3.2 FOXP3 gene is expressed among isolated Tregs

Semi-quantitative PCR analysis of actin, CD4 and FOXP3 expression for both the Treg and non-Treg $CD4^+$ T cell fractions revealed actin and CD4 expression among both fractions. FOXP3 expression was seen only among the Treg population (**Fig. 25**).

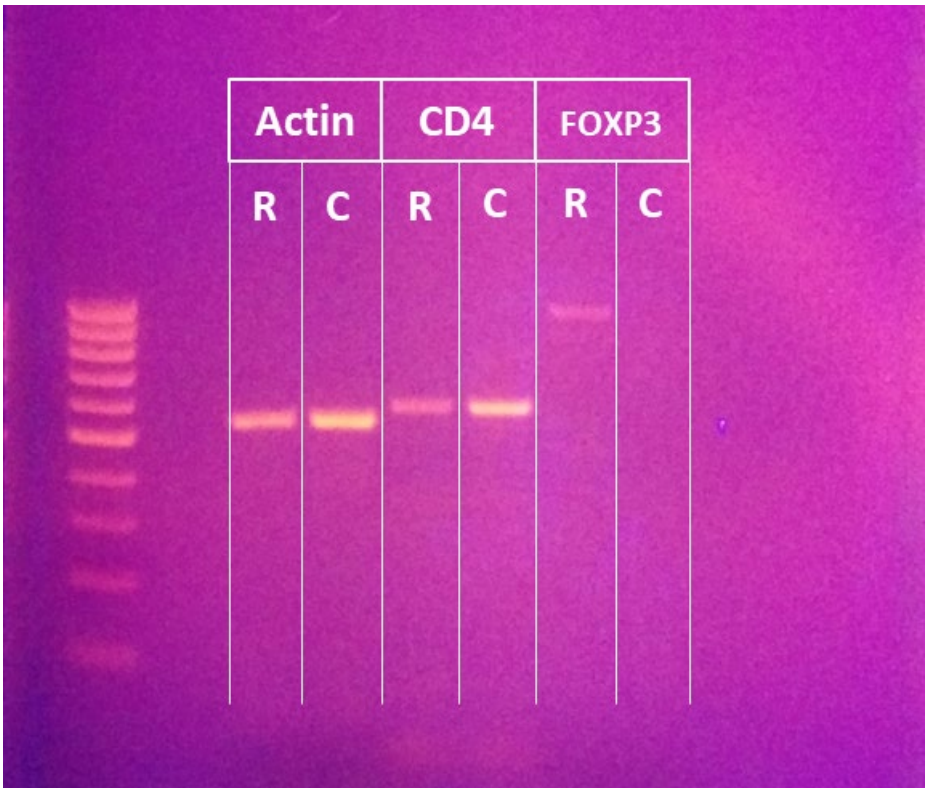

Figure 25.

FOXP3 is expressed among isolated human peripheral blood Tregs and absent among non-Treg $CD4^+$ T cells. Isolated human peripheral blood $CD4^+CD25^+CD127lo$ Tregs (R) and the negative fraction consisting of $CD4^+CD25^-$ T cells (C) demonstrated Actin and CD4 expression. Only the isolated Tregs had FOXP3 expression.

The Treg cDNA was used as a template for alpha-chain TCR amplification with the 32 alpha-chain family primers. The same process was repeated for beta-chain TCR amplification using the 24 beta-chain family primers. Two rounds of PCR amplifications (in a nested design) were carried out for each chain, followed by cloning and sequencing. The obtained TCR sequences were then analyzed using the IMGTV & Expasy softwares.

3.3.3 Treg TCR analysis among healthy donors revealed mostly a polyclonal distribution

The Treg cDNA was used as a template for alpha-chain TCR amplification with the 32 alpha-chain family primers. The same process was repeated for beta-chain TCR amplification using the 24 beta-chain family primers. Two rounds of PCR amplifications (in a nested design) were carried out for each chain, followed by cloning and sequencing. The obtained TCR sequences were then analyzed using the IMGTV & Expasy softwares.

ND1Treg

Sequence analysis of the beta-chain TCR transcripts of the 1st normal donor Treg sample (ND1Treg) revealed two quadruplets, a triplet, and five doublets (Table 2):

(1) clone ND1Treg-B-1: transcript Vβ11.2 Dβ1 Jβ1.2; CDR3 sequence CASSLEGGPQRGYTF accounted for 4 of 36 (11.11%) of the beta-chain TCR transcripts sequenced.

(2) clone ND1Treg-B-2: transcript Vβ5.1 Dβ1 Jβ1.4; CDR3 sequence CASSVDRGKEKLFF accounted for 4 of 36 (11.11%) of the beta-chain TCR transcripts sequenced.

(3) clone ND1Treg-B-3: transcript Vβ18 Dβ1 Jβ2.5; CDR3 sequence CASSPDSQETQYF accounted for 3 of 36 (8.33%) of the beta-chain TCR transcripts sequenced.

The following clones were doublets, and they accounted for 2 of 36 (5.56%) of the beta-chain TCR transcripts sequenced:

(4) clone ND1Treg-B-4: transcript Vβ6.5 Jβ1.1; sequence CASSYSRSMMNTEAFF,

(5) clone ND1Treg-B-5: transcript Vβ5.1 Dβ2 Jβ1.1; sequence CATRDGIGINTEAFF

(6) clone ND1Treg-B-6: transcript Vβ11.2 Dβ1 Jβ2.5; sequence CASSLVVGLPDF,

(7) clone ND1Treg-B-7: transcript Vβ5.1 Dβ2 Jβ1.1; sequence CASNLMGGRNTEAFF,

(8) clone ND1Treg-B-8: transcript Vβ2 Dβ1 Jβ2.1; sequence CASRPETGRNEQFF

The remainder of the TCR sequences demonstrated a polyclonal distribution (singlets).

Table 2. β-Chain TCR transcripts expressed in Tregs from 1st donor PBMCs.

Vβ	N-Dβ-N	Jβ	Gene usage
tgtgccagcagctt C A S S L	ggaagggggcccacagcg E G G P Q R	tggctacaccttc G Y T F	Vβ11.2 Dβ1 Jβ1.2 (4/36, 11.11%)
tgcgccagcagc C A S S	gtggacaggggaaa V D R G K	gaaaaactgtttttt E K L F F	Vβ5.1 Dβ1 Jβ1.4 (4/36, 11.11%)
tgtgccagctcacc C A S S P	tgacagt D S	caagagacccagtacttc Q E T Q Y F	Vβ18 Dβ1 Jβ2.5 (3/36, 8.33%)
tgtgccagcagttactc C A S S Y S	tcgctcgatga R S M	tgaacactgaagctttcttt M N T E A F F	Vβ6.5 Jβ1.1 (2/36, 5.56%)
tgtgccagcagcttag C A S S L	tcgtaggcctcccag V V G L P	acttc D F	Vβ11.2 Dβ1 Jβ2.5 (2/36, 5.56%)
tgcgcca C A	cgcgggacgggatcgggatc T R D G I G I	aacactgaagctttcttt N T E A F F	Vβ5.1 Dβ2 Jβ1.1 (2/36, 5.56%)
Tgcgccagca C A S	acttgatgggggggag N L M G G R	gaacactgaagctttcttt N T E A F F	Vβ5.1 Dβ2 Jβ1.1 (2/36, 5.56%)
Tgtgccagcag C A S R	accggagacaggccg P E T G R	caatgagcagttcttc N E Q F F	Vβ2 Dβ1 Jβ2.1 (2/36, 5.56%)
Tgcagcg C S	tcccctcactagggttg V P S L G L	aatgagcagttcttc N E Q F F	Vβ29.1 Dβ2 Jβ2.1 (1/36, 2.78%)

Table 2. *(Continued.)*

Tgtgcctggagtgt C A W S V	atcgtcagggatgtt S S G M F	tcagccccagcattt Q H F Q P	Vβ30 Dβ1 Jβ1.5 (1/36, 2.78%)
Tgcgccagcag C A S S	tgctttaaataggggcagt A L N R G S	tcctacaatgagcagttcttc S Y N E Q F F	Vβ4.1 Dβ1 Jβ2.1 (1/36, 2.78%)
Tgcagtgct C S A	gcccgggacgggggggag A R D G G S	cactgaagctttcttt T E A F F	Vβ20.1 Dβ2 Jβ1.1 (1/36, 2.78%)
tgcagtgctag C S A S	tgtcccaggaggtgg V P G G G	cactgaagctttcttt T E A F F	Vβ20.1 Dβ2 Jβ1.1 (1/36, 2.78%)
tgtgccagctcacc C A S S P	ggtccgg V R	gaagctttcttt E A F F	Vβ18 Dβ2 Jβ1.1 (1/36, 2.78%)
tgcagtgc C S A	caccgggacccccg T G T P	atcagccccagcatttt D Q P Q H F	Vβ20.1 Dβ1 Jβ1.5 (1/36, 2.78%)
Tgcagcg C S	ttgaaaggg V E R	accaagagacccagtacttc D Q E T Q Y F	Vβ29 Dβ1 Jβ2.5 (1/36, 2.78%)
tgtgccagcagtttat C A S S L	tgtccctgactcta L S L T L	gagcagttcttc E Q F F	Vβ27 Dβ2 Jβ2.1 (1/36, 2.78%)
tgcgccagcagcttgg C A S S L	accagccatctcga D Q P S R	ggctacaccttc G Y T F	Vβ5.1 Dβ1 Jβ1.2 (1/36, 2.78%)
tgcagtgctagaga C S A R D	tttgaa L K	gaacactgaagctttcttt N T E A F F	Vβ20.1 Jβ1.1 (1/36, 2.78%)
tgtgccagcagcttag C A S S L	tcgtaggcctcccag V V G L P	acttc D F	Vβ11.3 Dβ1 Jβ2.5 (1/36, 2.78%)
tgcagtgctag C S A S	tgtcccaggaggtggcacc V P G G G T	gaagctttcttt E A F F	Vβ20.1 Dβ2 Jβ1.1 (1/36, 2.78%)
tgcagtgctaga C S A R	atggctagcgggggggctattcgtag M A S G G A I R S	cgagcagtacttc E Q Y F	Vβ20.1 Dβ2 Jβ2.7 (1/36, 2.78%)
tgcgccagcagcttg C A S S L	accagccatttcga. T S H F -	ggctacaccttc G Y T F	Vβ5.1 Dβ1 Jβ1.2 (1/36, 2.78%)

For the sake of clarity, the above results will be referred to as ‘all-family’ amplifications. To further investigate the clonal sequences observed in the Vβ11 and Vβ5 families, ‘family-specific’ amplifications were carried out:

Frozen ND1Treg RNA was reverse transcribed, and the cDNA template was used for two rounds of PCR amplifications using the Vβ11 primer for one set of PCR reactions, and the Vβ5 primer for another set. Cloning and sequencing were performed.

Sequence analysis for the Vβ11 family-specific amplifications revealed (Table 3):

clone ND1Treg-BFS11-1: transcript Vβ11.2 Dβ2 Jβ2.1; CDR3 sequence CASSLVGGDWHEQFF accounted for 4 of 12 (33.3%) of the beta-chain TCR transcripts sequenced. All other sequences were singlets.

Table 3. ND1Treg Vβ11 family-specific TCR expression.

Vβ	N-Dβ-N	Jβ	Gene usage
Tgtgccagcagcttag C A S S L	Tcgggggggattggc V G G D W	atgagcagttcttc H E Q F F	Vβ11.2 Dβ2 Jβ2.1 (4/12; 33.3%)
Tgtgccagcagc C A S S	Ataggacaggggttg I G Q G L	aacattcagtacttc N I Q Y F	Vβ11.3 Dβ1 Jβ2.4 (1/12; 8.3%)
tgtgccagcagc C A S S	Ataggacaggggttg I G Q G L	aacattcagtacttc N I Q Y F	Vβ11.2 Dβ1 Jβ2.4 (1/12; 8.3%)
Tg C	cgccagcagcttagtcgggggggattggc A S S L V G G D W H	atgagcagttcttc E Q F F	Vβ11.3 Dβ2 Jβ2.1 (1/12; 8.3%)
Tgtgccagcagc C A S S	gccttcctagcgggggct A F L A G G	acaccggggagctgtttttt Y T G E L F F	Vβ11.1 Dβ2 Jβ2.2 (1/12; 8.3%)
tgtgccagcagc C A S S	ataggacaggggttgac I G Q G L T	cattcagtacttc I Q Y F	Vβ11.2 Dβ1 Jβ2.4 (1/12; 8.3%)

Table 3. *(Continued.)*

tgtgccagcagcttag C A S S L	tcgggggggattggcatgagcagtc V G G D W H E Q S	cttc F	Vβ11.2 Dβ2 Jβ2.1 (1/12; 8.3%)
tgtgccagcagc C A S S	gccttctttcccgggggct. A F F P G G #	.acaccggggagctgtttttt # T G E L F F	Vβ11.2 Dβ2 Jβ2.2 (1/12; 8.3%)
C	tgtgccagcagcgccttcccagcgggggggct L C Q Q R L P S G G A	.acaccggggagctgtttttt # T G E L F F	Vβ11.2 Dβ2 Jβ2.2 (1/12; 8.3%)

Family-specific nested PCR amplifications for the Vβ5 chain revealed (Table 4)**:** clone ND1Treg-BFS5-1: transcript Vβ5.1 Dβ1 Jβ1.6; CDR3 sequence CASRPGQFNPTFNSPLHF accounted for 4 of 6 (66.7%) of the beta-chain TCR transcripts sequenced.

Table 4. ND1Treg Vβ5 family-specific TCR expression.

Vβ	N-Dβ-N	Jβ	Gene usage
tgcgccagc C A S	cgtccgggacagttcaatcccagctt R P G Q F N P S F	taattcacccctccacttt N S P L H F	Vβ5.1 Dβ1 Jβ1.6 (4/6)
tg C	cgccagcagcttgggtttgggcac A S S L G L G T	gaacactgaagctttcttt N T E A F F	Vβ5.4 Dβ1 Jβ1.1 (1/6)
tg C	cgccagcagcgcgggggacaggtcg A S S A G D R S	actgaagctttcttt T E A F F	Vβ5.4 Dβ1 Jβ1.1 (1/6)

The expanded Vβ11 (CASSLEGGPQRGYTF) and Vβ5 (CASSVDRGKEKLFF) sequences obtained from the initial all-family amplifications (Table 4) did not match the sequences obtained from the later family-specific amplifications of the Vβ11 and Vβ5 families.

All-family amplification of the ND1Treg alpha-chain TCR transcripts, followed by cloning and sequencing, revealed a triplet and a doublet:

(1) clone ND1Treg-A-1: Vα4 Jα16 transcript; CDR3 sequence CLVGVSDGQKLLF accounted for 3 of 16 (18.75%) of the alpha-chain TCR transcripts sequenced.

(2) clone ND1Treg-A-2: Vα12.2 Jα58 transcript; CDR3 sequence CAVNGPETSGSRLTF accounted for 2 of 16 (12.5%) of the alpha-chain TCR transcripts sequenced.

Table 5. α-Chain TCR transcripts expressed in Tregs from 1st donor PBMCs.

Vα	N	Jα	Gene usage
Tgcctcgtgggtg C L V G		tttcagatggccagaagctgctcttt V S D G Q K L L F	Vα4 Jα16 (3/16, 18.75%)
Tgtgccgtgaac C A V N	Gggcc G P	agaaaccagtggctctaggttgaccttt E T S G S R L T F	Vα12.2 Jα58 (2/16, 12.5%)
tgcctcgtgggtg C L V G	ta V	tcagatggccagaagctgctcttt S D G Q K L L F	Vα4 Jα16 (1/16, 6.25%)
tgtgcagcaagt C A A S	gggtctcagggg G S Q G	ggaaatgagaaattaacctttt G N E K L T F	Vα13.1 Jα48 (1/16, 6.25%)
Tgt C	ccagccgaaaccagtggctctt P A E T S G S	ggttgaccttt W L T F	Vα41 Jα58 (1/16, 6.25%)
Tgt C	ccagcc P A	gaaaccagtggctctaggttgaccttt E T S G S R L T F	Vα41 Jα58 (1/16, 6.25%)
tgtgct C A	t	catcaggaggaagctacatacctacattt S S G G S Y I P T F	Vα17 Jα6 (1/16, 6.25%)
tgtgcagca C A A	gcagg A G	tacctcaggaacctacaaatacatcttt T S G T Y K Y I F	Vα13.1 Jα40 (1/16, 6.25%)
tgtgcagca C A A	gcaggtacctcg A G T S	ggaacctacaaatacatcttt G T Y K Y I F	Vα13.1 Jα40 (1/16, 6.25%)

Table 5. *(Continued.)*

C	ctgcaaggttacaactggtggagcaacctatggcc P A R L Q L V E Q P M A	.agctgacattt - A T F	Vα12.3 Jα52 (1/16, 6.25%)
Tg	agctgtgccc A V P	cagggcggatctgaaaagctggtcttt Q G G S E K L V F	Vα21 Jα57 (1/16, 6.25%)
-	-	-	Vα4 Jα43 (1/16, 6.25%)

Vα4 family-specific amplifications, cloning and sequencing revealed (Table 6):

clone ND1Treg-A4FS-1: Vα4 Jα20 transcript; CDR3 sequence CLVGDRDYKLSF accounted for 18 of 23 (78.3%) of the alpha-chain TCR transcripts sequenced.

A clonal expansion was observed of the Vα4 Jα20 TCR transcript sequence CLVGDRDYKLSF with 18/23 identical copies of the sequence present. This constituted 78.3% of the sequences; the remainder of the sequences were singlets.

Table 6. ND1Treg Vα4 family-specific TCR expression

Vα	N	Jα	Gene usage
tgcctcgtgggtgaca C L V G D	ga R	gactacaagctcagcttt D Y K L S F	Vα4 Jα20 (18/23; 78.3%)

ND2Treg

Analysis of the ND2Treg beta chain TCR transcripts revealed a polyclonal distribution of the 19 TCR transcript sequences analyzed (Table 7):

Table 7. β-Chain TCR transcripts expressed in Tregs from 2nd donor PBMCs

Vβ	N-Dβ-N	Jβ	Gene usage
tgtgccagcag C A S S	cctgtacccgacagggaa L Y P T G N	ctacgagcagtacttc Y E Q Y F	Vβ27 Dβ1 Jβ2.7 (1/19, 5.26%)
tgtgccagcagccaag C A S S Q	gggatcc G D P	caatgagcagttcttc N E Q F F	Vβ14 Dβ1 Jβ2.1 (1/19, 5.26%)
tgtgccagctcacc C A S S P	gggactagcgggag G L A G	cagatacgcagtatttt A D T Q Y F	Vβ18 Dβ2 Jβ2.3 (1/19, 5.26%)
tgtgcctgg C A W	agtatgagcagac S M S R	acgagcagtacttc H E Q Y F	Vβ30 Dβ1 Jβ2.7 (1/19, 5.26%)
tgcgccagcag C A S R	gacggacaagcc T D K P	caccggggagctgtttttt T G E L F F	Vβ5.1 Dβ1 Jβ2.2 (1/19, 5.26%)
tgcagtgctagag C S A R	tgcggag V R S	ctcctacaatgagcagttcttc S Y N E Q F F	Vβ20.1 Dβ2 Jβ2.1 (1/19, 5.26%)
tgcagtgctag C S A S	tggcag G S	ctacgagcagtacttc Y E Q Y F	Vβ20.1 Dβ1 Jβ2.7 (1/19, 5.26%)
tgcagtgctagag C S A R	gtcacgggggc G H G G	aacactgaagctttcttt N T E A F F	Vβ20.1 Dβ1 Jβ1.1 (1/19, 5.26%)
tgtgcctgg C A W	gcccacaccttcg A H T F	acactgaagctttcttt D T E A F F	Vβ30 Dβ1 Jβ1.1 (1/19, 5.26%)
tgtgccagca C A S	ccaccgccggacggag T T A G R S	ctcctacaatgagcagttcttc S Y N E Q F F	Vβ28 Dβ1 Jβ2.1 (1/19, 5.26%)
tgcgccagcagct C A S S	ggggggggacta W G G L	caagagacccagtacttc Q E T Q Y F	Vβ5.1 Dβ2 Jβ2.5 (1/19, 5.26%)
tgcagtgc C S A	ctcccgggacggg S R D G	aactatggctacaccttc N Y G Y T F	Vβ20.1 Dβ1 Jβ1.2 (1/19, 5.26%)
tgcagtgc C S A	cagcgccactacaggggctacgagcagtacc S A T T G G Y E Q Y	tc L	Vβ20.1 Dβ1 Jβ2.7 (1/19, 5.26%)
tgcgccagcagcttgg C A S S L	g G	ctctggggccaacgtcctgactttc S G A N V L T F	Vβ5.1 Jβ2.6 (1/19, 5.26%)
tgcgccagcagct C A S S	ctccgggacaggggcgg S P G Q G A	actatggctacaccttc D Y G Y T F	Vβ5.1 Dβ1 Jβ1.2 (1/19, 5.26%)

Table 7. *(Continued.)*

tgtgccagcagtt C A S S	ctcgacagggcgag S R Q G E	tatggctacaccttc Y G Y T F	Vβ27 Dβ1 Jβ1.2 (1/19, 5.26%)
tgtgccagca C A S	ccaggacaggggtactgg T R T G G T G	tggctacaccttc G Y T F	Vβ28 Dβ1 Jβ1.2 (1/19, 5.26%)
tgtgccagcagccaag C A S S Q	gggagagg G E R	gatacgcagtatttt D T Q Y F	Vβ14 Dβ2 Jβ2.3 (1/19, 5.26%)
tgtgccagcagcg C A S S	cccacgggacaggggg A H G T G G	tcacccctccacttt S P L H F	Vβ9 Dβ1 Jβ1.6 (1/19, 5.26%)

Analysis of the ND2Treg alpha chain TCR transcripts (Table 8), on the other hand, revealed a triplet and a doublet:

(1) clone ND2Treg-A-1: transcript Vα22 Jα57; CDR3 sequence CAVKSQGGSEKLVF accounted for 3 of 24 (12.5%) of the alpha-chain TCR transcripts sequenced

(2) clone ND2Treg-A-1: transcript Vα39 Jα40; CDR3 sequence CAVEIPGTYKYIF accounted for 2 of 24 (12.5%) of the alpha-chain TCR transcripts sequenced following two sets of nested all-family amplifications.

Table 8. α-Chain TCR transcripts expressed in Tregs from 2nd donor PBMCs

Vα	N	Jα	Gene usage
tgtgctgtg C A V	aagt K	ctcagggcggatctgaaaagctggtcttt S Q G G S E K L V F	Vα22 Jα57 (3/24, 12.5%)
tgtgccgtgga C A V E	gatcc I	caggaacctacaaatacatcttt P G T Y K Y I F	Vα39 Jα40 (2/24, 8.3%)
tgtgctct C A L	ccc P	ctctggggctgggagttaccaactcactttc S G A G S Y Q L T F	Vα6 Jα28 (1/24, 4.16%)

Table 8. *(Continued.)*

tgtgcagagaata C A E N	aggccccggacgactacaagctcaa K A P D D Y K L N	cttt F	Vα13.2 Jα20 (1/24, 4.16%)
tgtgctgtggagcg C A V E R	g	gggtacagcagtgcttccaagataatcttt G Y S S A S K I I F	Vα22 Jα3 (1/24, 4.16%)
tgtgctgggcag C A G Q	caac Q	gttctaacgactacaagctcagcttt R S N D Y K L S F	Vα35 Jα20 (1/24, 4.16%)
tgtggag C G	gagg G G	ctcaggaacctacaaatacatcttt S G T Y K Y I F	Vα34 Jα40 (1/24, 4.16%)
tgtgctg C A	gg G	acaggctttcagaaacttgtattt T G F Q K L V F	Vα22 Jα8 (1/24, 4.16%)
tgtgctctaga C A L D		taaccagggaggaaagcttatcttc N Q G G K L I F	Vα6 Jα23 (1/24, 4.16%)
tgtgctgtggagc C A V E	gcggtagcg R G S	actatcagttaatctgg D Y Q L I W	Vα22 Jα33 (1/24, 4.16%)
tgtggagcagac C G A D	ccggaaagaacctgcaaaaac P E R T C K N	atcttt I F	Vα34 Jα40 (1/24, 4.16%)
tgtgctctaga C A L D		taaccagggaggaaagcttatcttc N Q G G K L I F	Vα6 Jα23 (1/24, 4.16%)
tgt C	gtggttaccctagtc V V T L V	ggaacctacaaatacatcttt G T Y K Y I F	Vα10 Jα40 (1/24, 4.16%)
tgtgctct C A L	caa K	gatttataaccagggaggaaagcttatcttc I Y N Q G G K L I F	Vα9.2 Jα23 (1/24, 4.16%)
tgtgc C A	cggcgtgaattatggaggaagccag G V N Y G G S Q	ggaaatctcatcttt G N L I F	Vα6 Jα42 (1/24, 4.16%)
c	tgtgctgtggaggatcaggaggaagctacatacct L C C G G S G G S Y I P	actttt T F	Vα2 Jα6 (1/24, 4.16%)
tgtgctgtcag C A V S	tgataagggcggatatgaaaagct. D K G G Y E K L	gtcttt V F	Vα41 Jα57 (1/24, 4.16%)
tgtgccg C A	gcccaaaaagaggagggg..caaggaaatct G P K R G G - Q G N L	catcttt I F	Vα39 Jα42 (1/24, 4.16%)
tgtgc C A	tgctaacttgggaaaaaaga.. A N L G K K -	aaattaaccttt K L T F	Vα25 Jα48 (1/24, 4.16%)

Table 8. *(Continued.)*

tgt C	ttttttcccggaggggaaggaa. F F P E G K E	gaaatgagaaattaaccttt - N E K L T F	Vα13.1 Jα48 (1/24, 4.16%)
tgtgctctag C A L	ccggtaaccattttcttt. A G N H F L -	Tttt F	Vα6 Jα49 (1/24, 4.16%)

Using the same ND2Treg RNA, Vα22 family-specific PCR amplification of the cDNA product (Table 9), revealed a doublet:

Clone ND2Treg-A22FS-1: Vα22 Jα4 transcript; CDR3 sequence CAVHSGGYNKLIF accounted for 2 of 11 (18.8%) of the Vα22 TCR transcripts sequenced. The remainder were singlets.

Table 9. ND2Treg Vα22 family-specific TCR expression

Vα	N	Jα	Gene usage
tgtgctgt C A V	cca H	ttctggtggctacaataagctgattttt S G G Y N K L I F	Vα22 Jα4 (2/11: 18.18%)
tgtgctgt C A V	ccattcc H S	ggtggctacaataagctgattttt G G Y N K L I F	Vα22 Jα4 (1/11: 9.09%)
tgtgctg C A		ggatggatagcagctataaattgatcttc G M D S S Y K L I F	Vα22 Jα12 (1/11: 9.09%)
tgtgctg C A	ggatggatagcagcc G M D S S	ataaattgatcttc H K L I F	Vα22 Jα12 (1/11: 9.09%)
tgtgctgt C A V	ttt L	agaaaccagtggctctaggttgaccttt E T S G S R L T F	Vα22 Jα58 (1/11: 9.09%)
tgtgctgtgg C A V		ggtacagcagtgcttccaagataatcttt G Y S S A S K I I F	Vα22 Jα3 (1/11: 9.09%)
tgtgctgtg C A V	aggg R	atagtggaggtagcaactataaactgacattt D S G G S N Y K L T F	Vα22 Jα53 (1/11: 9.09%)

Table 9. *(Continued.)*

tgtgct C A	tcccg S R	gaacagagatgacaagatcatcttt N R D D K I I F	Vα22 Jα30 (1/11: 9.09%)
tgtgctgtggagc C A V E	cc P	aacaccaatgcaggcaaatcaaccttt N T N A G K S T F	Vα22 Jα27 (1/11: 9.09%)
tgtgctgt C A V	agc A	tactggagccaatagtaagctgacattt T G A N S K L T F	Vα22 Jα56 (1/11: 9.09%)

ND3Treg

The third Treg isolation ND3Treg sample revealed unique sequences for both chains, indicating a polyclonal distribution among the Tregs. 17 beta chains and 13 alpha chains were sequenced.

ND4Treg

The fourth Treg isolation ND4Treg sample similarly revealed unique TCR transcript sequences for both chains; 21 beta chains and 18 alpha chains were sequenced.

ND5Treg

The fifth Treg isolation ND5Treg sample produced three doublets in the alpha chain (Table 10):

(1) clone ND5Treg-A-1: transcript Vα22 Jα42; CDR3 sequence CAVGRGGSQGNLIF accounted for 2 of 24 (8.33%) of the alpha-chain TCR transcripts sequenced

(2) clone ND5Treg-A-2: transcript Vα34 Jα21; CDR3 sequence CGAATGWDKFYF accounted for 2 of 24 (8.33%) of the alpha-chain TCR transcripts sequenced

(3) clone ND5Treg-A-3: transcript Vα6 Jα12; CDR3 sequence CALLDSSYKLIF accounted for 2 of 24 (8.33%) of the α-chain TCR transcripts sequenced.

Table 10. α-Chain TCR transcripts expressed in Tregs from 5th donor PBMCs.

Vα	N	Jα	Gene usage
tgtgctgtgg C A V	gtcgg G R	ggaggaagccaaggaaatctcatcttt G G S Q G N L I F	Vα22 Jα42 (2/24; 8.33%)
tgtggagcag C G A	cgacagggtggg A T G W	acaaattttacttt D K F Y F	Vα34 Jα21 (2/24; 8.33%)
tgtgctcta C A L	t	tggatagcagctataaattgatcttc L D S S Y K L I F	Vα6 Jα12 (2/24; 8.33%)
tgtgc C A	ccaggggagagatgacaagg Q G R D D K	tcatcttt V I F	Vα6 Jα30 (1/24; 4.17%)
tgtgcaatgagaga C A M R D	tcag Q	tcaggaaacacacctcttgtcttt S G N T P L V F	Vα14 Jα29 (1/24; 4.17%)
tgtgctgtca C A V	ctct T L	caccgacaagctcatcttt T D K L I F	Vα41 Jα34 (1/24; 4.17%)
tgtgcagag C A E	ca Q	aggaagctacatacctacattt G S Y I P T F	Vα5 Jα6 (1/24; 4.17%)
t	tggcaatgagtccaaaccccggtaaccagttctt L A M S P N P G N Q F F	tttt F	Vα14 Jα49 (1/24; 4.17%)
tgtcttct C L L	cctctctgc L S A	ggataactatggtcagaattttgtcttt D N Y G Q N F V F	Vα40 Jα26 (1/24; 4.17%)
tgtgctctga C A L	cctatc T Y	cttataacaccgacaagctcatcttt P Y N T D K L I F	Vα9.2 Jα34 (1/24; 4.17%)
tgtgctgtg C A V	a	caggaaacacacctcttgtcttt T G N T P L V F	Vα2 Jα29 (1/24; 4.17%)
tgtgcg C A	catggcat H G I	ctcaggaacctacaaatacatcttt S G T Y K Y I F	Vα17 Jα40 (1/24; 4.17%)

Table 10. *(Continued.)*

tgtgcagca C A A	ggag G	acaccgacaagctcatcttt D T D K L I F	Vα29 Jα34 (1/24; 4.17%)
tgtgctg C A	ggttca G F	tgttttctggtggctacaataagctgatttt M F S G G Y N K L I F	Vα22 Jα4 (1/24; 4.17%)
tgtgctgtggagg C A V E		ggatggatagcagctataaattgatcttc G M D S S Y K L I F	Vα2 Jα12 (1/24; 4.17%)
tgtgctacggacg C A T D	cggg A G	ctatggtcagaattttgtcttt Y G Q N F V F	Vα17 Jα26 (1/24; 4.17%)
tgtgc C A	ccagggg Q G	agagatgacaagatcatcttt R D D K I I F	Vα6 Jα30 (1/24; 4.17%)
tgtgct C A	ctt L	aacaccggtaaccagttctatttt N T G N Q F Y F	Vα36 Jα49 (1/24; 4.17%)
tgtgccgt C A V	cccgggg P G	ggtagcaactataaactgacattt G S N Y K L T F	Vα39 Jα53 (1/24; 4.17%)
tgtgctgggcag C A G Q	tcttatcagggagcccagaagctggtatc S Y Q G A Q K L V S	T	Vα35 Jα54 (1/24; 4.17%)
tgtgcagcaagt C A A S	ctgaatgcaggcaaatcaacc L N A G K S T	ttt F	Vα13.1 Jα27 (1/24; 4.17%)

ND6Treg

The sixth Treg isolation ND6Treg sample had unique TCR transcript sequences for the beta chain sequences (Table 11).

Table 11. β-Chain TCR transcripts expressed in Tregs from 6th donor PBMCs.

Vβ	N-Dβ-N	Jβ	Gene usage
tgtgccag C A S	tagcttacttgcgactaa S L L A T N	ctctggaaacaccatatatttt S G N T I Y F	Vβ11.2 Dβ2 Jβ1.3 (1/23: 4.35%)
tgtgccagcagc C A S S	ctgggtgacgggtctc L G D G S	acaatgagcagttcttc H N E Q F F	Vβ11.2 Dβ2 Jβ2.1 (1/23: 4.35%)
tgtgccagcag C A S S	tactaggcggggag T R R G	ctgaagctttcttt A E A F F	Vβ11.2 Dβ2 Jβ1.1 (1/23: 4.35%)
tgtgccagcagc C A S S	ccgggggcaggggggcgg P G A G G G	caccggggagctgtttttt T G E L F F	Vβ11.2 Dβ1 Jβ2.2 (1/23: 4.35%)
tgtgccagcagctt C A S S F	tcaggagaactatggca Q E N Y G	acaccttc N T F	Vβ11.2 Dβ1 Jβ1.2 (1/23: 4.35%)
tgtgccagcagctt C A S S F	tcaggag Q E	aactatggctacaccttc N Y G Y T F	Vβ11.2 Dβ1 Jβ1.2 (1/23: 4.35%)
tgtgccagctc C A S S	ccccggccgcgccgggggccg P G R A G G R	caatgagcagttcttc N E Q F F	Vβ18 Dβ1 Jβ2.1 (1/23: 4.35%)
tgtgccagctcaccac C A S S P	tcgggacaggggggcggg L G T G G G	aatgagcagttcttc N E Q F F	Vβ18 Dβ1 Jβ2.1 (1/23: 4.35%)
tgtgccagctcac C A S S	aacaaggagggga Q Q G G D	taatgaaaaactgtttttt N E K L F F	Vβ18 Dβ2 Jβ1.4 (1/23: 4.35%)
tgtgccagcagt C A S S	cacggactagcgggggtctt H G L A G G L	gatacgcagtatttt D T Q Y F	Vβ6.1 Dβ2 Jβ2.3 (1/23: 4.35%)
tgtgccagc C A S	gcacctacggctagcgggggggcgg A P T A S G G G G	ctcctacaatgagcagttcttc S Y N E Q F F	Vβ6.1 Dβ2 Jβ2.1 (1/23: 4.35%)
tgcagtg C S	ggcaggggcta G Q G L	acagatacgcagtatttt T D T Q Y F	Vβ20.1 Dβ1 Jβ2.3 (1/23: 4.35%)
Tgcag C R	agctagaggcagggtaacggg A R G R V T G	cggggagctgtttttt G E L F F	Vβ20.1 Dβ1 Jβ2.2 (1/23: 4.35%)
tgtgccag C A S	cagaccgggactagcgggggtggt R P G L A G V V	agatacgcagtatttt D T Q Y F	Vβ3.1 Dβ2 Jβ2.3 (1/23: 4.35%)
tgcgccagcag C A S R	acgtcaggtct R Q V	caactaatgaaaaactgtttttt S T N E K L F F	Vβ5.1 Dβ1 Jβ1.4 (1/23: 4.35%)

Table 11. *(Continued.)*

tgtgccagcagcc C A S S	gccagggaggaaggtc R Q G G R S	cactgaagctttcttt T E A F F	Vβ14 Dβ2 Jβ1.1 (1/23: 4.35%)
tgtgccagcag C A S S	ccatatcagggaggggggg H I R E G G	ctatggctacaccttc Y G Y T F	Vβ25.1 Dβ2 Jβ1.2 (1/23: 4.35%)
tgtgccatcagtga C A I S E	agttcgg V R	gaaaaactgtttttt E K L F F	Vβ10.3 Dβ2 Jβ1.4 (1/23: 4.35%)
tgtgccag C A R	aagattgataagtag R L I S S	ctcctataattcacccctccacttt S Y N S P L H F	Vβ2 Dβ2 Jβ1.6 (1/23: 4.35%)
tgtgcctggag C A W S	tttcagcagtaaa F S S K	tatggctacaccttc Y G Y T F	Vβ30 Dβ1 Jβ1.2 (1/23: 4.35%)
tgtgccagcagttt C A S S F	tgggc G	cgaattcacccctccacttt P N S P L H F	Vβ27 Dβ1 Jβ1.6 (1/23: 4.35%)
tgcgccagcagcttgg C A S S L	cggcagat A A D	tatggctacaccttc Y G Y T F	Vβ1 Dβ1 Jβ1.2 (1/23: 4.35%)
tgtgccagcagct C A S S	cgaggacaggggg S R T G G	ctacaatgagcagttcttc Y N E Q F F	Vβ11.3 Dβ1 Jβ2.1 (1/23: 4.35%)

All-family Nested PCR amplifications revealed a quadruplet (Table 12):

clone ND6Treg-A-1: transcript Vα22 Jα45; CDR3 sequence CAVERFGRGGADGLTF accounted for 4 of 26 (15.4%) of the alpha-chain TCR transcripts sequenced following the all-family PCR amplifications.

Table 12. α-Chain TCR transcripts expressed in Tregs from 6th donor PBMCs.

Vα	N	Jα	Gene usage
tgtgctgtggagc C A V E	Ggttcggaa R F G	gaggaggtgctgacggactcaccttt R G G A D G L T F	Vα22 Jα45 (4/26: 15.4%)
tgtgctgtgga C A V E	atctaacgacc S N D	acaagctcagcttt H K L S F	Vα22 Jα20 (1/26: 3.85%)
tgtgctgtgga C A V E	a	tctaacgactacaagctcagcttt S N D Y K L S F	Vα22 Jα20 (1/26: 3.85%)
tgtgctg C A	ctaga A R	tcttataacaccgacaagctcatcttt S Y N T D K L I F	Vα22 Jα34 (1/26: 3.85%)
tgtggagcagaca C G A D	tacc I P	caccaatgcaggcaaatcaaccttt T N A G K S T F	Vα22 Jα34 (1/26: 3.85%)
tgtgctgtgg C A V		gcggatctgaaaagctggtcttt G G S E K L V F	Vα22 Jα57 (1/26: 3.85%)
tgtgctgtcaga C A V R	gagc E	ctggtggtactagctatggaaagctgacatt P G G T S Y G K L T F	Vα41 Jα52 (1/26: 3.85%)
tgtgctgtca C A V		ccggtaaccagttctatttt T G N Q F Y F	Vα41 Jα49 (1/26: 3.85%)
tgtgctgtcaga C A V R	tcg S	ggcggtgctacaaacaagctcatcttt G G A T N K L I F	Vα41 Jα32 (1/26: 3.85%)
tgtgcagagagta C A E S	gaccgggggcaaacaacctcttct R P G A N N L F	tt F	Vα5 Jα36 (1/26: 3.85%)
tgtgcagag C A E	tccaac S N	aaccagggaggaaagcttatcttc N Q G G K L I F	Vα5 Jα23 (1/26: 3.85%)
tgtgcagaga C A E	cccctact T P T	ttttctggtggctacaataagctgattttt F S G G Y N K L I F	Vα5 Jα4 (1/26: 3.85%)
g	gagcaccgaacgatagggccagggaggaaagctc G A P N D R G Q G G K L	atcttc I F	Vα29 Jα23 (1/26: 3.85%)
tgtgtggtgaac C V V N	gatttctggggtacgggcaggagagcacttacc D F W G T G R R A L T	ttt F	Vα12.1 Jα5 (1/26: 3.85%)
tgtggagc C G A	ccgcagggg R R G	cggcactgccagtaaactcaccttt G T A S K L T F	Vα34 Jα44 (1/26: 3.85%)

Table 12. *(Continued.)*

tgtcttct C L L	c	ggaggaggtgctgacggactcaccttt G G G A D G L T F	Vα40 Jα45 (1/26: 3.85%)
tgtgccgtg C A V	ggtg G	attctgggggttaccagaaagttaccttt D S G G Y Q K V T F	Vα12 Jα13 (1/26: 3.85%)
tgtgc C A	ccctcgcgcagctggaggcttcaaaactatcttc P R A A G G F K T I F		Vα6 Jα9 (1/26: 3.85%)
tgtgctgtgcagg C A V Q	aatatat E Y I	caccaatgcaggcaaatcaaccttt T N A G K S T F	Vα20 Jα27 (1/26: 3.85%)
tgtgccgtgg C A V	tccttac V L T	gaacagagatgacaagatcatcttt N R D D K I I F	Vα39 Jα30 (1/26: 3.85%)
tgtgccgtgga C A V E	gag S	tgcaggcaacatgctcaccttt A G N M L T F	Vα39 Jα39 (1/26: 3.85%)
tgtgctacggac C A T D	tacgg Y G	taatgctggtggtactagctatggaaagctgacattt N A G G T S Y G K L T F	Vα17 Jα52 (1/26: 3.85%)
tgtgcagcaa C A A	cccct T P	tacagcagtgcttccaagataatcttt Y S S A S K I I F	Vα13 Jα3 (1/26: 3.85%)

Vα22 family-specific PCR amplification of the ND6Treg RNA material revealed a triplet and a doublet (Table 13):

(1) clone ND6Treg-A22FS-1; TCR transcript Vα22 Jα12; CDR3 sequence CAGMDSSYKLIF accounted for 3 of 21 (14.3%) of the Vα22 transcripts sequenced.

(2) clone ND6Treg-A22FS-2; TCR transcript Vα22 Jα26; CDR3 sequence CALNDNYGQNFVF accounted for 2 of 21 (9.5%) of the Vα22 transcripts sequenced.

Table 13. ND6Treg Vα22 family-specific TCR expression.

Vα	N	Jα	Gene usage
tgtgctg C A		ggatggatagcagctataaattgatcttc G M D S S Y K L I F	Vα22 Jα12 (3/21: 14.3%)
tgtgct C A	ctgaac L N	gataactatggtcagaattttgtcttt D N Y G Q N F V F	Vα22 Jα26 (2/21: 9.5%)
tgtgctgtgg C A V	gt G	aataacaatgccagactcatgttt N N N A R L M F	Vα22 Jα31 (1/21: 4.76%)
tgtgctgtgg C A V	gtaataacaatgccagactcatgtc G N N N A R L M S	t	Vα22 Jα31 (1/21: 4.76%)
tgtgctg C A G		gagatgacaagatcatcttt D D K I I F	Vα22 Jα30 (1/21: 4.76%)
tgtgctg C A	gagatgacaagatcatcttc G D D K I I F		Vα22 Jα30 (1/21: 4.76%)
tgtgctgt C A V	cca H	ttctggtggctacaataagctgattttt S G G Y N K L I F	Vα22 Jα4 (1/21: 4.76%)
tgtgctgt C A V	agc A	tactggagccaatagtaagctgacattt T G A N S K L T F	Vα22 Jα56 (1/21: 4.76%)
tgtgctgtgga C A V D	tagaactggggcaaacaat R T G A N N	ctcttcttt L F F	Vα22 Jα36 (1/21: 4.76%)
tgtgctgtggagc C A V E	ttc L	attcaggaaacacacctcttgtcttt H S G N T P L V F	Vα22 Jα29 (1/21: 4.76%)
tgtgctgtg C A V	tgtcgtgt C R V	tagcaactatcagttaatctgg S N Y Q L I W	Vα22 Jα33 (1/21: 4.76%)
tgtgctgtgg C A V	g G	ccaggcaggaactgctctgatcttt Q A G T A L I F	Vα22 Jα15 (1/21: 4.76%)
tgtgctgtggag C A V E	agagctg R A	ccggcactgccagtaaactcaccttt A G T A S K L T F	Vα22 Jα44 (1/21: 4.76%)
tgtgctg C A	gg G	aatactggaggcttcaaaactatcttt N T G G F K T I F	Vα22 Jα9 (1/21: 4.76%)
tgtgctgtg C A V	atccca I P	tacaacttcaacaaattttacttt Y N F N K F Y F	Vα22 Jα21 (1/21: 4.76%)

Table 13. *(Continued.)*

Tgtgctg C A	ctaga A R	tcttataacaccgacaagctcatcttt S Y N T D K L I F	Vα22 Jα34 (1/21: 4.76%)
Tgtgctg C A	ggggggggt G G G	acaataacaatgacatgcgcttt Y N N N D M R F	Vα22 Jα43 (1/21: 4.76%)
tgtgctgtggag C A V E	gggcgc G R	ggctctggcaacacaggcaaactaatcttt G S G N T G K L I F	Vα22 Jα37 (1/21: 4.76%)

ND7Treg

The seventh Treg isolation ND7Treg sample revealed unique TCR transcript sequences for both chains; 15 beta chains and 25 alpha chains were sequenced.

CHAPTER 4

DISCUSSION

4.1 NPT phenotypic changes

NPT was previously shown to eliminate 4T1 breast cancer tumors as well as N1-S1 rat liver tumors to induce a vaccine effect suggesting immunotherapeutic potential. Unlike other immunotherapeutic agents, NPT actively kills cancer cells and stimulates the host's immune system. It was shown in the 4T1-luc model (92), as others have reported in other cancer models (98), that NPT induces the release of damage-associated molecular patterns (DAMPs) and activates dendritic cells *ex vivo* and *in vivo*. Data supports the role of NPT as a non-drug immunogenic cell death inducer. Given that immunosuppression in the TME is the bane of immunotherapy, I was interested to determine more specifically the mechanisms by which NPT breaks this barrier to promote host-induced immunity in a predominantly immunosuppressive TME in mouse 4T1-luc breast cancer.

I have shown in this study that NPT reduces the local and systemic tumor immunosuppressive burden by reducing activated Tregs, TAMs and MDSCs in the tumor and other tissues (**Fig. 26**). While it was shown previously that NPT induces apoptosis in liver cancer tissue (99), the cell types that underwent caspase-mediated cell death were not defined. Here I show that Tregs (in the dLN) and TAMs (in both, the tumor and dLN), but not conv T-cells, are among the apoptotic cell population most adversely impacted by NPT. These findings contrast with those seen in radiotherapy treatment, which was shown to increase the frequency, phenotypic characteristics, and functional capacity of

Tregs in the TME (90). Although it was previously shown that a successful local NPT reduces the number of Tregs and MDSCs (92), this is the first study to investigate how NPT alters the phenotypic and functional dynamics of local Tregs.

4.2 NPT-induced differential changes in T cell subset frequencies

When evaluating the differences among T cell subsets, I found that NPT reduced intratumoral Tregs more aggressively than conventional CD4 TILs. To better understand this observation, I evaluated the Tconv/Treg ratio and found it significantly elevated in all the tissues post-treatment, suggesting that the CD4 cells shifted away from a suppressive Treg population and towards an effector T cell profile. Interestingly in the dLN, Tregs were found to be more prone to apoptotic changes post-treatment when compared to their CD8 and CD4 T effector counterparts. A study by Plaza-Servant et al. demonstrated that Tregs have an increased sensitivity to apoptosis in relation to Tconv (100). This sensitivity was correlated with a lower expression of c-Flip$_L$, a member of the extrinsic apoptosis pathway, among Tregs when compared to Tconv. Among Tregs, the increased sensitivity to apoptosis was mostly restricted to activated CD44$^+$CD62L$^-$ Tregs when compared to naïve CD44$^-$CD62L$^+$ Tregs (100). The lower c-Flip$_L$ expression in Tregs may be the reason why they are more vulnerable, than their Tconv counterparts, to apoptotic changes resulting from NPT.

4.3 Reduction in Treg activation and function post-NPT

Since Tregs are critical in keeping the immune system from attacking self-antigens, a non-selective Treg depletion approach, such as using anti-CD25, results in autoimmunity (80). Treg depletion in Foxp3DTR-GFP mouse tumor models initially results in tumor clearance, but the mice later succumb to systemic autoimmunity (6,101-103). It

is therefore critical to selectively deplete activated Tregs, or ideally tumor-specific Tregs in the TME. In order to find which subgroups of Tregs were most affected by NPT, I analyzed the expression of different Treg activation markers and found 4-1BB to be exclusively expressed among Foxp3$^+$ CD4 Tregs in tumor-bearing mice, absent among other T cell subsets, and entirely absent in naïve mice T cells. Treg 4-1BB expression was also clearly and consistently downregulated post-treatment, making it an excellent marker to track the impact of NPT on the local and systemic Treg dynamics.

Overall, I found NPT shifted the Treg phenotypic dynamics from a predominantly activated (CD44$^+$CD62L$^-$) population with higher TGFβ and 4-1BB expression to a predominantly naïve (CD44$^-$CD62L$^+$) population with lower 4-1BB expression, which is consistent with a reduced functional suppressive capability. Studies have shown that *in vivo* depletion of 4-1BB$^+$ Tregs inhibits tumor growth, and Tregs lacking 4-1BB have an impaired suppressive function (104).

Interestingly, I also observed a transient peak in both apoptotic and 4-1BB$^+$ Tregs in the dLN at 4 hours post-treatment followed by their reduction in the following days, hinting that these Tregs may have a transient spike in activation and suppressive function before dying. Although apoptotic Tregs are described in literature as being more efficient at their suppressive function (105), a Treg suppression assay would be needed to confirm whether these apoptotic Tregs at 4 hours post-NPT truly have an increased functional capacity. Nevertheless, the elevation of 4-1BB$^+$ Tregs lasts less than 24 hours after NPT. Considering DC activation observed at Day 2 post-NPT (92) and M1-polarization occurring at Day 3 post-treatment, these cells unlikely have a significant impact on the initiation of antitumor immunity.

4.4 Activation of the antitumor immune branch

Studies on NPT have shown an increase in activated DCs and cytotoxic and memory T cells responsible for tumor clearance and antitumor immunity (92). These findings are concurrent with 100% rejection of the secondary tumor challenge following a successful treatment of the primary tumor with 100 ns NPT (92). In this current study I demonstrated a shift in both innate and adaptive immune branches from a pro-tumor to an antitumor profile. In the innate immune arm, I saw an immediate TAM apoptosis and a gradual MDSC reduction post-treatment, with a concomitant upregulation of antitumor activated $CD86^{+}$ M1 TAMs. Blood MDSCs, which accurately reflect changes in the overall tumor burden (92), also demonstrated a gradual decrease post-treatment. Meanwhile in the adaptive immune branch, I observed a phenotypic and functional post-treatment decrease in Tregs followed by a gradual increase in resident memory CD8 T cells at days 3 and 7. Thus, NPT encouraged coordinate host changes in both the lymphoid and myeloid immune systems to shift from an immunosuppressive to an immunostimulatory performance as part of NPT-induced immune responses.

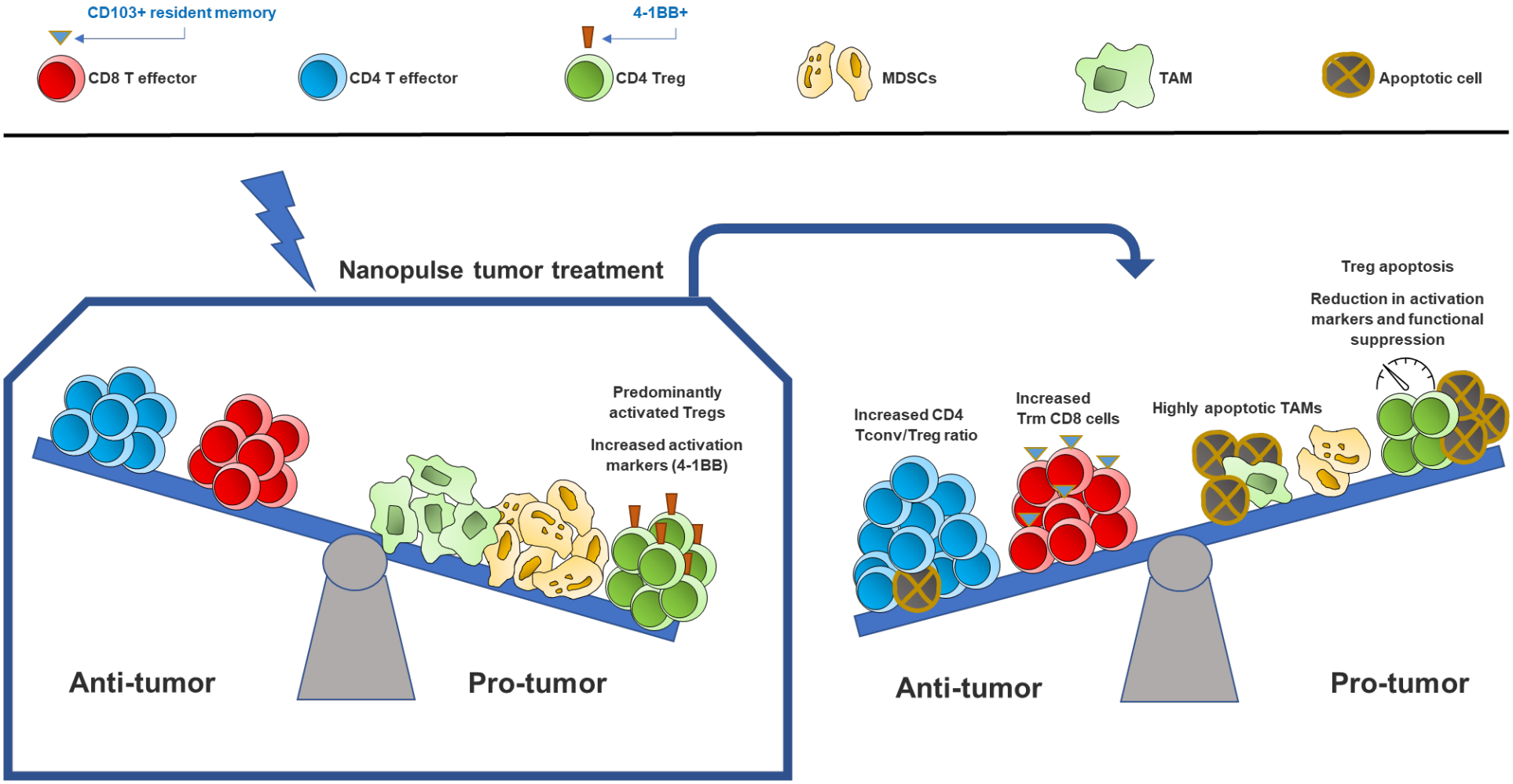

Figure 26.

The impact of NPT on the TME in breast cancer. NPT treatment shifts the immune cell dynamics from a pro-tumor to an anti-tumor environment. Suppressor cells including Tregs, TAMs and MDSCs are downregulated. Tregs undergo apoptosis, exhibit a shift from an activated 4-1BB^{+} to a naïve 4-1BB^{-} phenotype, and demonstrate reduced functional suppression capacity post-treatment. Anti-tumor CD4 Tconv increase in frequency and CD8^{+} CD103^{+} resident memory T cells are upregulated following treatment.

4.5 Underlying mechanisms of differential changes in intratumoral immune cells

When comparing the impact of NPT on different immune cells in the TME, I found that while intratumoral Tregs swiftly decreased following NPT, they did not demonstrate significant post-treatment apoptosis as seen among dLN Tregs.

While I observed a rapid shift to apoptosis in intratumoral TAMs following NPT, I do not yet know why the treatment reduced intratumoral Tregs without similarly inducing their apoptosis in the TME. I speculate that such a rapid TIL depletion following NPT may have been the result of an immediate (possibly accidental) cell death mechanism that was no longer detected after 4 hours, an electro-expulsive force causing a massive TIL exodus, or an abrogation of tumor signaling factors, whether cell-contact dependent proteins or tissue-specific chemo-attractants, that had previously kept Tregs confined to the TME.

Co-culturing healthy dLN lymphocytes with *in vitro* pulsed 4T1-luc tumor cells demonstrated that Tregs heavily rely on a healthy tumor presence for their survival and that NPT has an antitumor impact on both the host immune cells as well as the TME. This finding confirms that NPT induces a dual specificity effect in cancer cell elimination and reprogramming the host's immune system to participate in the antitumor effects through natural immunity in the 4T1-luc model. Future studies of the post-treatment changes in the TME-Treg signaling mechanism and local T cell trafficking patterns will help further to clarify these findings. Pulsing Tregs *in vitro* will reveal what direct impact NPT has on the Treg signaling and cell death mechanism.

4.6 Treg TCR clonality

Investigating the impact NPT may have on the Treg and Tconv TCR clonality in mice will help bring our studies closer to clinical trials. Our control studies on the blood of healthy individual donors indicated that human peripheral $CD4^+$ Tregs are mostly polyclonal in nature.

A recent study on the Treg TCR in patient tumors suggested that tumors contain activated Tregs that proliferate in an antigen specific manner (61). I speculate that the downregulation of the 4-$1BB^+$ Tregs and shift from a predominantly activated to a predominantly naïve Treg population is a result of NPT-induced downregulation of the accumulated tumor antigen-specific Tregs. An investigation of the Treg TCR clonality before and after treatment will further reveal whether NPT reduces clonally expanded antigen-specific Tregs. Investigating for changes in the CD8 T cell TCR clonality in parallel with the above study will further demonstrate whether a rise in antigen-specific CD8 T cells, indicative of an antigen-mediated antitumor response, ensues post-treatment.

CHAPTER 5

CONCLUSION

NPT confers local and systemic benefits by reducing the immunosuppressive burden and eliciting protective antitumor immunity. Therefore, it is critical to understand how the treatment impacts Tregs, a key player of the immunosuppressive barrier, and how it tips the Treg/Teff axis from a tumorigenic to a tumor-eliminative response.

These studies enhance the concept that NPT is a potent TME modifier that differentially affects immune cells in the tumor. NPT diminished local and systemic Treg frequencies, their expression of activation markers and their functional suppressive capacity. The treatment also reduced local TAMs and systemic MDSCs. Tregs in the dLN and intratumoral TAMs were further found to undergo a rapid increase in apoptosis post-treatment. Along with the diminution of immunosuppressive cells, NPT also preserved CD4 and CD8 Tconv, increased the CD8 Trm frequency, and promoted the M1-polarization of surviving TAMs, indicating the initiation of antitumor immunity post-NPT.

These discoveries, along with our previous work, suggest that NPT is a novel non-drug ICD inducer and a promising *in situ* vaccination approach to reduce the risk of metastatic disease, the major cause of breast cancer death. Other local cancer therapies, such as radiotherapy, require several immune modulators to ablate tumors and create a long-term protective effect. In contrast, a single nanopulse treatment has been demonstrated to elicit effective antitumor immunity. These findings make NPT a promising immunotherapeutic candidate for future clinical trial investigations.

REFERENCES

1. Jin M-Z, Jin W-L. The updated landscape of tumor microenvironment and drug repurposing. Signal Transduct Target Ther 2020;5(1):166
2. Baghban R, Roshangar L, Jahanban-Esfahlan R, Seidi K, Ebrahimi-Kalan A, Jaymand M*, et al.* Tumor microenvironment complexity and therapeutic implications at a glance. Cell Commun Signal 2020;18(1):59
3. Sakaguchi S. Naturally arising CD4(+) regulatory T cells for immunologic self-tolerance and negative control of immune responses. Annu Rev Immunol 2004;22:531-62.
4. Plitas G, Rudensky AY. Regulatory T Cells: Differentiation and Function. Cancer Immunol Res 2016;4(9):721-5.
5. Toker A, Nguyen LT, Stone SC, Yang SYC, Katz SR, Shaw PA, et al. Regulatory T cells in ovarian cancer are characterized by a highly activated phenotype distinct from that in melanoma. Clin Cancer Res 2018;24(22):5685-96.
6. Overacre-Delgoffe AE, Vignali DAA. Treg Fragility: A prerequisite for effective antitumor immunity? Cancer Immunol Res 2018;6(8):882-7.
7. Tanchot C, Terme M, Pere H, Tran T, Benhamouda N, Strioga M, et al. Tumor-infiltrating regulatory T cells: phenotype, role, mechanism of expansion in situ and clinical significance. Cancer Microenvironment 2013;6(2):147-57.
8. Quezada SA, Peggs KS, Curran MA, Allison JP. CTLA4 blockade and GM-CSF combination immunotherapy alters the intratumor balance of effector and regulatory T cells. J Clin Invest 2006;116(7):1935-45.
9. Curiel T. Managing regulatory T cells to improve cancer immunotherapy. Cancer Immunotherapy: Springer New York; 2013. p 281-314.
10. Strauss L, Bergmann C, Szczepanski M, Gooding W, Johnson JT, Whiteside TL. A unique subset of CD4+CD25highFoxp3+ T cells secreting interleukin-10 and transforming growth factor-beta1 mediates suppression in the tumor microenvironment. Clin Cancer Res 2007;13(15 Pt 1):4345-54.
11. Strauss L, Bergmann C, Szczepanski MJ, Lang S, Kirkwood JM, Whiteside TL. Expression of ICOS on human melanoma-infiltrating CD4+CD25highFoxp3+ T regulatory cells: implications and impact on tumor-mediated immune suppression. J Immunol 2008;180(5):2967-80.
12. Wang HY, Wang RF. Antigen-specific CD4(+) regulatory T cells in cancer: implications for immunotherapy. Microbes Infect 2005;7(7-8):1056-62.
13. Peng DJ, Liu R, Zou W. Regulatory T cells in human ovarian cancer. J Oncol 2012;2012:345164.
14. Woo EY, Chu CS, Goletz TJ, Schlienger K, Yeh H, Coukos G, et al. Regulatory CD4(+)CD25(+) T cells in tumors from patients with early-stage non-small cell lung cancer and late-stage ovarian cancer. Cancer Res 2001;61(12):4766-72.
15. Ormandy LA, Hillemann T, Wedemeyer H, Manns MP, Greten TF, Korangy F. Increased populations of regulatory T cells in peripheral blood of patients with hepatocellular carcinoma. Cancer Res 2005;65(6):2457-64.
16. Schott AK, Pries R, Wollenberg B. Permanent up-regulation of regulatory T-lymphocytes in patients with head and neck cancer. Int J Mol Med 2010;26(1):67-75.

17. Alvaro T, Lejeune M, Salvado MT, Bosch R, Garcia JF, Jaen J, et al. Outcome in Hodgkin's lymphoma can be predicted from the presence of accompanying cytotoxic and regulatory T cells. Clin Cancer Res 2005;11(4):1467-73.
18. Liyanage UK, Moore TT, Joo HG, Tanaka Y, Herrmann V, Doherty G, et al. Prevalence of regulatory T cells is increased in peripheral blood and tumor microenvironment of patients with pancreas or breast adenocarcinoma. J Immunol 2002;169(5):2756-61.
19. Gil Del Alcazar CR, Alečković M, Polyak K. Immune Escape during Breast Tumor Progression. Cancer Immunol Res 2020;8(4):422-7.
20. Ge Y, Böhm H-H, Rathinasamy A, Xydia M, Hu X, Pincha M, et al. Tumor-specific regulatory T cells from the bone marrow orchestrate antitumor immunity in breast cancer. Cancer Immunol Res 2019;7(12):1998-2012.
21. Curiel TJ, Coukos G, Zou LH, Alvarez X, Cheng P, Mottram P, et al. Specific recruitment of regulatory T cells in ovarian carcinoma fosters immune privilege and predicts reduced survival. Nat Med 2004;10(9):942-9.
22. Ayyoub M, Pignon P, Classe JM, Odunsi K, Valmori D. CD4+ T effectors specific for the tumor antigen NY-ESO-1 are highly enriched at ovarian cancer sites and coexist with, but are distinct from, tumor-associated Treg. Cancer Immunol Res 2013;1(5):303-8.
23. Jacobs JFM, Nierkens S, Figdor CG, de Vries IJM, Adema GJ. Regulatory T cells in melanoma: the final hurdle towards effective immunotherapy? Lancet Oncol 2012;13(1):E32-E42.
24. deLeeuw RJ, Kost SE, Kakal JA, Nelson BH. The Prognostic Value of FoxP3+ Tumor-Infiltrating Lymphocytes in Cancer: A Critical Review of the Literature. Clin Cancer Res 2012;18(11):3022-9.
25. Sato E, Olson SH, Ahn J, Bundy B, Nishikawa H, Qian F, et al. Intraepithelial CD8+ tumor-infiltrating lymphocytes and a high CD8+/regulatory T cell ratio are associated with favorable prognosis in ovarian cancer. Proc Natl Acad Sci U S A 2005;102(51):18538-43.
26. Ichihara F, Kono K, Takahashi A, Kawaida H, Sugai H, Fujii H. Increased populations of regulatory T cells in peripheral blood and tumor-infiltrating lymphocytes in patients with gastric and esophageal cancers. Clin Cancer Res 2003;9(12):4404-8.
27. Yang Y, Yang Y, Yang J, Zhao X, Wei X. Tumor Microenvironment in Ovarian Cancer: Function and Therapeutic Strategy. Front Cell Dev Biol 2020;8(758).
28. Atretkhany KSN, Drutskaya MS. Myeloid-derived suppressor cells and proinflammatory cytokines as targets for cancer therapy. Biochemistry (Moscow) 2016;81(11):1274-83.
29. Ostrand-Rosenberg S, Fenselau C. Myeloid-Derived Suppressor Cells: Immune-Suppressive Cells That Impair Antitumor Immunity and Are Sculpted by Their Environment. J Immunol 2018;200(2):422-31.
30. Rodriguez PC, Quiceno DG, Zabaleta J, Ortiz B, Zea AH, Piazuelo MB, et al. Arginase I production in the tumor microenvironment by mature myeloid cells inhibits T-cell receptor expression and antigen-specific T-cell responses. Cancer Res 2004;64(16):5839-49.

31. Srivastava MK, Sinha P, Clements VK, Rodriguez P, Ostrand-Rosenberg S. Myeloid-derived suppressor cells inhibit T-cell activation by depleting cystine and cysteine. Cancer Res 2010;70(1):68-77.
32. Hanson EM, Clements VK, Sinha P, Ilkovitch D, Ostrand-Rosenberg S. Myeloid-derived suppressor cells down-regulate L-selectin expression on CD4+ and CD8+ T cells. J Immunol 2009;183(2):937-44.
33. Sakuishi K, Jayaraman P, Behar SM, Anderson AC, Kuchroo VK. Emerging Tim-3 functions in antimicrobial and tumor immunity. Trends Immunol 2011;32(8):345-9.
34. Gabrilovich DI, Ostrand-Rosenberg S, Bronte V. Coordinated regulation of myeloid cells by tumours. Nat Rev Immunol 2012;12(4):253-68.
35. Law AMK, Valdes-Mora F, Gallego-Ortega D. Myeloid-Derived Suppressor Cells as a Therapeutic Target for Cancer. Cells 2020;9(3).
36. Cha YJ, Koo JS. Role of Tumor-Associated Myeloid Cells in Breast Cancer. Cells 2020;9(8):1785.
37. Gabrilovich DI. Myeloid-Derived Suppressor Cells. Cancer Immunol Res 2017;5(1):3-8.
38. Molon B, Ugel S, Del Pozzo F, Soldani C, Zilio S, Avella D, et al. Chemokine nitration prevents intratumoral infiltration of antigen-specific T cells. J Exp Med 2011;208(10):1949-62.
39. Murray PJ, Allen JE, Biswas SK, Fisher EA, Gilroy DW, Goerdt S, et al. Macrophage activation and polarization: nomenclature and experimental guidelines. Immunity 2014;41(1):14-20.
40. Laoui D, Movahedi K, Van Overmeire E, Van den Bossche J, Schouppe E, Mommer C, et al. Tumor-associated macrophages in breast cancer: distinct subsets, distinct functions. Int J Dev Biol 2011;55(7-9):861-7.
41. Ojalvo LS, King W, Cox D, Pollard JW. High-density gene expression analysis of tumor-associated macrophages from mouse mammary tumors. Am J Pathol 2009;174(3):1048-64.
42. Pucci F, Venneri MA, Biziato D, Nonis A, Moi D, Sica A, et al. A distinguishing gene signature shared by tumor-infiltrating Tie2-expressing monocytes, blood "resident" monocytes, and embryonic macrophages suggests common functions and developmental relationships. Blood 2009;114(4):901-14.
43. Movahedi K, Laoui D, Gysemans C, Baeten M, Stangé G, Van den Bossche J, et al. Different tumor microenvironments contain functionally distinct subsets of macrophages derived from Ly6C(high) monocytes. Cancer Res 2010;70(14):5728-39.
44. Stewart DA, Yang Y, Makowski L, Troester MA. Basal-like breast cancer cells induce phenotypic and genomic changes in macrophages. Mol Cancer Res 2012;10(6):727-38.
45. Rippaus N, Taggart D, Williams J, Andreou T, Wurdak H, Wronski K, et al. Metastatic site-specific polarization of macrophages in intracranial breast cancer metastases. Oncotarget 2016;7(27):41473-87.
46. Zhang M, Yan L, Kim JA. Modulating mammary tumor growth, metastasis and immunosuppression by siRNA-induced MIF reduction in tumor microenvironment. Cancer Gene Ther 2015;22(10):463-74.

47. Arlauckas SP, Garris CS, Kohler RH, Kitaoka M, Cuccarese MF, Yang KS, et al. In vivo imaging reveals a tumor-associated macrophage-mediated resistance pathway in anti-PD-1 therapy. Sci Transl Med 2017;9(389).
48. Ring A, Nguyen C, Smbatyan G, Tripathy D, Yu M, Press M, et al. CBP/β-Catenin/FOXM1 Is a Novel Therapeutic Target in Triple Negative Breast Cancer. Cancers (Basel) 2018;10(12).
49. Platsoucas CD, Fincke JE, Pappas J, Jung WJ, Heckel M, Schwarting R, et al. Immune responses to human tumors: Development of tumor vaccines. Anticancer Res 2003;23(3A):1969-96.
50. Kreider JW, Bartlett GL, Butkiewicz BL. Relationship of Tumor Leukocytic Infiltration to Host Defense-Mechanisms and Prognosis. Cancer Metast Rev 1984;3(1):53-74.
51. Platsoucas CD. Human Autologous Tumor-Specific T-Cells in Malignant-Melanoma. Cancer Metast Rev 1991;10(2):151-76.
52. Mihm MC, Clark WH, From L. Clinical Diagnosis, Classification and Histogenetic Concepts of Early Stages of Cutaneous Malignant Melanomas. New Engl J Med 1971;284(19):1078.
53. Clemente CG, Mihm MG, Bufalino R, Zurrida S, Collini P, Cascinelli N. Prognostic value of tumor infiltrating lymphocytes in the vertical growth phase of primary cutaneous melanoma. Cancer 1996;77(7):1303-10.
54. Benvenuto M, Focaccetti C, Izzi V, Masuelli L, Modesti A, Bei R. Tumor antigens heterogeneity and immune response-targeting neoantigens in breast cancer. Semin Cancer Biol 2019.
55. Peng M, Mo Y, Wang Y, Wu P, Zhang Y, Xiong F, et al. Neoantigen vaccine: an emerging tumor immunotherapy. Mol Cancer 2019;18(1):128.
56. Zhang X, Kim S, Hundal J, Herndon JM, Li S, Petti AA, et al. Breast Cancer Neoantigens Can Induce CD8(+) T-Cell Responses and Antitumor Immunity. Cancer Immunol Res 2017;5(7):516-23.
57. Zacharakis N, Chinnasamy H, Black M, Xu H, Lu YC, Zheng Z, et al. Immune recognition of somatic mutations leading to complete durable regression in metastatic breast cancer. Nat Med 2018;24(6):724-30.
58. Lesterhuis WJ, Haanen JB, Punt CJ. Cancer immunotherapy--revisited. Nat Rev Drug Discov 2011;10(8):591-600.
59. Nishikawa H, Sakaguchi S. Regulatory T cells in tumor immunity. Int J Cancer 2010;127(4):759-67.
60. Bonertz A, Weitz J, Pietsch DHK, Rahbari NN, Schlude C, Ge YZ, et al. Antigen-specific Tregs control T cell responses against a limited repertoire of tumor antigens in patients with colorectal carcinoma. J Clin Invest 2009;119(11):3311-21.
61. Ahmadzadeh M, Pasetto A, Jia L, Deniger DCA-Ohoo, Stevanovic SA-Ohoo, Robbins PF, et al. Tumor-infiltrating human CD4(+) regulatory T cells display a distinct TCR repertoire and exhibit tumor and neoantigen reactivity. Sci Immunol 2019;4(31).
62. Bayraktar S, Batoo S, Okuno S, Glück S. Immunotherapy in breast cancer. J Carcinog 2019;18:2.

63. Hodi FS, O'Day SJ, McDermott DF, Weber RW, Sosman JA, Haanen JB, et al. Improved Survival with Ipilimumab in Patients with Metastatic Melanoma. New Engl J Med 2010;363(8):711-23.
64. Leach DR, Krummel MF, Allison JP. Enhancement of antitumor immunity by CTLA-4 blockade. Science 1996;271(5256):1734-6.
65. Topalian SL, Hodi FS, Brahmer JR, Gettinger SN, Smith DC, McDermott DF, et al. Safety, Activity, and Immune Correlates of Anti–PD-1 Antibody in Cancer. New Engl J Med 2012;366(26):2443-54.
66. Guo ZS. The 2018 Nobel Prize in medicine goes to cancer immunotherapy (editorial for BMC cancer). BMC Cancer 2018;18(1):1086.
67. Vonderheide RH, LoRusso PM, Khalil M, Gartner EM, Khaira D, Soulieres D, et al. Tremelimumab in combination with exemestane in patients with advanced breast cancer and treatment-associated modulation of inducible costimulator expression on patient T cells. Clin Cancer Res 2010;16(13):3485-94.
68. McArthur HL, Diab A, Page DB, Yuan J, Solomon SB, Sacchini V, et al. A Pilot Study of Preoperative Single-Dose Ipilimumab and/or Cryoablation in Women with Early-Stage Breast Cancer with Comprehensive Immune Profiling. Clin Cancer Res 2016;22(23):5729-37.
69. Lipson EJ, Forde PM, Hammers H-J, Emens LA, Taube JM, Topalian SL. Antagonists of PD-1 and PD-L1 in Cancer Treatment. Semin Oncol 2015;42(4):587-600.
70. Nanda R, Chow LQM, Dees EC, Berger R, Gupta S, Geva R, et al. Pembrolizumab in Patients With Advanced Triple-Negative Breast Cancer: Phase Ib KEYNOTE-012 Study. J Clin Oncol 2016;34(21):2460-7.
71. Ventola CL. Cancer Immunotherapy, Part 3: Challenges and Future Trends. P T 2017;42(8):514-21.
72. Rugo HS, Delord J-P, Im S-A, Ott PA, Piha-Paul SA, Bedard PL, et al. Safety and Antitumor Activity of Pembrolizumab in Patients with Estrogen Receptor–Positive/Human Epidermal Growth Factor Receptor 2–Negative Advanced Breast Cancer. Clin Cancer Res 2018;24(12):2804-11.
73. Nikanjam M, Patel H, Kurzrock R. Dosing immunotherapy combinations: Analysis of 3,526 patients for toxicity and response patterns. Oncoimmunology 2017;6(8):e1338997.
74. Yang L, Yu H, Dong S, Zhong Y, Hu S. Recognizing and managing on toxicities in cancer immunotherapy. Tumour Biol 2017;39(3):1010428317694542.
75. Takeuchi Y, Nishikawa H. Roles of regulatory T cells in cancer immunity. Int Immunol 2016;28(8):401-9.
76. Gobert M, Treilleux I, Bendriss-Vermare N, Bachelot T, Goddard-Leon S, Arfi V, et al. Regulatory T Cells Recruited through CCL22/CCR4 Are Selectively Activated in Lymphoid Infiltrates Surrounding Primary Breast Tumors and Lead to an Adverse Clinical Outcome. Cancer Res 2009;69(5):2000-9.
77. Yi G, Guo S, Liu W, Wang H, Liu R, Tsun A, et al. Identification and functional analysis of heterogeneous FOXP3+ Treg cell subpopulations in human pancreatic ductal adenocarcinoma. Sci Bull 2018;63(15):972-81.

78. Tan MCB, Goedegebuure PS, Belt BA, Flaherty B, Sankpal N, Gillanders WE, et al. Disruption of CCR5-Dependent Homing of Regulatory T Cells Inhibits Tumor Growth in a Murine Model of Pancreatic Cancer. J Immunol 2009;182(3):1746-55.
79. Xie F, Liang R, Li D, Li B. Regulatory T Cells and Their Clinical Applications in Antitumor Immunotherapy. Engineering 2019;5(1):132-9.
80. Ohue Y, Nishikawa H. Regulatory T (Treg) cells in cancer: Can Treg cells be a new therapeutic target? Cancer Sci 2019;110(7):2080-9.
81. Sugiyama D, Nishikawa H, Maeda Y, Nishioka M, Tanemura A, Katayama I, et al. Anti-CCR4 mAb selectively depletes effector-type FoxP3+CD4+ regulatory T cells, evoking antitumor immune responses in humans. Proc Natl Acad Sci U S A 2013;110(44):17945-50.
82. Kurose K, Ohue Y, Sato E, Yamauchi A, Eikawa S, Isobe M, et al. Increase in Activated Treg in TIL in Lung Cancer and In Vitro Depletion of Treg by ADCC Using an Antihuman CCR4 mAb (KM2760). J Thorac Oncol 2015;10(1):74-83.
83. Kurose K, Ohue Y, Wada H, Iida S, Ishida T, Kojima T, et al. Phase Ia Study of FoxP3+ CD4 Treg Depletion by Infusion of a Humanized Anti-CCR4 Antibody, KW-0761, in Cancer Patients. Clin Cancer Res 2015;21(19):4327-36.
84. Knochelmann HM, Dwyer CJ, Bailey SR, Amaya SM, Elston DM, Mazza-McCrann JM, et al. When worlds collide: Th17 and Treg cells in cancer and autoimmunity. Cell Mol Immunol 2018;15(5):458-69.
85. Zhou G, Drake CG, Levitsky HI. Amplification of tumor-specific regulatory T cells following therapeutic cancer vaccines. Blood 2006;107(2):628-36.
86. Ebert LM, MacRaild SE, Zanker D, Davis ID, Cebon J, Chen W. A cancer vaccine induces expansion of NY-ESO-1-specific regulatory T cells in patients with advanced melanoma. PLoS One 2012;7(10):e48424-e.
87. Zou WP. Regulatory T cells, tumour immunity and immunotherapy. Nat Rev Immunol 2006;6(4):295-307.
88. Moreno Ayala MA, Li Z, DuPage M. Treg programming and therapeutic reprogramming in cancer. Immunology 2019;157(3):198-209.
89. Guo S, Burcus NI, Hornef J, Jing Y, Jiang C, Heller R, et al. Nano-Pulse Stimulation for the Treatment of Pancreatic Cancer and the Changes in Immune Profile. Cancers 2018;10(7):217.
90. Muroyama Y, Nirschl TR, Kochel CM, Lopez-Bujanda Z, Theodros D, Mao W, et al. Stereotactic Radiotherapy Increases Functionally Suppressive Regulatory T Cells in the Tumor Microenvironment. Cancer Immunol Res 2017;5(11):992-1004.
91. Beebe SJ, Lassiter BP, Guo S. Nanopulse Stimulation (NPS) Induces Tumor Ablation and Immunity in Orthotopic 4T1 Mouse Breast Cancer: A Review. Cancers 2018;10(4):97.
92. Guo S, Jing Y, Burcus NI, Lassiter BP, Tanaz R, Heller R, et al. Nano-pulse stimulation induces potent immune responses, eradicating local breast cancer while reducing distant metastases. Int J Cancer 2018;142(3):629-40.
93. Geng F, Bao X, Dong L, Guo Q-Q, Guo J, Xie Y, et al. Doxorubicin pretreatment enhances FAPα/survivin co-targeting DNA vaccine anti-tumor activity primarily through decreasing peripheral MDSCs in the 4T1 murine breast cancer model. Oncoimmunology 2020;9(1):1747350.

94. Steenbrugge J, Vander Elst N, Demeyere K, De Wever O, Sanders NN, Van Den Broeck W, et al. Comparative Profiling of Metastatic 4T1- vs. Non-metastatic Py230-Based Mammary Tumors in an Intraductal Model for Triple-Negative Breast Cancer. Front Immunol 2019;10:2928.
95. Xu B, Sakkas LI, Goldman BI, Jeevanandam V, Gaughan J, Oleszak EL, et al. Identical α-chain T-cell receptor transcripts are present on T cells infiltrating coronary arteries of human cardiac allografts with chronic rejection. Cell Immunol 2003;225(2):75-90.
96. Sakkas LI, Xu B, Artlett CM, Lu S, Jimenez SA, Platsoucas CD. Oligoclonal T Cell Expansion in the Skin of Patients with Systemic Sclerosis. J Immunol 2002;168(7):3649-59.
97. Hanahan D. Studies on Transformation of Escherichia-Coli with Plasmids. J Mol Biol 1983;166(4):557-80.
98. Nuccitelli R, McDaniel A, Anand S, Cha J, Mallon Z, Berridge JC, et al. Nano-Pulse Stimulation is a physical modality that can trigger immunogenic tumor cell death. J Immunother Cancer 2017;5:32.
99. Lassiter BP, Guo S, Beebe SJ. Nano-Pulse Stimulation Ablates Orthotopic Rat Hepatocellular Carcinoma and Induces Innate and Adaptive Memory Immune Mechanisms that Prevent Recurrence. Cancers (Basel) 2018;10(3).
100. Plaza-Sirvent C, Schuster M, Neumann Y, Heise U, Pils MC, Schulze-Osthoff K, et al. c-FLIP Expression in Foxp3-Expressing Cells Is Essential for Survival of Regulatory T Cells and Prevention of Autoimmunity. Cell Reports 2017;18(1):12-22.
101. Kim J, Lahl K, Hori S, Loddenkemper C, Chaudhry A, deRoos P, et al. Cutting Edge: Depletion of Foxp3+ Cells Leads to Induction of Autoimmunity by Specific Ablation of Regulatory T Cells in Genetically Targeted Mice. J Immunol 2009;183(12):7631-4.
102. Bos PD, Plitas G, Rudra D, Lee SY, Rudensky AY. Transient regulatory T cell ablation deters oncogene-driven breast cancer and enhances radiotherapy. J Exp Med 2013;210(11):2435-66.
103. Delgoffe GM, Woo SR, Turnis ME, Gravano DM, Guy C, Overacre AE, et al. Stability and function of regulatory T cells is maintained by a neuropilin-1-semaphorin-4a axis. Nature 2013;501(7466):252-6.
104. Freeman ZT, Nirschl TR, Hovelson DH, Johnston RJ, Engelhardt JJ, Selby MJ, et al. A conserved intratumoral regulatory T cell signature identifies 4-1BB as a pan-cancer target. J Clin Inves 2020;130(3):1405-16.
105. Maj T, Wang W, Crespo J, Zhang H, Wang W, Wei S, et al. Oxidative stress controls regulatory T cell apoptosis and suppressor activity and PD-L1-blockade resistance in tumor. Nat Immunol 2017;18(12):1332-41.

VITA

Anthony Nanajian received his B.S. and M.S. degrees in Biological Sciences from Old Dominion University and his M.D. degree from St. George's University in Grenada. He is currently completing his Ph.D. degree in Biomedical Sciences at Old Dominion University under the guidance of Dr. Stephen J. Beebe and Dr. Siqi Guo. His research focus is on investigating changes in immune cell dynamics, particularly among regulatory T cells, in tumors following nanopulse treatment. He is currently a medical resident at the University of Central Florida Internal Medicine program in Gainesville and plans to specialize in Hematology-Oncology and become involved in cancer immunotherapy clinical trials.